2011

The Effect of Sliding Contact Friction on Surface Quality of Aluminum Sheet Products

Olufisayo Gali
University of Windsor

The Effect of Sliding Contact Friction on Surface Quality of Aluminum Sheet Products

by

Olufisayo Gali

A Thesis
Submitted to the Faculty of Graduate Studies
through Engineering Materials
in Partial Fulfillment of the Requirements for
the Degree of Master of Applied Science at the
University of Windsor

Windsor, Ontario, Canada

2011

The Effect of Sliding Contact Friction on Surface Quality of Aluminum Sheet Products

by

Olufisayo Gali

APPROVED BY:

_____

Dr A. Fartaj
Department of Mechanical, Automotive and Materials Engineering

_____

Dr. A Alpas
Department of Mechanical, Automotive and Materials Engineering

_____

Dr. A Riahi, Advisor
Department of Mechanical, Automotive and Materials Engineering

_____

Dr. H. Hu, Chair of Defence
Department of Mechanical, Automotive and Materials Engineering

February 07, 2011

DECLARATION OF ORIGINALITY

I hereby certify that I am the sole author of this thesis and that no part of this thesis has been published or submitted for publication.

I certify that, to the best of my knowledge, my thesis does not infringe upon anyone's copyright nor violate any proprietary rights and that any ideas, techniques, quotations, or any other material from the work of other people included in my thesis, published or otherwise, are fully acknowledged in accordance with the standard referencing practices. Furthermore, to the extent that I have included copyrighted material that surpasses the bounds of fair dealing within the meaning of the Canada Copyright Act, I certify that I have obtained a written permission from the copyright owner(s) to include such material(s) in my thesis and have included copies of such copyright clearances to my appendix.

I declare that this is a true copy of my thesis, including any final revisions, as approved by my thesis committee and the Graduate Studies office, and that this thesis has not been submitted for a higher degree to any other University or Institution.

ABSTRACT

The surface defects of aluminum alloys that have undergone high temperature processing are studied.

The effects of rolling passes and forward speed on the generation of a disturbed layer on aluminum alloy sheet surfaces were investigated with a hot rolling simulator. The results showed that by increasing the forward speed and number of rolling passes, the localized shear deformation became more pronounced on the surface. However, when the two rolling passes were in opposite directions, the defects induced by the localized shear deformation were embedded into the aluminum surface.

The use of WS_2 as a solid lubricant in hot forming of AA5083 aluminum alloy was also explored. The results show that the method of WS_2 application is crucial to its performance. An aerosol WS_2 spray was developed which recorded a lower COF than BN and a WS_2 coating sandblasted to the substrate. WS_2 also showed better durability regardless of application method than BN.

DEDICATION

To my mother;

I wouldn't be anywhere without you nor would I want to be

My grandfather, Mr F O C Akinpelu, and my nephews;

You are the love and inspiration that keep me going

Arike,

Without you, the clocks would stop ticking, the world would stop spinning and all life would stop breathing.

Thank you for giving my life meaning.

ACKNOWLEDGEMENTS

First, I would like to express my sincere gratitude to Dr Riahi, for his guidance, support and encouragement during this journey. His continuous drive for research, mentorship and interest in me are much more than appreciated. My thanks to Dr Alpas, for his continual support, valuable suggestions and taking a chance on me. My sincere appreciation is extended to Dr K. Januszkiewicz for his comments, support and vital suggestions during this work and also to Dr A Morales for her support and cooperation.

I would like to thank Dr Fartaj and Dr Hu, for their time, insight and for always having an open door. My deepest thanks to Dr Edrisy for all her guidance, care and support, I truly appreciate your friendship.

My special thanks goes to the technical support team; Mr. A. Jenner, for always making out time and bringing our designs and ideas to life; Mr. J. Robinson, for his constant help and training; Mr. P. Seguin, for all his constant assistance and wisdom; Ms B. Tattersall and Ms R. Gignac, for their enduring administrative assistance and constant understanding. My sincere gratitude is also extended to Dr X. Meng-Burrany for all her encouragement.

I am very indebted to my new family the past and present researchers of the IRC in Tribology of Lightweight Materials for their friendship and contributions to this research work.

I would also like to extend my thanks to Novelis Global Technology Centre, General Motors of Canada Limited and Natural Sciences and Engineering Research Council of Canada (NSERC) for their support and funding of this study.

Finally I would like to pay tribute to my father; whose strength, love and support I have always relied on, my brother, for constantly believing in me despite the odds, supporting me and just being there, my sister for her constant love and support.

TABLE OF CONTENTS

LIST OF TABLES

LIST OF FIGURES

NOMENCLATURE

Abbreviations

A.S.	Aerosol Sprayed
COF	Coefficient of Friction
EDS	Energy Dispersive X-Ray Spectroscopy
EPMA	Electron Probe Micro-Analyzer
FFC	Filiform Corrosion
FIB	Focused Ion Beam
GDOES	Glow Discharge Optical Emission Spectroscopy
QPF	Quick Plastic Forming
S.B.	Spray/Sand Blasted
SEM	Scanning Electron Microscope
SPF	Superplastic Forming
TEM	Transmission Electron Microscope

CHAPTER I

INTRODUCTION

1.1 Background

Non-heat-treatable wrought aluminum alloys have found widespread use in industries that require not just a good strength-to-mass ratio but an attractive surface finish that eliminates the need for hard polishing or other finishing operations [1]. These alloys also offer good corrosion resistance, weldability, and high ductility/good formability [2, 3]. They include alloys in the series 1XXX (Pure Al), 3XXX (Al-Mn), 4XXX (Al-Si), and 5XXX (Al-Mg). These alloys are referred to as non-heat-treatable because they do not respond to heat treatments such as precipitation or age hardening and therefore rely solely on solid solution strengthening and strain-hardening practices [4].

The non-heat-treatable alloys of major interest are those alloys that contain magnesium, manganese, or both as major additions; these are alloys in the 3XXX (Al-Mn) and 5XXX (Al-Mg) series. Aluminum-magnesium (Al-Mg) alloys are also considered to be lighter than other aluminum alloys [4]. Manganese additions in the aluminum increase its strength without loss of the corrosion resistance of the alloy. The solubility of manganese is limited to about 1.5 wt. %; it forms dispersoids such as Al_6(Mn,Fe) and α–$Al_{15}(Fe,Mn)_3Si_2$ which strengthen the alloy, the distribution of these dispersoids determine the amount of strengthening that occurs [5, 6]. They also control recrystallized grain size by pinning the grain and subgrain boundaries [4, 6]. Magnesium additions increase the tensile strength of the alloy as well as raise the recrystallization temperature [2]. They promote work hardening in the alloy by reducing the stacking fault energy, which reduces the inclination for dynamic recovery [4].

Magnesium has a high solubility in aluminum up to 17.4 wt. %, and as shown on, the Al-Mg phase diagram (Figure 1), it undergoes precipitation hardening for it possesses a positively sloping solvus. Commercially however, this is not the case as the formation of the required second-phase precipitates (Al_3Mg_2) is difficult, and therefore they cannot be heat-treated [6]

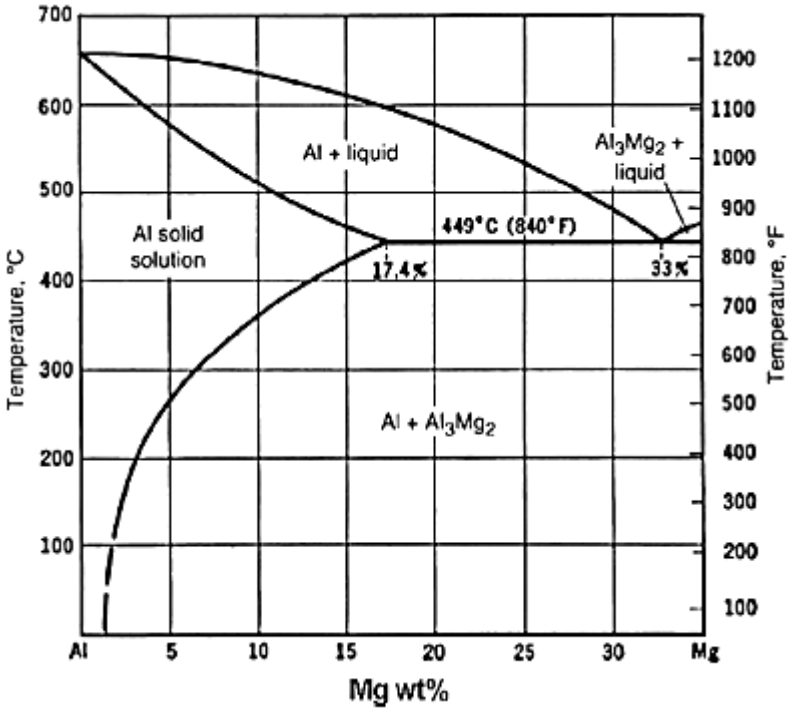

Figure 1 Phase diagram of binary Al-Mg system. The magnesium concentration is in wt. % [6]

The processing of alloys, which is performed to change the shape of the workpiece, usually involves bulk plastic forming processes [7, 8]. These processes are grouped under primary mechanical working processes (processing operations) and secondary mechanical working processes (fabrication operations). The former involve

processes that are designed to induce significant deformation and shape changes in the form of reduction of an ingot or billet to a standard simpler shape, that is, sheet, strip or plate, whereas the latter are performed on the sheet products produced by the previous process to produce a final finished shape. The latter are usually referred to as sheet metal working processes. They include forming processes such as hot forming, quick plastic forming, superplastic forming, and warm forming, whereas the former include such methods as rolling, extrusion, and drawing [7, 9].

Aluminum alloys are usually processed through thermo-mechanical processes which enhance the formability of these alloys by reducing the stress concentrators which initiate failure [3]. For most non-heat-treatable aluminum alloys, the process usually first involves hot rolling, which produces the sheet and strip products on which later forming operations are performed to attain the desired final product. It is vital to know the thermo-mechanical processes the alloy goes through as these affect their surface quality during subsequent thermo-mechanical treatments. Rolling is the most common method of work-hardening non-heat-treatable alloys [3]. Hot rolling temperatures are usually in the range of $0.6T_m$, where T_m is the melting temperature, with strain rates reaching as high as $5s^{-1}$. The deformation of metals during rolling subjects them to high compressive stresses from the rolls and surface shear stresses from the friction between the rolls and the metal [9]. During hot rolling, aluminum alloys experience significant changes in their microstructure and texture, and this determines the product quality [3].

Forming operations are used for the production of various shapes needed by the industry; these shapes can be complex with a high production rate. Forming operations at

elevated temperatures are preferred in the industry as elevated temperatures result in greater productivity and the formation of complex shapes by taking advantage of the increased formability of materials at these temperatures. Some aluminum alloys experience high formability at elevated temperatures with some experiencing up to 500% elongation under uniform tension without failure [10]. These are referred to as superplastic alloys; they possess a fine, stable grain size microstructure. In Al-Mg alloys, this microstructure is achieved through static or dynamic recrystallization and the presence of small amounts of second phase particles that stabilize the fine grain size structure [3, 11]. Forming operations at elevated temperatures are grouped into hot forming operations and warm forming operations.

Hot forming involves forming operations at temperatures above recrystallization whereas warm forming operations occur below recrystallization but well above room temperature. Warm forming temperatures range between 250^{o}C – 300^{o}C for aluminum alloys. At these temperatures, alloys such as 5XXX series are able to maintain most of their original strength after forming while producing parts with *enhanced capabilities* [10]. Hot forming operations include processes such as superplastic forming and quick plastic forming. These processes are of interest as they have a growing niche not only in the automobile industry, but also in other industries. They take advantage of the superplastic properties of alloys, relying on the hot gas blowing forming process to form a heated blank into a single-sided tool with the use of pressurized air [12, 13].

SPF and QPF are quite similar; they both have a high strain rate sensitivity and occur under high forming temperatures in excess of 400^{o}C. QPF was developed by GM

and boasts higher production volumes than SPF. This is because SPF uses slow forming rates under which maximum strain sensitivity occurs to obtain a uniform final thickness distribution. The SPF manufacturing process has been described to occur at temperatures ranging between 450^{o}C – 500^{o}C at strain rates of $10^{-4}s^{-1}$. The material deformation occurs mainly due to grain boundary sliding. QPF on the other hand occurs at lower temperatures of about 400^{o}C – 510^{o}C at strain rates greater than $10^{-3}s\text{-}^{1}$. Metal deformation here occurs due to both grain boundary sliding and dislocation mechanisms. [13, 14, 15].

High friction has been observed with elevated temperature metal processing as those discussed above. It occurs between the die and the workpiece due to their close contact and the high pressures which drive the surfaces together. High friction is undesirable as it is associated with the increase in the rate of material transfer between the aluminum workpiece and the harder tool surface, prevents the stretching of the sheet, and induces welding of the sheet to the die. All of these contribute to the reduction of the required fine surface finishing of the final aluminum products by the induction of various surface defects [8, 9].

Lubrication which is used to mitigate high friction is thus critical during elevated temperature processing. Lubricants are selected for their compatibility with aluminum alloys and are metal working process specific [11]. In hot rolling, oil-in-water emulsions are industrially used to reduce friction and aid in the cooling of the rolls, whereas in hot forming, lubricants are based on formulations of boron nitride and graphite to facilitate the smooth movement of the aluminum workpiece over the die [16]. Even with

lubrication, relatively high coefficients of friction still occur during high temperature metal working, and lubrication breakdown is also known to occur which can lead to adhesion between the die and the workpiece.

1.2 Thesis Objective

There has been limited tribological work done in the area of high temperature forming for aluminum sheet products to date. The current study examines the surface defects that occur during two processing routes for Al-Mg alloys. These processing routes can be and are used in succession (usually with hot forming following hot rolling), this research examined these processes individually, pertaining to the particular surface defects that occur during each process and the parameters that affect them. A different alloy is observed during each study pertaining to two different processes.

The first part of the study examines the surface defects that occur during hot rolling of an Al-Mn-Mg alloy. The alloy AA3104 has found major use in the production of beverage cans. Here the interest pertains to how processing parameters as forward speed and the number of passes affect the development of surface defects.

The second part of the study concentrates on the hot forming in relation to the QPF process with specific interest given to Al-Mg alloys. These alloys, particularly AA5083, are used in the automotive and aeronautic industry due to their high superplastic properties. Their processing conditions for the QPF have been optimized but high COF is still a major concern [11, 13]. The interest here lies in the possible use of an alternate lubricant for this process and a comparison of this lubricant with others that are currently used.

1.3 Organization of Thesis

This thesis is arranged into six different chapters, each of which is briefly described below.

Chapter 1 introduces the thesis, giving background information into the research and the research objectives. It focuses on the aluminum-magnesium alloys, its uses in today's market as well as some processing routes used.

Chapter 2 is a literature survey relating to the thesis. It contains information on previous research work that has been done so far. It is sectioned into two parts, the first of which focuses on the disturbed layer, a surface defect occurring in aluminum alloys during thermo-mechanical processing. The second section covers the effect of hot forming on the surface of aluminum alloys. It focuses mainly on the effect that high COF and adhesion have on surface defects and the work done so far in mitigating these by the use of solid lubrication.

Chapter 3 delves into the experimental procedures undertaken. This includes the experimental setup devised for this research, the conditions under which they were carried out, the parameters that were monitored, and the materials that were used. It is divided into two parts, the first handling the simulations for hot rolling, and the second, the simulations for hot forming. It describes the simulators designed for the purpose of the research as well as the analytical tools used to examine the surface defects on the specimen surfaces.

Chapter 4 introduces the results gathered, from SEM, FIB, EDS, and GDOES examination of the surface features observed. This chapter is divided into two sections,

one handling the results for the hot rolling simulations, one for the hot forming experiments.

Chapter 5 discusses the results obtained, first pertaining to the effect the monitored parameters have on the formation and evolution of the disturbed layer during hot rolling, as well as the mechanisms involved in its formation. It then moves on to the performance of the different solid lubricants displayed during the hot forming simulations with particular attention to the material transfer that occurred during the experiments.

Chapter 6 is a summary chapter of the entire thesis. It presents a summary of the results obtained from the research and the discussions made.

CHAPTER II

REVIEW OF LITERATURE

2.1 Introduction to the Review

As stated in the Introduction, typical aluminum processing methods involve the hot rolling of the ingot into sheet or foil products, which are then hot formed to the desired final shape. While some final products may not require hot forming, both processing procedures have the tendency to introduce undesirable surface defects unto the aluminum sheet. Aluminum alloys have a high tendency to adhere to tool steel, which is usually the material that the die is made of. Also as stated earlier, elevated temperature processes are plagued by high COF which add to the occurrence of surface defects. We shall fist look into the occurrence of surface defects during the hot rolling process and then proceed to friction and adhesion during the hot forming process.

2.2 The Effect of Hot Rolling on Al-Mg Surfaces

The process of hot rolling has been observed to alter the composition of the surface and subsurface regions of aluminum alloys. This microstructure evolution of the sheet during hot rolling has been observed to depend on the strain, strain rate, and temperature of the sheet metal with the surface receiving a different thermo-mechanical treatment from the bulk of the material [17, 18]. This affects such properties of the surface of the alloy as the optical appearance, adhesion, formability, corrosion resistance, and weldability of the metal as these are determined by the composition of the non-heat treatable alloys [19, 20, 21]. The high compressive stresses, along with the high temperatures experienced by the alloy during hot rolling, change its composition and

cause the formation of a deformed or altered surface layer on the alloy called the disturbed layer.

2.2.1 The Disturbed Layer

The disturbed layer was first observed by Leth-Oslsen et al [21] while researching filiform corrosion (FFC), a thread-like form of corrosion that occurs under painted and plated surfaces of especially aluminum alloys [21, 22, 23]. At the time they believed the susceptibility of aluminum alloys to this corrosion to be related to the disturbed layer, stating that its presence made the surface more prone to corrosion attacks than the underlying bulk alloy [21, 24]. Its formation has been attributed to the much higher strains experienced by the surface of the alloy as compared with that of the bulk, resulting in the difference in microstructural characteristics between them [18]. The high strains are due to the high shear deformation processes that the surface undergoes such as sliding and grinding [25]. Research showed that the region is more electrochemically reactive than the bulk region, thus reducing the metal's resistance to filiform corrosion [26, 27 28]. Originally referred to as the Beilby layer and thought to be amorphous, this region is now referred to as: the tribolayer, the white layer, the flow zone, the near-surface layer, and the deformed layer [25]. It has been observed on aluminum alloys in the 1XXX, 3XXX, 5XXX, 6XXX and 8XXX series and its formation noted to depend on the chemistry of the alloy and its thermal treatment [29]

The disturbed layer has been discovered to be made up of a surface and subsurface layer [21]. The surface layer is comprised of continuous metal oxides. The oxides include MgO, γ-Al_2O_3, $MgAl_2O_4$ and amorphous aluminum oxide. The subsurface

layer has a makeup of a refined grain structure (small grained metal) aligned in the rolling direction with rolled-in oxide particles and a fine distribution of intermetallic phases and dispersoids which are responsible for pinning the grain boundaries [19, 21, 28, 30, 31] (see Figure 2). The pinning of the grain boundaries prevents recrystallization of this layer on further heat treatments [23]. Carbon has also been observed from the lubricant which is also rolled in, either with the oxide or on its own [31]. The layers are non-uniform in thickness and composition, with cracks and voids observed [20]. The rolled-in layers of lubricant and oxides are non-continuous but distributed over the metal surface.

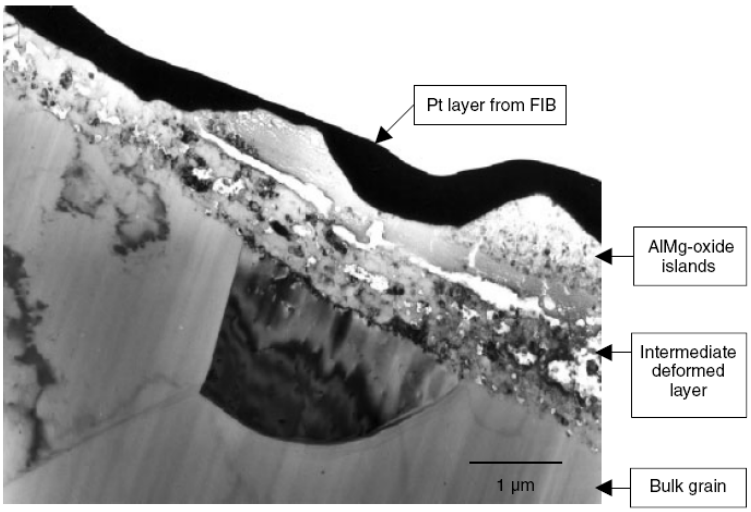

Figure 2 Bright-field TEM analysis of the near-surface of a cross-section of hot rolled and annealed AlMg0.5 [30]

2.2.2 The Formation of the Disturbed Layer

The formation of these layers is dependent on the tribological conditions at the tool and metal surface during rolling. The disturbed layer is produced due to the high shear experienced by asperity contacts of the roll tool and the metal piece under lubricated conditions [19, 32]. Therefore it is noted that friction conditions between the two surfaces play an important role in the formation, and therefore the state of lubrication, position of the neutral point, roughness of the rolls, and roll speed are important parameters to take note of.

The surface deformation during hot rolling was first schematically represented (Figure 3) by Fishkis and Lin by using TEM to take the plane and cross sectional view of an Al-Mg alloy (the alloy composition was not specified) [19, 21]. They discovered that the subsurface layer possessed voids and cracks and proposed that the formation of holes was due to the lower ductility of the surface layer and shear stress. Proposing that the lower ductility at the surface was due to the following [19]:

(i) The aluminum and magnesium oxides that covered the surface which made it brittle

(ii) Surface cooling which leads to the surface compound having lower ductility than the bulk region.

They thus proposed that the subsurface layer was formed in the following three-step process which occurred during rolling [19]:

(i) Holes are formed by ploughing, adhesive wear, delamination wear, or transverse surface cracking in the process of rolling

(ii) The holes are filled with the wear debris which consisted of metal and oxide fines mixed with lubricants

(iii) The holes are covered over with thin metal layers during the continuing rolling process which leads to a *shingled* surface appearance.

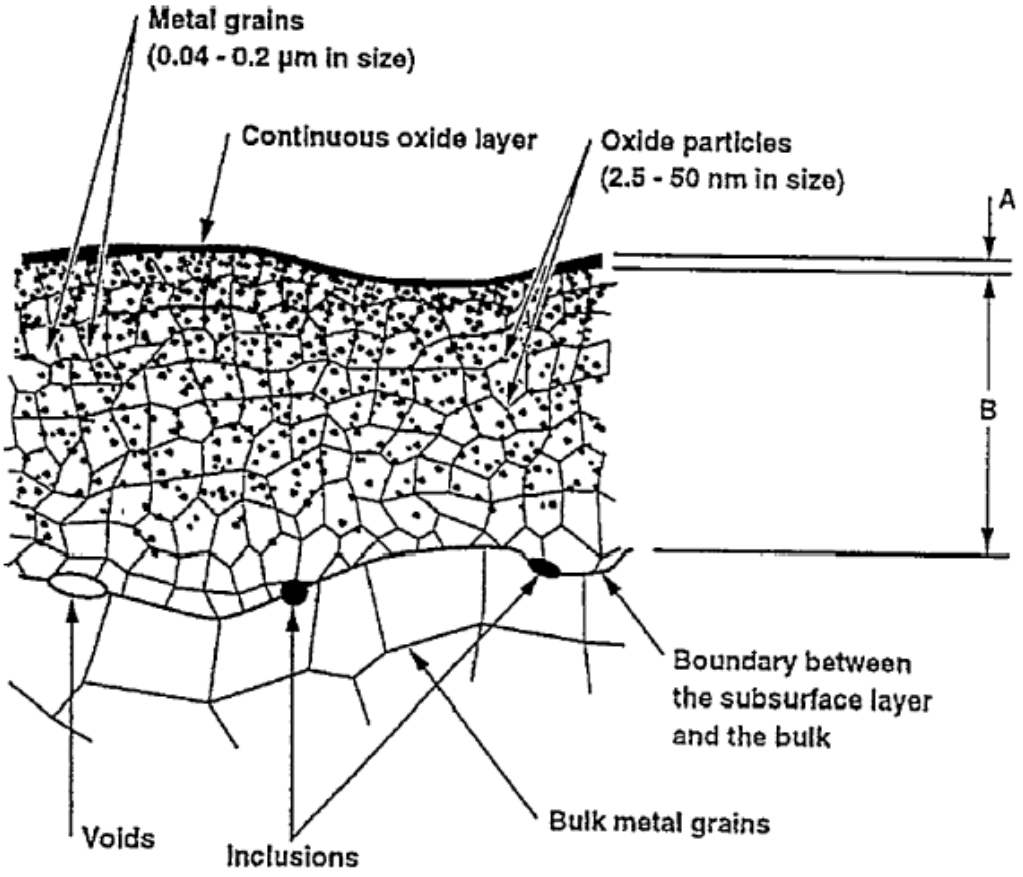

Figure 3 Schematic representation of subsurface layer containing microcrystalline oxides mixed with small grained material and covered with a continuous surface oxide. A represents the surface oxide layer and B represents the subsurface ultrafine grained layer [21]

2.2.3 Mechanisms of Disturbed Layer Formation

Early research by Fishkis and Lin [19] proposed that during hot rolling, metal transfer occurs from the surface of the workpiece to the roll surface. The transferred metal is oxidized and can be transferred back to the metal surface from the tool. This produces surface disturbances which influence the properties of the surface. Thus the altered surface and subsurface disturbed layer that forms affects the formability, weldability and the effects of finishing operations on the surface appearance [19].

Frolish et al.[22], from their simulation of industrial rolling proposed that the mechanism causing the disturbed layer and the mixing in of the oxide particles was from slip occurring at the interface of the roll and workpiece and the action of the roll surface asperities on the workpiece surface.

Scamans [33] later suggested the severe surface shear experienced during hot rolling as the reason the surface of the alloy was ploughed and re-welded back together. This, he noted, caused the integration of the oxide and explained the sharp transition observed from the disturbed surface to the bulk-grained microstructure beneath it. On subsequent hot rolling, the surface is consolidated and the micro-grained layer developed and thinned. He observed that most thermo-mechanical treatments were able to cause the development of a disturbed layer after his having observed its ultra-fine grain size structure after processes such as mechanical grinding.

2.2.4 The Ultra-fine Grained Structure of the Sub-Surface Layer

The refined grain size of the subsurface layers was proposed to be stabilized through Zener pinning of the grain boundaries by small oxide particles [19, 21]. Zener

proposed [34] that grain growth could be inhibited by very small particles, presenting a restraining force which balanced the driving pressure of grain growth [19]. The oxides thus prevent grain growth and prevent the complete recrystallization of the surface layer during subsequent heating [31].

Frolish et al.[21] noted that the diffusion of magnesium to the surface of the alloy, which was observed to occur rapidly and increase in intensity with time, was in part responsible for the formation of the subsurface layers as its oxides were observed to provide the Zener pinning of the grain boundaries thus producing the fine grain features . They suggested that the depth of the magnesium content correlated with the thickness of the subsurface layer, although noting that the subsurface layer structure depended on the alloy composition and the processing conditions [21].

Xia, [34] in his experiments observed precipitates also involved in the Zener pinning of grains which prevented subgrain growth during the hot rolling of aluminum alloys. Premendra et al. [23], also observed broken intermetallics on the surface of the metal at grain boundaries, which he suggested were involved in pinning grains.

Work by Plassart et al. on cold-rolled aluminum alloys also showed a disturbed layer with recrystallized refined grain structure [35]. Magnesium precipitation to the surface layer during rolling has been associated with the increased corrosion susceptibility [31].

2.2.5 The Effect of Rolling Passes on the Surface Layer

Fishkis et al. were one of the first to observe that each pass during hot rolling contributes to the extent of deformation, although the experimental conditions were not

stated [19, 32]. On the Al 3XXX series they worked with, the oxide formation at the surface varied with each pass, and the surface was observed to became smoother [19]. They were able to map out the oxides formed at each pass of the roll during hot rolling with the use of a controlled surface layer removal technique combined with electron imaging and X-ray maps obtained from electron probe micro-analysis (EPMA) [19, 21, 31] .

During the first and second pass amorphous Al_2O_3, MgO, γ-Al_2O_3 and $MgAl_2O_4$ are present in the surface layer. Carbon, as stated earlier, has also been observed, the source of which is the rolled-in lubricant. The lubricant has been observed to undergo entrapment on either being rolled-in or slipping into surface defects such as holes and being covered on subsequent rolling passes [23].

The oxide film is noticed to be continuous by the second pass; during the fourth pass, the ratio of metallic aluminum to oxide concentrations is higher than observed in the first and second pass. The oxides by the fourth pass present in the surface region are MgO, which is the dominant oxide, and γ-Al_2O_3, which is now only found in specific areas [19, 21].

The fifth pass brings about a more uniform surface microstructure, with MgO and γ-Al_2O_3 still present but in smaller amounts. The surface microstructure becomes *more metal like* by the sixth pass, with the dominant surface element being aluminum with MgO found in some areas. Frolish et al [21] discovered that during heating, Mg constantly precipitates to the surface of the aluminum alloys that have it as an addition. The observed that the concentration of Mg increased at the surface of the alloy with

longer heating periods.

The thickness of the surface region is noted to decrease with each succeeding pass or stage of rolling from 8-5μm to about 2-1.5μm by the 6th pass [19, 21].

2.2.6 Filiform Corrosion and the Disturbed Layer

Filiform corrosion is a case of *concentration-cell* corrosion that occurs on certain metals coated with organic films by the formation of thread-like filaments containing corrosion products [29, 36, 37, 38]. It is described as a cosmetic form of localized corrosion, also known as *underfilm corrosion* and *worm-track corrosion* which initiates at surface defects in the protective films [37, 39, 40, 41]. It was first referred to as filamentary corrosion and has been observed to attack steel, aluminum, magnesium, and zinc [36, 37, 40, 41, 43, 44].

Filiform attack is characterized by narrow fine filaments propagating in random directions from one or more points with propagation in any one direction reaching relatively long lengths [29, 37, 45]. Although it has been described to produce aesthetic damage affecting the mechanical integrity of the metal directly, it degrades the protective barrier properties of the coatings, reducing its the resistance of the substrate to damaging forms of corrosion like crevice and pitting corrosion as well as stress cracking corrosion [29, 37, 44]. The filaments have been observed to grow in the rolling direction of the substrate material [29, 37].

Filiform attack in aluminum is very severe particularly in warm coastal, tropical and industrial regions [29]. It is able to propagate at relative humidities as low as 30% in the presence of HCL vapour. This is thought to be due to the presence of hygroscopic

corrosion products formed in the filament head [29, 46]. It comprises a filament head containing alumina gel with the possible evolution of hydrogen gas bubbles in a cathodic reaction if the head is very acidic [29], and a tail that appears white with corrosion products being hydroxides and oxides (see Figure 4) [29, 46]. When the filaments dry out, they take on a clear appearance due to internal reflection of light [29]. These filaments can remain dormant during these conditions and then reinitiate propagation once humidity increases [46].

In aluminum alloys, the disturbed layer enhances the occurrence of filiform by increasing the number density of filiform tracks and kinetics of track propagation [29]. It affects filament orientation growth as it directs the filament growth in the direction of the mechanical extrusion [29]. The anodic activity of the disturbed layer has been attributed to the fine grain size and magnesium intermetallic particles which are dispersed over the surface of the metal [29, 47]. Rolling and grinding are known to induce the preferential precipitation of dispersiods in the disturbed layer [47]. The density of these dispersiods in the near surface region is related to susceptibility to filiform corrosion [47, 48].They are thought to set off its electrochemical activity of the metal by forming microgalvanic couples with the surrounding matrix.

Intermetallics are of importance to where filiform is initiated as they increase the probability of initiation [46]. Also in relation to their electrochemical characteristics to the matrix, they can act either as cathodes or anodes and thus influence the rate of electrochemical process by promoting the dissolution of aluminum [46, 48]. When located at the front head of the filament they act as cathodes for hydrogen reduction in as

much as aluminum oxides are not present (see Figure 5) [48]. They increase the cathodic surface area as well as the corrosion current density [48]. In the presence of a thin electrolyte film formed due to humidity and salt concentration, chloride ions will migrate to anodic areas around the intermetallics [46]. Aluminum dissolves around the intermetallics until either it is detached or a new one is reached [48]. As the filament grows, the anodic section in the head eventually becomes cathodic; the intermetallic now acts as a cathodic area, reducing oxygen in the cathodic portion of the head [48]. With more intermetallics on the surface, the anodic or cathodic surface becomes larger [48].

Scamans related the corrosion susceptibility to the manganese content with manganese-rich dispersiods being preferentially predicated in the disturbed surface relative to the less deformed bulk area during annealing. While he agreed that the susceptibility of this surface is directly related to the density of precipitated dispersiods he noted that this precipitation depends on the manganese solid solution levels along with the temperature and annealing time [33].

Examining the Al-Mg alloys in the AA5XXX series, he notes that their disturbed layers do not differ significantly from the underlying bulk in terms of electrochemical properties or corrosion behaviour. These alloys do not display the high filiform corrosion susceptibility as Al-Mn alloys [33]. He states that particle break-up is less significant to dispersoid precipitation in inducing the susceptibility to filiform [49].

2.2.7 The Optical Appearance of the Disturbed Layer

The disturbed layer affects the optical appearance of the aluminum alloy by reducing its total reflectance. This is calculated as the amount of incident light reflected

by the surface of the alloy. Premendra et al. observed that the surface oxide patches in the surface area of the disturbed layer where rich in carbon, derived from the lubricant. They proposed that this was responsible for the reduction of the total reflectance of the surface (now between 50-60%) in comparison to that of the bulk alloy directly below the disturbed layer (measured at between 80-90%) [31]. Rolling had been noted to reduce the total reflectance by < 10% on its own [30]. They proposed that the rolled-in oxides did not just prevent recrystallization from occurring by pinning the grain boundaries of the surface layer, but were also responsible for the low total reflectance value observed at the near surface (see Figure 6). They also noted that carbon on its own reduced the total reflectance as well as the adhesion properties of the material. They proposed that with total reflectance measurements, one could approximately calculate the average thickness of the disturbed layer with the use of the total reflectance curve they had plotted [31].

2.2.8 The Influence of Surface Treatments on the Disturbed Layer

It has been observed that cold rolling after hot rolling reduces the thickness of the disturbed layer. It has been proposed that this action breaks up and smears out the rolled-in oxides into the near-surface region of the rolled alloy [30, 33, 50].

Alkaline etching was observed to attack the aluminum matrix while preserving the rolled-in oxide rich subsurface regions. On sufficient etching, these drop out of the substrate with the small, thin oxides being removed faster than the larger, thicker ones [28]. CrO_3/H_3PO_4 treatments worked better, dissolving the oxide rich regions first while leaving the aluminum matrix un-attacked, and removing the subsurface layer with much less weight loss when compared with alkaline etching [28].

Scamans has suggested the use of thermal treatments prior to hot rolling; these would promote the precipitation of manganese from the alloy, which he suggested is responsible for promoting the precipitation of dispersiods to the surface region, thus reducing the surface activation of the alloy during further annealing treatments [33]. This method does not aid in the removal of the oxide rich surface layer which is responsible for reducing the total reflectance of the surface of the alloy. As noted in the Introduction, the high surface finishing is one of the properties that make non-heat treatable aluminum alloys in high demand. Therefore further treatments are still required to remove the oxide layers and thus increase the adhesion and optical reflectance properties of the alloys.

The electrochemically active layers of the disturbed region need to be removed for aluminum alloys to effectively resist filiform corrosion; therefore effective etch cleaning operations, conversion pre-treatments, or anodizing treatments are preformed on aluminum alloys [33, 49]. These treatments are usually performed after extensive cold rolling facilitates cleaning by reducing the thickness of the disturbed layer that is, the amount of metal which needs to be removed [33. 49]. During acid and alkaline etch treatments; caution must be taken to avoid copper accumulation on the surface which is quite common in aluminum alloys during these treatments. Desmutting treatments (an anodizing process that entails rinsing the alloy in an acid solution) are performed to remove the copper from these surfaces [49, 51]. Conversion treatments are performed to increase the adhesion properties of the alloy; they are used to enhance the natural oxide layer of the aluminum alloy [49]. Conversion treatments like anodizing, hydrothermal treatments in water or steam, coil line treatments, and fluorotitanic acid-based

pretreatments have been commonly used, each with their advantages and disadvantages [49]. Treatments with silanes, which are most effective when applied as monolayers, have been looked into in combination with other anodizing treatments to enhance the adhesion properties [49].

2.3 The Effect of Hot Forming on Al-Mg Surfaces

In sheet metal working, previous processing history is important as surface defects that might have been incurred during these processes can quite easily be carried on to the next processes. During hot forming, the aluminum alloy is heated until it is relatively soft so that it can intimately conform to the tool surface; the surface quality of the tool has an important influence on the surface quality of the final product [16].The surface composition and topography of the tool are very important; they are constantly being heated and, like the work-piece, have metal oxides constantly being formed on their surfaces. The oxides characteristics constantly change due to their interaction with the workpiece. They also change the die surface characteristics so that forming with a previously unused die differs from forming with an already used die. The oxide layer formed on the die is not uniform in thickness due to constant die surface oxidation and oxide loss to wear. Oxidation degrades the die surface with die coating being unable to completely mitigate such effects. Research has gone into self lubricating oxide coating for the die tool, the oxides can act as a parting agent during hot forming, unlike the oxides of the disturbed layer which are not known to aid the thermo-mechanical process. These oxides form on the die rather than the workpiece [13].

The tribological conditions that prevail between the tool die and the work-piece

are of great interest as they influence productivity efficiency, the quality of the final surface finishing, as well as sheet formability [13, 52, 53]. The tribological factors and their interactions that occur at tool die and workpiece surfaces as the work piece slides across the surface of the tool are very complex, some of which are responsible for the surface defects that may occur on the work-piece [12, 54]. These mechanisms occur simultaneously and include friction, material transfer, wear, and deformation [12]. The wear mechanisms of interest that have been identified include adhesion, mechanical interaction of surface asperities, abrasion, deformation and/or fracture of the surface oxides layer which forms during high temperature operations, and tribo-chemical wear [12, 52, 53]

2.3.1 Friction in Hot Forming

During hot forming, friction occurs due to the sliding of the workpiece against the die. It influences the material flow as well as the stress and strain distribution that occur in the workpiece [52]. Friction is vital in the control of the workpiece deformation during the forming process [55]. The workpiece undergoes bulk plastic deformation which induces local surface deformations [55]. Friction behaviour is quite complex, comprising interacting variables that change constantly during the forming processes. These variables include deformation magnitude, forming speed, sheet and tool material, surface roughness, and tool geometry, the most significant of these being contact pressure and sliding velocity [56, 57].

Friction increase is observed with increasing temperature and strain rate, factors on which the SPF ($500^{o}C/10^{-4}s^{-1}$) and QPF ($450^{o}C/10^{-3}s^{-1}$) operations are quite dependent.

The evolution or development of the microstructure of the workpiece during forming is dependent on the strain rate applied, which in turn depends on the friction at the interface of the tool and the workpiece. Friction also influences the state of stress at the interface between the tool and the workpiece. [58].

The level of friction is very important as it can be neither too high nor too low in order to attain the required surface quality [13, 52]. Low friction has been observed to lead to slippery panels, which lead to handling problems later. It also results in increasing the possibility of necking occurring on areas of a workpiece that have sharp radii [13, 52]. The main influence of high friction has been observed to be its detrimental effect to surface quality of the aluminum sheet workpiece, in the wear of the die and tool, and the process energy consumption [9, 59]. It is able to hinder the movement of the workpiece over the die by increasing the constraint to plastic flow of the material while reducing the material flow and causing failure within the workpiece [13, 58]. The surface quality is thus reduced by high friction-induced scratches on the final product [52].

Friction is related to adhesion which is another mechanism detrimental to hot forming. It has been stated in the literature to be controlled by adhesive forces and deformation forces [52]. High friction has being observed to increase the rate of material transfer; adhesion is also noted to be a mechanism of high friction in superplastic forming [8, 14].

2.3.2 Adhesion in Hot Forming

Adhesion, the material transfer of the softer workpiece material to the harder tool, causes critical issues during forming operations. If the material is *welded* to the tool

surface, it leads to the material build-up on the surface and consequent scratching of the workpiece during forming [52, 60]. This kind of surface damage during sliding contact due to material adhesion is often referred to as galling, scuffing, or scoring [52]. It is a form of severe wear that reduces the conformity of its contact, can lead to seizure of the surfaces, and causes gross failure of the forming system.

The workpiece, under the influence of adhesion, experiences mechanisms of hardening which include work hardening, grain refinement, and oxide particle inclusion [60]. During high temperature sheet metal processing, oxides are easily formed on the surfaces of the tool as on well as the workpiece. High contact pressure experienced by the surface of the workpiece can break the oxides of the workpiece exposing fresh surfaces, and these oxide particles may be intermixed into the material adhered on the tool surface [55, 61].

Adhesion and material transfer tends to be dependent on such factors as temperature, tool roughness and surface composition, contact pressure, and sliding velocity. [16, 52, 60, 61, 62]. On increasing most of these factors, the tendency of adhesion and material transfer increases. Hanson et al. [62] have reported that there is no critical surface roughness for the occurrence of adhesive transfer and that the process occurs instantaneously. As stated earlier, high friction is often associated with adhesion, it has been recorded as increasing the rate of material transfer, and an increase in friction is used as an indicator of galling [8, 61]. Material transfer was observed by Hanson et al. [60] to give low friction when it formed thin layers on the tool surface, but on build up, was associated with high friction.

The surface of aluminum is known to be naturally covered with a thin layer of oxide, aluminum oxide, and in the case of Al-Mg alloys, magnesium oxide as well [63, 64]. Aluminum however is observed to adhere to all surfaces even at low loads when the softer metal beneath the oxide is exposed due to oxide breakup [16, 60, 64]. The thickness of the transfer layer depends on the size of the oxide fragments, which must be small to induce a thin film [60]. The material transfer and adhesion experienced is not easily removed by normal industrial cleaning systems [13]. Adhesion of Al-Mg alloys has also been observed to be less for alloys with higher magnesium content in contact with steel surfaces [63].

In light of the surface finishing required, the hot forming process would require a moderate coefficient of friction, minimal adhesion, and material transfer, highlighting the need for lubrication during these processes.

2.3.3 Lubrication in Hot Forming

Lubrication is introduced into forming processes to control friction, resist the onset of metal adhesion, and facilitate metal flow [65]. It provides complete separation of the workpiece from the tool by either a thick film of fluid; various thinner fluid films; molecular layers which are absorbed on the metal surfaces; surface films formed through a chemical reaction; or low shear solids [66]. The relative motion of the bodies in these cases thus occurs through the shearing of the film [66].

The lubrication of the aluminum alloy surface is complex as its composition and properties at the surface differ from that of the bulk material, reflecting its processing history as indicated earlier. The composition and thickness of the oxide layer aluminum

readily forms at high temperatures depend on the processing history. The oxide formed depends on the aluminum alloy being processed and the rate of diffusion of the alloying elements. Amorphous Al_2O_3 has been noted as a major oxide formed, α-Al_2O_3 and γ-Al_2O_3 have also been observed and MgO formed in alloys containing Mg additions. Unlike other metals, its oxide layer does not offer any form of friction reduction or protection to the aluminum workpiece, as it is brittle and allows adhesion to occur once it is breached, exposing the underlying metal [67]. Oxides that offer protection to the substrate are usually ductile at the interface or, if they are not, break up into a powder form [67]. These oxides should also have a critical thickness of 0.01μm in order to act as a lubricant [66].

Lubricants for aluminum metal working are selected for their compatibility with the alloys and their suitability for the metal working process taking place [65]. This implies that whereas certain groups of lubricants work well for one high temperature metal working process, they are not necessarily applicable in other metal working processes. Lubrication of aluminum metal working is best described in connection white the process the lubrication fits best. Lubricants used with high temperature forming operations need to be able to withstand high temperatures and pressures.

In hot forming, the lubricant must facilitate the smooth movement of the aluminum workpiece over the die features. It must complement the die design and be able to be applied in very thin evenly distributed layers needing to adhere to the aluminum surface. The lubricant must be able to function without allowing metal transfer or build-up of aluminum at the die, yet avoiding the lubricant accumulating on the dies [16].

Solid lubricants are preferred over oil lubricants due to their high deep drawing performance, notably in the use of complex shaped body panels [67, 68]. They improve the stretch flangeability and drawing formability of aluminum alloy sheets, as well as increase the *homogenous sheet thickness distribution* that can be obtained during this process [68, 69]. They are chosen based on temperature as there are few with melting behaviours that are suitable for aluminum metal working. They must possess lower shear strength than the workpiece, have good film forming ability, ductility, good adhesion to the substrate and film continuity [52, 65].

In hot forming, lamellar solids have commonly been used for lubrication. They are able to act in this function because of their easily sheared layer structure and their ability to slide over one another, which comprise their lubricating behaviour. [16]. Lamellar solids such as boron nitride, graphite, and their variations have been used to control the high friction and resist against the onset of metal adhesion during hot forming [16, 70]. The inclusion of molybdenum disulfide has also been practiced to reduce friction during these high temperature processes [16]. Boron nitride has a hexagonal layered crystal lattice structure similar to graphite, and like graphite, its lattice layers can be easily shifted. It has high thermal stability and oxidation resistance, up to temperatures of 1800^{o}C [71]. It offers good lubrication and has been observed to be limited not only by its requirement of an *applicable thickness*, it is influenced by the thickness of the coating, but also by its difficulty in bonding to the substrates [72, 73]. Graphite on the other hand tends to flake after forming and is difficult to remove from the formed part [13]. Molybdenum disulfide lubricating properties come from the low shear it experiences at

its basal planes due to the van der Waals forces bonding its covalently bonded layers. It is stable in air temperatures up to 350^{o}C at which point it begins to oxidize, and like graphite, is difficult to remove from formed surfaces [13]. The major issue with industrial lubricants however has been the price issue; when the application technique is factored in, they are considered relatively expensive as it is difficult to apply a uniform coating [13].

2.3.4 Research into Alternate Lubricants for Hot Forming

Much research has gone into the behaviour of Al-Mg alloys at high temperature and into finding alternate solid lubricants that can be used in their hot forming. Riahi et al. looked into the use of non-hydrogenated DLC and observed that they displayed comparable COF results with those of uncoated steel at 420^{o}C [74]. In their work, vitreous and devitrifying enamels at a temperature of 470^{o}C were observed to be effective lubricants but were found to contain lead [75]. Morales [76] has shown that the final surface characteristics of formed aluminum alloy depend on the lubricant on the die. Her work with several dry lubricants showed the possible use of Ni-P-PTFE coatings, but it did not fully mitigate adhesion. Krajewski et al. [13] in their review paper on QPF issues, mentioned that work was being done with lead-tin sheets as lubricants, noting that its high volume application was not viable. They mention the requirements for a good lubricant being used in hot forming processes, which include the ability to be applied uniformly, lubricant not accumulating on the tool surface and its easy removal after the forming process [13]. The present research looks into the use of tungsten disulphide as a possible solid lubricant in hot forming.

2.3.5 Tungsten Disulphide (WS_2)

Tungsten disulphide (WS_2) has been used extensively in the aeronautical industry, NASA, medical fields, automotive industry, and the military. It is a lamellar solid with lubricating and structural properties similar to molybdenum disulphide (MoS_2) but offers better thermal stability and oxidation resistance. Its lubricating properties have been extensively looked into at room temperature by researchers [77, 78].

It has a hexagonal crystal structure composed of layered sheets stacked on one another. Each sheet is tri-layered so that each layer of tungsten atoms is sandwiched between two hexagonally packed sulphur layers (see Figure 7a) [79, 80]. The sheets make up a covalently bonded S– W–S sandwiched layer, so that each tungsten atom is covalently bonded to six sulphur neighbours with an elemental ratio of 25.86% (S) to 74.14% (W) [81]. These sandwiched layers (with bonds between the sulphur atoms shown in Figure 7b) are held together by weak van der Waals forces resulting in an interlamellar structure that is easily sheared [79, 82, 83].

The basal planes are subject to intercrystalline slip, that is, shearing easily occurs; the basal planes slide back and forth over one another and cause interlamellar mechanical weakness [79, 80, 84]. It is responsible for the low friction surface and high load carrying capabilities of WS_2 [79].

This structure is similar for most transition metal dichalcogenides, especially MoS_2. WS_2 has thus been deemed a direct replacement for MoS_2 because of their similar properties due to their crystal structures (MoS_2 and WS_2, like most metal dichalcogenides, have the same lamellar crystal structure) and mild differences in the

physical properties [79]. WS_2 is more thermally stable than MoS_2, more resistant to oxidation at elevated temperatures and provide an additional 100^oC to MoS_2 operating temperature [79, 80]. The friction behaviour of WS_2 has been observed to be stable up to a temperature of 500^oC in air, at which point oxidation begins to occur [77, 85]. One of the oxides formed, WO_3 is a soft oxide with low shear strength and provides low interfacial friction at high temperatures. It is slightly more protective than the oxide formed by MoS_2 at high temperature, MoO_3 [85]. WS_2 has a coefficient of friction of between 0.1 – 0.15 at ambient temperatures in air [78]. Its stability is such that industrial companies have stated its working temperature as between -188^oC – 650^oC at normal atmosphere and up to 1316^oC in a vacuum [86].

MoS_2 has been the more common lubricant due to its lower price, easier availability and stronger marketing when compared to WS_2. In the last few years, their prices have become comparable with coating companies paying more attention to WS_2 due to its high potential and superior properties [87]. Another reason MoS_2 is more commonly used is that it is occurs naturally while WS_2 is synthetic [79].

As a solid lubricant, WS_2 offers low friction coefficients due to (a) the development of a transfer film on the counterface to accommodate interfacial sliding, (b) reorientation of the basal plane parallel to the sliding direction in the wear track, and (c) the absence of contaminants such as oxygen, carbon, and water [80]. The basal layer is composed of a layer of sulphur atoms and is inert in this state [79]. The research of Isshiki et al. has shown that when an external stress is applied, successive glides of 1/3a<120> between the S-S layers occur easily (see Figure 8). On this plane, friction

occurs only against the van der Waals interaction and is thus very low [82]. Transfer films induced by wear are quite common with lamellar solids with their formation, in addition to the environmental stability, determining friction between moving parts [84].

Coefficients of friction measured have proven to be different under different environmental conditions, 0.03 - 0.05 being reported in dry nitrogen [80, 85, 88] whereas in humid air COF has been observed to jump up to 0.10 – 0.15 [80, 84, 88]. This change is due to the oxidation of WS_2 films in air (humid environments) producing WO_3 and SO_2 which results in an increase in the COF as WO_3 is not lubricious at room temperature, possesses a poor wear behaviour, and interferes with the formation of the WS_2 transfer layer [80, 88]. The oxidation occurs due to dangling or unsaturated bonds which lie at the edge of basal planes, (whereas WS_2 coated surfaces are inert, if a crack exists on the surface, more unsaturated bonds occur) these activated sites react with moisture and oxygen to form WO_3 [89, 80]. The wear behaviour is also affected by the environment with lower wear rates being observed in nitrogen environment compared to that of air [84].

The transfer films of WS_2 were observed in air and nitrogen, and it was observed that whereas those in air were patchy and powdery by nature, those in nitrogen were very thin plate-like crystallite with an ability to bend and cover the contours of the other surface [84, 88]. The transfer platelets have been observed to be very thin, less than 60 nm in size [84]. In light of this, WS_2 coatings have been advertised [87] industrially to have a standard coating thickness of 0.5μm and to take on the characteristics of the substrate.

WS_2 can be applied in a number of ways; industrially advertised application methods include: burnishing/impingement, spraying, tumbling and buffing with aerosol sprays being recently introduced. Spraying also referred to as spray blasting, involves sand blasting the substrate with alumina powder after it has been cleaned thoroughly for better WS_2 adhesion. After which, the substrate is cleaned again to remove any trace of the alumina dust.WS_2 powder is then sand blasted on the substrate at a high pressure of 120psi (0.8Mpa) with dry, cool pneumatic air till the substrate turns a silver grey. This application method can be carried out at ambient temperatures and does not require the use of a binder. Buffing and tumbling are both slow and laborious methods that depend on speed and friction for the effective bonding of WS_2 to the substrate. Power tools are usually advised for both application methods. With buffing the WS_2 powder is mixed with isopropyl alcohol creating a paste which is applied unto the substrate and the power tool, for example a buffering wheel. The paste is left to dry after which the substrate is buffed with the buffing wheel till it is silver grey in appearance. The tumbling application is mostly used for bullets and could require up to 5hrs for application. All these methods are based on WS_2 platelets being mechanically interlocked into the crevices of the substrate, in the case of spray blasting these are created by pre-sand blasting with aluminum oxide. It can also be mixed with other liquid lubricants such as oil, grease and paraffin, increasing the lubricating properties of the mixture and the high temperature and pressure resistance of the mixture [87, 88].

Other methods of producing WS_2 films include: pulsed laser deposition, atomic layer deposition, physical vapour deposition techniques such as sputter deposition, metal

organic chemical vapour deposition, vapour phase transport and sulphurization of sputtered tungsten films [90]. Scharf et al. have used atomic layer deposition to deposit WS_2 thin films using gas precursors WF_6 and $H2_S$ at a temperatures between 300^oC – 350^oC [80]. Prasad et al. has mainly worked with pulsed layer deposition at room temperatures [78, 84]. The method of deposition is of interest as it is known to affect the behaviour of WS_2 films deposited, for example, COF reported for pulsed laser deposited and sputtered coatings both in dry nitrogen are 0.03 - 0.05 and 0.02 - 0.06 respectively [80, 85]. This could be attributed to the different crystal structure of the deposited film. Pulse laser deposition of WS_2 performed at room temperature was observed to be amorphous in nature, possessing sufficient short-range order [78, 79]. The structure of atomic layer deposition of WS_2 film, which is similar to PVD WS_2 films, was observed to be more crystalline in nature [91]. Ion beam induced formation of WS_2 films were observed also be crystalline in nature, while DC magnetron sputtered films were amorphous but on ion-irradiation they were observed to have an induced crystalline structure [77]. Prasad et al., observed that the WS_2 film properties, such as, the crystallinity, stoichiometry, morphology and dopand concentration were adjustable by varying the deposition parameters [79]. Amorphous films deposited at room temperature with pulsed laser deposition, could be crystallize by mechanical actions such as rubbing at room temperature, thermal and laser anneals could also induce the same effect. The mechanical action like rubbing inducing crystallinity in these coatings has been termed; *stress induced crystallization*, and is due to the increase in energy input [78, 79]. It can be said that WS_2 films deposited at room temperatures are amorphous while those deposited

at higher temperatures are more crystalline in nature; that is the crystalline structure of the coating depends on the deposition temperature. Cohen et al., have also observed that randomly oriented WS_2 platelets are more prone to corrosion than the highly oriented WS_2 film [92].

2.4 Short Summary of Literature Survey

Much of the research into the disturbed layer has been carried out to understand the composition, the effect these layers have on the alloy properties and on treatments to eliminate these layers after formation. It also has primarily been done on as-received hot rolled samples, with few researchers stating the full conditions under which the deformed layer was observed. It is understood that the friction between the rolls and the work piece is an important parameter [9, 21]. The friction between the rolls and the workpiece causes the surface layer to be subjected to higher levels of strain than the underlying bulk material [18]. It is difficult to measure the variation in friction coefficient during rolling, and parameters such as roll speed are known to influence it [19]. However, research on the parameters which affect or induce the formation of these layers has been lacking and is needed. While a lot of time and money is put into treatments to remove these layers after they are formed, controlling processing parameters so as to control, or better still eliminate, their formation would be a better solution. For a proper study, the laboratory replication of the conditions under which these layers are formed in the industry would be quite useful [21]. This research is aimed at looking into the effect of forward slip in hot rolling on the formation of the disturbed layer by the use of a laboratory simulation of the hot rolling process.

Lubrication is quite essential for the surface finish during hot forming. A lot of research has gone into finding lubricants that offer low friction, good adhesion, and no accumulation on the die surface which mitigates aluminum adhesion. Tungsten disulfide has been used as a solid lubricant in many industries, being advertised to have extremely low coefficient of friction at room temperature. Also being advertised as a high temperature lubricant, it has gained popularity as a solid lubricant in various industries [84, 87]. Although it has been used in the automobile industry to reduce friction in braking systems, until now it has not been tested as a possible hot forming lubricant under the conditions of high temperature stretching. The second part of this work focused on the possible use of tungsten disulfide as a solid lubricant for hot forming. This involved measuring the COF of various lubricants under forming conditions as a base comparison at an elevated temperature of 723 K. The purpose of the test was to simulate hot forming while observing the stability of these lubricants and their effectiveness at mitigating adhesion.

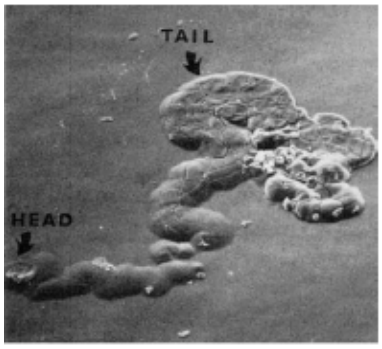

Figure 4 Advancing head and cracked tail section of a filiform cell [29]

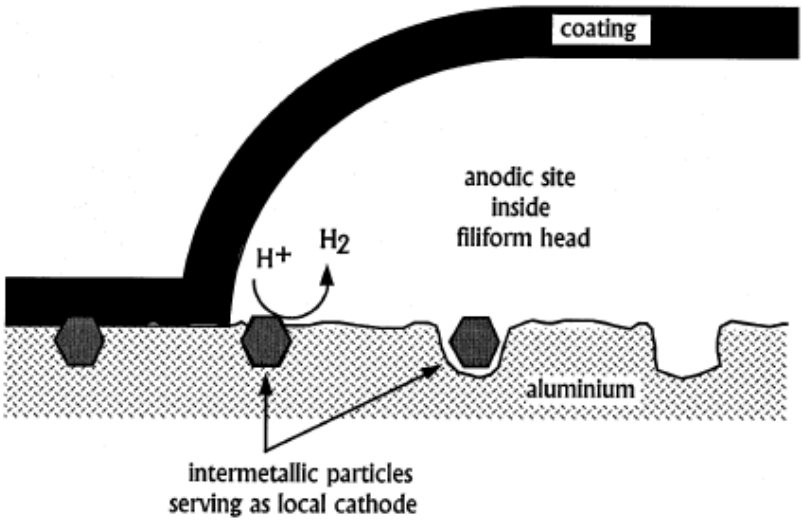

Figure 5 Effects of intermetallic particles on the propagation behaviour of filiform filaments [49]

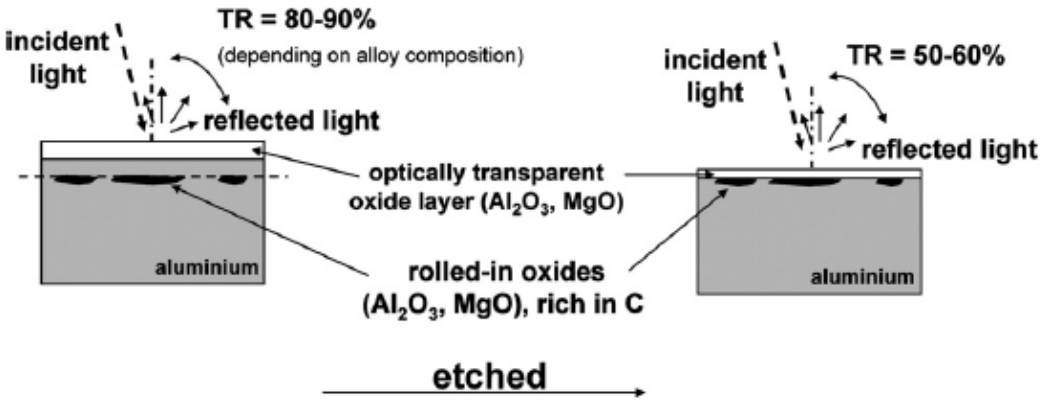

Figure 6 Schematic of the influence of the rolled-in oxides on the Total Reflectance (TR) [31]

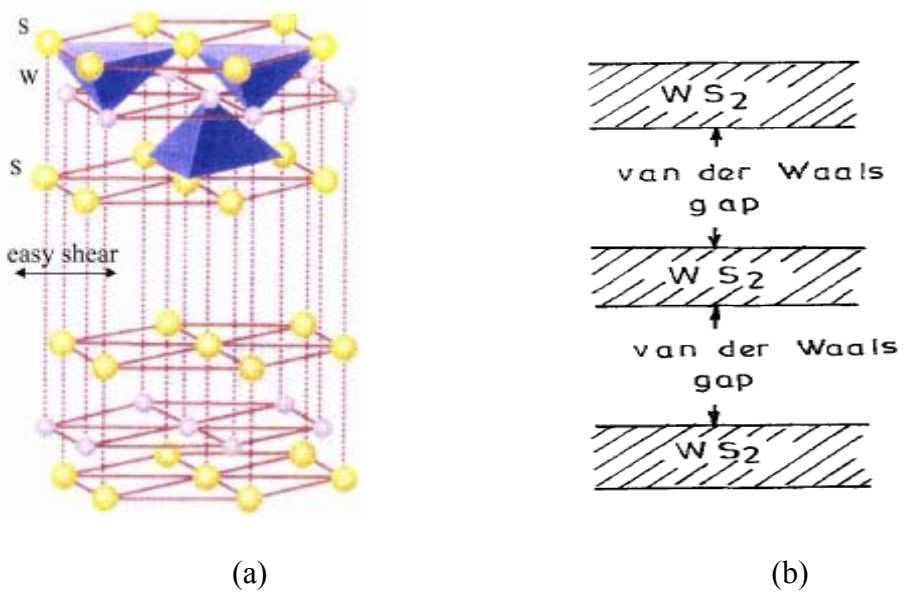

(a) (b)

Figure 7 (a) Crystal structure of hexagonal 2H –WS_2 with easy shear direction [82], (b) structure showing stacking of layers [84]

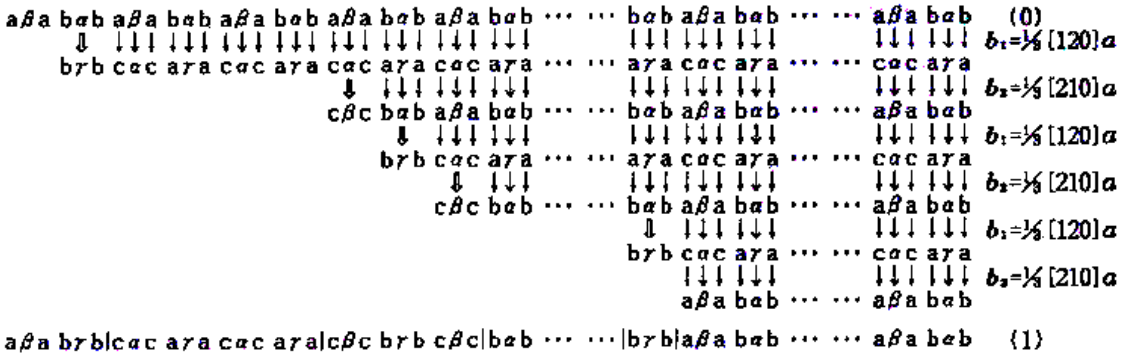

Figure 8 Formation mechanism from an original perfect hexagonal WS_2 crystal (0) to the structure (1) in the lowest part of the crystal: ↓, atoms shifts by slipping between S-S layers; ‖ local shifts of W atoms. b_1 and b_2 are glide vectors, which are partial in the complete Burger vector b=a[110].

CHAPTER III

DESIGN AND METHODOLOGY

3.1 Hot Rolling Experiment

3.1.1 The Workpiece

The alloy investigated was an Al-Mn alloy, AA3104, and its composition is given in Table 1. The material, in the form of small billets, was provided by Novelis Global Technology Centre, and samples were subsequently machined to the required dimensions of 10.5 x 30 x 96 mm. The 10.5 x 96 mm edge face of the samples was polished using 1μm diamond paste and then cleaned ultrasonically in acetone for five (5) minutes to remove surface contaminants.

3.1.2 The Roller

The roller used for the experiments was made of a steel alloy AISI 52100 with its composition given in Table 2. An optical profile of the roll surface was taken to show a surface roughness of Ra = 0.2 μm (shown in Figure 9). It had a diameter of 21 mm and was less than 1/10 the size of rolls used in the industry.

3.1.3 Laboratory Simulation

The simulation was carried out using a CNC machine with a stage built for the purpose of holding the sample. Movement of the stage was controlled in both the x and y axes. The schematic and the image of the experimental setup are shown in Figures 10a and 10b with a general view of the set up shown in Figure 10c. The stage was made of stainless steel and was fixed on the controlled stage of the machine. Two full bridge thin beam load cells with 5 pound capacity (Omega LCL series) were attached to the back of

the stage to measure the shear force due to coefficient of friction and the normal force (rolling force). Two cartridge heaters and thermocouples were attached to the stage to heat the stage and monitor the temperature.

Prior to each experiment the roller was cleaned with a 15 % (wt/wt) sodium hydroxide solution (to remove any transferred aluminum). An oil-in-water emulsion was used as lubricant and was applied continuously during the test. It was prepared by shearing neat oil in water usually at 4 % (v/v) concentration, using a homogenizer at 15,000 rpm for approximately five (5) minutes.

The sample was fixed on the stage and heated to 763 K while the roller was set to spin at the desired rpm. The stage was then moved in the desired direction, allowing the roller to run across the face of the sample, simulating rolling and sliding. To avoid excess lubricant being burnt into the surface of the sample during rolling, pressurized air was sprayed on the sample surface immediately after the contact with the roller. The time required to reach 763 K was fourteen to fifteen (14 to 15) minutes with the temperature dropping to 745K to 756 K during rolling. A list of the process parameters considered in the experiments is in Table 3.

During the rolling process the load was 860 -1130 N, providing a contact pressure of 30.7 - 40.4 MPa. Under these rolling conditions, the reduction in thickness of the aluminum specimen was 0.6 - 0.7 mm.

Forward slip is defined here as the difference between the speed of the stage and that of the (linear) speed of the roller, divided by the speed of the stage, multiplied by 100. A scanning electron microscope (SEM) equipped with energy dispersive X-ray

spectroscopy (EDS) was used to study the sample surfaces after each test. The subsurface cross-sections were characterized using cross-sectional focused ion beam (FIB/SEM). The composition profiles of the sample surfaces were determined using a glow discharge optical emission spectrometry (GDOES).

Focused ion beam works similar to the scanning electron microscope (SEM) except it makes use of focused beams of ions operated at low beam currents. The ions are rastered on the surface of the sample sputtering either ions, atoms, or secondary electrons as the beam hits the surface. These are collected and analyzed as signals which are used to form an image on a screen as the primary beam scans the surface. The intensity of the primary beam current determines the amount of material sputtered from the surface.

Glow discharge optical emission spectroscopy is used to measure the elemental concentrations of materials. It comprises a glow discharge source, optical spectrometer and a vacuum pump. The sample is placed in an analysis chamber where an electric current is applied directly to it. The sample acts as the cathode of the glow discharge cell. Plasma is created in the analysis chamber by an applied voltage created between a tubular grounded anode and the cathode. Argon is used as the carrier gas and is ionized by the plasma. The potential difference between the plasma and the sample accelerates the argon ions toward the sample, bombarding its surface milling atoms and free electrons (secondary electrons) from the surface of the sample. The sputtered atoms are excited in the plasma discharge through collisions with electrons or argon gas atoms. The plasma activity is maintained by the secondary electrons accelerating towards the plasma. The excited sample atoms are relaxed to their energetic ground state by the emission of

characteristic photons which are observed through an observation window and used to characterize and qualify the sample composition.

3.2 Hot Forming Experiment

3.2.1 The Workpiece

The alloy simulating the workpiece was an aluminum-magnesium alloy, AA5083 with its composition given in Table 4. It was in the form of strips 5mm wide, 1mm thick and 150mm long. The strips were in five (5) conditions, two (2) were coated with solid lubricants, and the other three (3) were uncoated. The uncoated strips tested were either in their as-received state or in a polished state.

The as-received state indicates that no work has been performed on the surface, that is, in the state it was received from the industry. It is expected that such strips possess a disturbed layer from previous high temperature processing operations like hot rolling. There is therefore a high concentration of continuous oxides, most significantly MgO on the surface of the strips. The polished state indicates that the surface was polished to a 1μm mirror finish, and all evidence of previous processing and oxides has been removed from the surface. The solid lubricant coated strips were either coated industrially or coated by aerosol spray in the laboratory.

3.2.2 The Die

The function of the die was simulated with a cylindrical P20 steel pin with the dimensions 25 mm length and an 11.7 mm diameter. P20 tool steel is the major tool material used for QPF applications in the automotive industry. The length of the pin was divided into four sections of 5 mm each with a spacing of 3 mm between sections. Its

composition is given in Table 5. The pins were all polished to a 1μm mirror finish and tested in either the polished uncoated state or coated with a solid lubricant. The solid lubricants used in these experiments are given below. There were six pins used, one (1) polished and uncoated and five (5) coated with different solid lubricants.

3.2.3 The Solid Lubricants

The coatings used for the strips were WS_2 and BN, whereas for the pins WS_2, BN, DLC TriboBond 40, and DLC TriboBond 41 were used. Figure 11 displays pictures of the coated pins. See Table 2 for the combinations in which the coatings were tested. The WS_2 coating was performed in one of two ways:

(1) The samples were first cleaned to increase the coating adhesion. Next they were lightly sand blasted with aluminum oxide (alumina). Then they were cleaned thoroughly to completely remove the aluminum oxide dust from the surface and then finally coated with WS_2 by sand blasting under high pressure at ambient temperature. The aluminum oxide was first sprayed to create crevices for the WS_2 platelets to mechanically interlock with the substrate. These samples are referred to as S.B.WS_2 henceforth, referring to spray/ sand blasted WS_2 samples

(2) The samples were coated in the laboratory with a WS_2 aerosol spray. These samples are referred to as A.S. WS_2 henceforth referring to samples being aerosol sprayed with WS_2.

The BN coating was performed in the laboratory with an aerosol spray purchased from ZYP coatings. The DLC coating was performed by the use of physical vapour deposition (PVD) at IonBond Tribological coatings. DLC TriboBond 40 (referred to later

as TB 40) is a non-hydrogenated form of DLC with a hardness (HV) between 800-1800, whereas DLC TriboBond 41 (referred to as TB 41) is a hydrogenated DLC with hardness (HV) between 1500-3000. Both DLC coatings had a tungsten metal addition in their chemical composition. The S.B WS_2 was provided by Dry Lube of Michigan and had a Rockwell hardness of 30HRc (1.0-1.5 Moh's scale). The A.S. WS_2 and WS_2 powder were purchased from M K Impex Canada. The chemical formula of all the coatings and their maximum working temperatures are given in Table 6.

3.2.4 Laboratory Simulation

The hot forming process was simulated with the use of a high temperature tribometer designed in collaboration with the GM Global Research Centre. It simulated the stretching of the workpiece as well as the sliding contact that occurs during hot forming with a pin-on-strip configuration. The pin represented the tool die, whereas the strip was the workpiece.

The setup (see Figure 12) comprised a 500 W cartridge heater inside a stainless steel roller (the hot roller), a COF measurement assembly made up of load cells and two linear actuators (a slave and a master). The strip was connected on each end to one of each of the actuators, passing it over the stainless steel hot roller which rotates freely. The slave was allowed to move at a higher speed than the master so that the strip moved forward at a constant strain rate, the strain rate being controlled by varying the speed of the slave.

The hot roller was 20 mm in outer diameter with only a small portion of the strip in contact with it at any point in time. Boron nitride was applied to its surface to

minimize friction between it and the sliding strip. The strip was then heated and on attaining the required temperature, with its bottom face in contact with the hot roller, it was allowed to slide and stretch by the movement of the actuators. The pin, which was attached to a COF measurement assembly, was then brought down into contact with the top face of the strip. The COF assembly consists of a load cell attached to the pin holder. The load cell transmits data to a data acquisition unit (an InstruNet acquisition unit) which sends the data to a computer where, with the use of calibration equations, COF graphs are plotted. The schematic of this can be seen in Figure 13. The COF between the stretching strip and the pin was measured at a normal load of 0.27 N with a constant temperature and strain rate of 723 K and $0.04s^{-1}$ respectively.

The experiments were carried out to suit a wide range of combination of surface conditions for the steel pins and aluminum strips. In most cases each of the pins was tested against all the surface conditions of strips, but this was not so for all the pins. The experimental conditions are given in Table 7.

Table 1 Composition of alloy under investigation, wt-% (Al3104)

Mn	Mg	Fe	Si	Cu	Zn	Ti	Al
1.40	1.30	0.80	0.60	0.25	0.25	0.10	Bal

Table 2 Composition of SAE 52100 steel, wt-%

C	Mn	Si	Cr	Fe
1.00	0.35	0.30	1.40	Bal

Table 3 Pass schedules and forward speeds in the experiments

	Roller Roughness Ra 0.2mm		
Forward Slip (%)	Temperature (^{O}C)	No. of Passes	Direction of Passes
-1	480	1	F
-1	480	2	F - F
-1	480	2	F - R
1	480	1	F
1	480	2	F - F
1	480	2	F - R
6.5	480	1	F
6.5	480	2	F - F
6.5	480	2	F - R
12	480	1	F
12	480	2	F - F
12	480	2	F - R

Table 4 Compositions of alloy under investigation, wt-% (Al 5083)

Mn	Mg	Cr	Al
0.70	4.40	0.15	Bal

Table 5 Compositions of alloy P20 steel, wt-%

C	Mn	Si	Cr	Mo	Fe
0.40	1.00	0.40	1.20	0.35	Bal

Table 6 Composition of solid lubricant coatings

Coating	Chemical formulae	Maximum Temperature ^{O}C
Tungsten disulphide	WS_2	650
DLC TriboBond 40	a-C:H:W	400
DLC TriboBond 41	a-C:H:W + a-C:H	350
Boron Nitride	BN	1800

Table 7 Experimental conditions for the hot forming experiments

Steel Pin	AA5083 Strip
Polished Uncoated	As Received
	Polished
	S.B. WS_2 Coated
	A.S. WS_2 Coated
	BN Coated
S.B. WS_2 Coated	As Received
	Polished
	S.B. WS_2 Coated
	BN Coated
BN Coated	As Received
	Polished
	S.B. WS_2 Coated
	BN Coated
A.S. WS_2 Coated	Polished
	A.S. WS_2 Coated
TB 40	As Received
	Polished
	S.B. WS_2 Coated
	BN Coated
TB 41	As Received
	Polished
	S.B. WS_2 Coated
	BN Coated

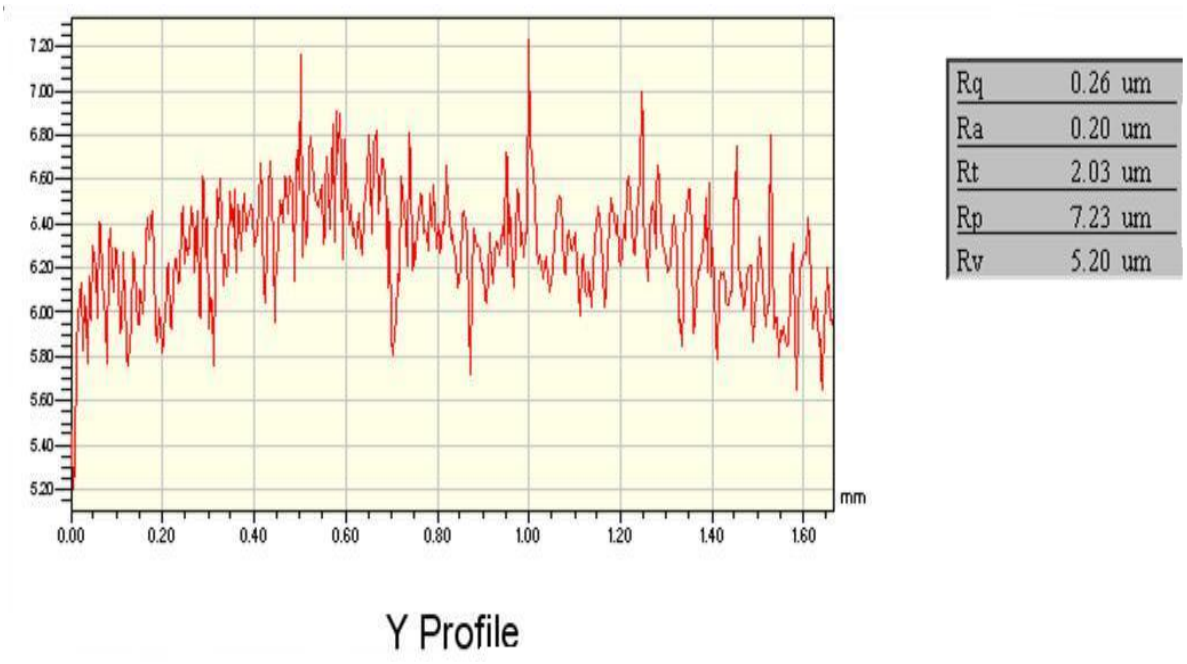

Figure 9 Optical profilimetry of the roll surface morphology consisted of discontinuous grooves

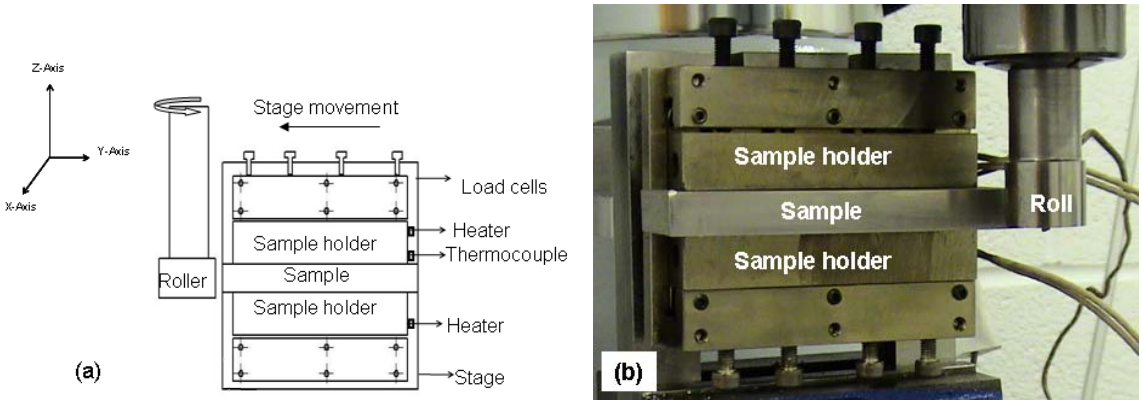

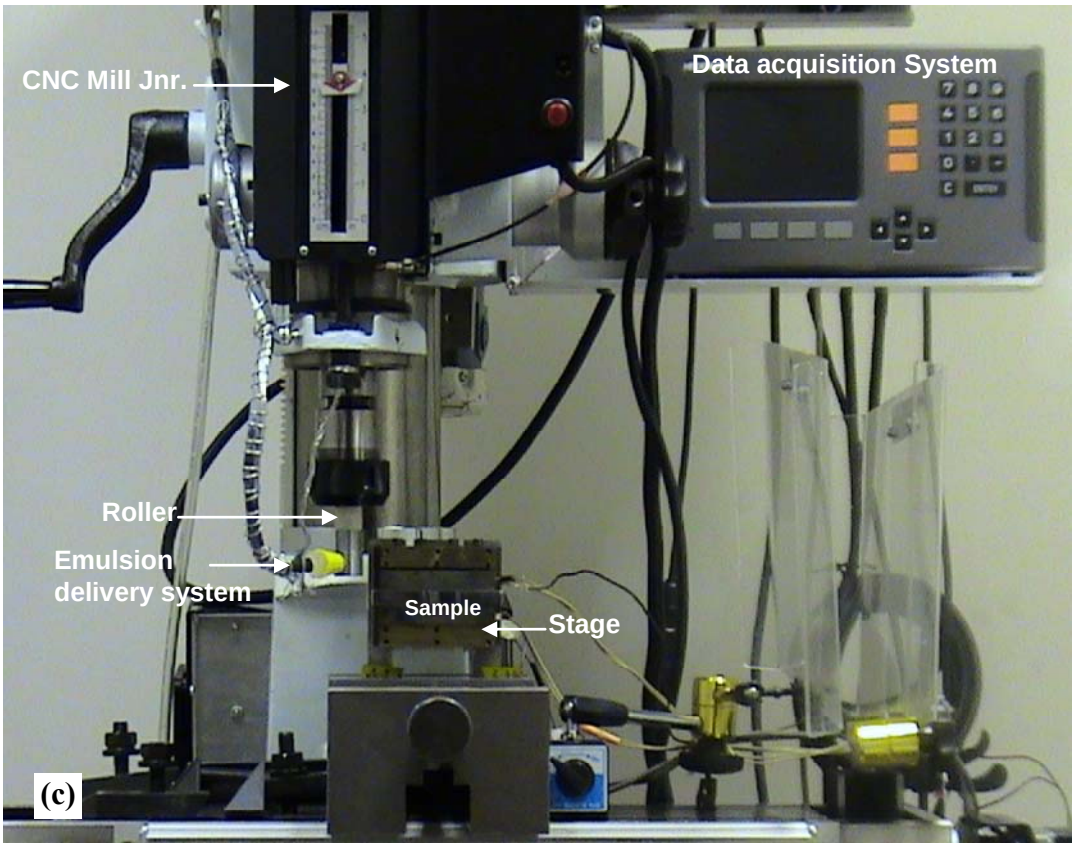

Figure 10 (a) Schematic of the front and top view of laboratory experimental setup with the arrows showing the direction of motion; (b) image of the experimental setup (c) general view of he CNC Mill with stage and sample

Figure 11 Picture showing the pins used in the order from left to right: the uncoated pin, the S.B. WS2 coated pin, the A.S. WS2 coated pin, the TB 40 coated pin, the TB 41 coated pin, and lastly the BN coated pin

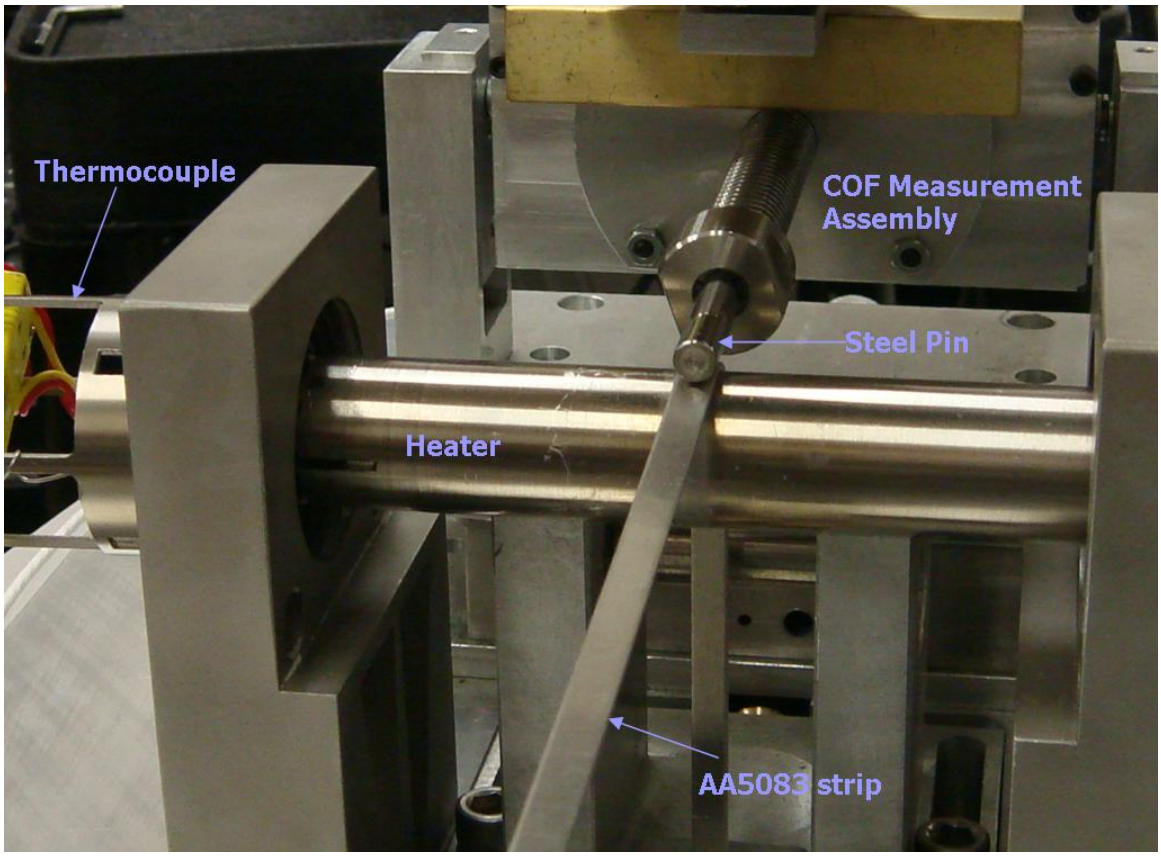

Figure 12 Experimental set-up for the high temperature tribometer designed to simulate hot forming operations

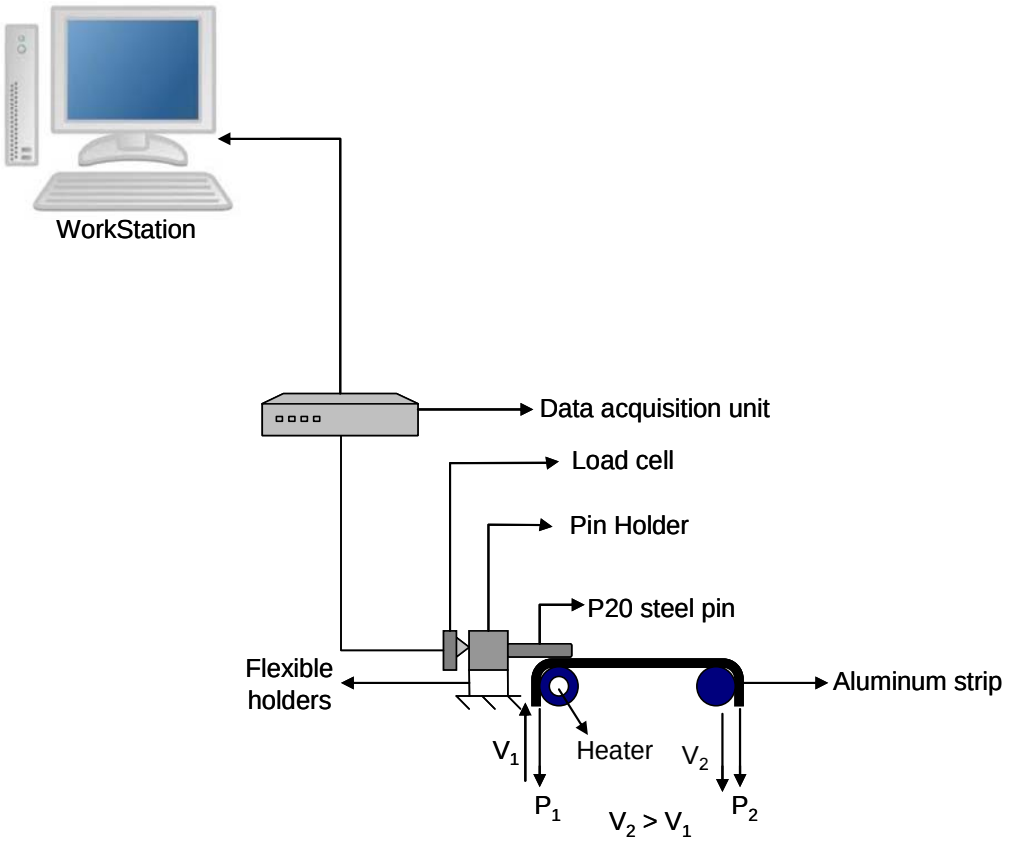

Figure 13 A Schematic diagram of the coefficient of friction measurement

CHAPTER IV

RESULTS

4.1 Hot Rolling Experiments

The SEM image of the surface of a sample rolled by industrial reversing mill (before rolling with tandem mills) was first taken as a basis of understanding of the surface features of an industrially rolled alloy. It shows oxide flakes and cracks distributed across the alloy surface (Figure 14a). The EDS of this surface seen in Figure 14b shows the surface to be rich in Al, Mg, and O, serving as evidence of the oxide flakes on the metal surface.

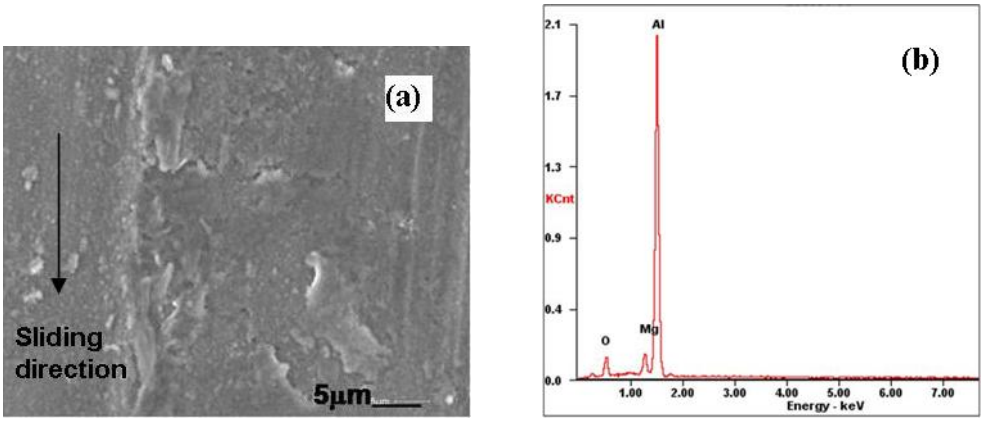

Figure 14 (a) SEM image from the surface of an AA3104 sample rolled by industrial reversing mill (before rolling with tandem mills), (b) EDS analysis from the surface shows oxygen

The SEM image of the surface of the AA3104 alloy rolled in one pass at 1% forward slip is shown in Figure 15a. It shows oxide flakes and intermetallics. The surface of the alloy at the same forward speed but after two passes in the same direction can be seen in Figure 15b and shows cavities developing on the surface in addition to the oxide flakes. Figure 15c shows the surface after two passes, first in the forward direction and

subsequently in the reverse direction at the same forward speed. Long narrow gorges are observed covering the surface of the alloy with oxide flakes observed at the edges of the gorges. The surface is also more heavily covered with intermetallics. The surface features observed under this condition appear more embedded. EDS comparison between the oxide flakes and the bulk surfaces show both surfaces to be rich in Al, Mg, O, and C, but the flakes have a higher concentration of both O and Mg, as seen in Figures 15d and 15e.

Figure 16a shows the surface of the alloy after one pass at a forward slip of 6.5%. There are surface cavities, cracks, and surface deformation in the form of shingles. These features are more pronounced on the surface after two passes at the same forward speed as seen in Figure 16b. The cavities and shingles here are wider, and less cracking is observed. Figure 16c shows a surface covered with deformation with more pronounced, wider, and longer cavities with larger shingles. This surface is developed after two passes, first in the forward direction and next in the reverse direction. The EDS again shows a surface rich in Al, Mg, O, and C with the shingles and cavity edges having a higher concentration of O and Mg, as seen in Figure 16d and 16e.

The SEM image of the surface of the alloy rolled in one pass at 12% forward slip is shown in Figure 17a. It shows localized shear deformation in the form of shingles. The magnified image of the marked square area in plate 16a is shown as the inserted image in Figure 17a. FIB milling was used to expose the cross-section along the dashed line in the inserted image. The surface was first platinum coated in order to avoid damaging due to the exposure to ion beam. Figure 17b shows a low magnification image of the trench after FIB milling. The image from the cross-section in Figure 17c shows cracks formed

approximately 7 μm beneath and parallel to the rolled surface. Under the same rolling condition, a different area on the aluminum surface is shown in Figures 18a and 18b. FIB milling was performed along the dashed line in Figure 18b. A high magnification image of the cross-section, Figure 18c, shows a layer with an average thickness of 150 nm and different composition than the bulk. The near surface layer consists of voids, and its composition in the area marked as d is shown in Figure 18d. This near surface area of the shingle is rich of Mg, O, C, and Al. The elements Pt and Ga are from the protective coating and the ion source respectively. An EDS spectrum of the bulk material from the area marked as e is shown in Figure 18e.

Figure 19a shows a dimple shape defect on the surface of the sample rolled with 12% forward slip for two passes, both in the same direction. The dashed line in the inserted image shows the path of FIB milling and the trench is shown in Figure 19b. The SEM image in Figure 19c, from the cross-section, shows a layered feature on the left side of the defect. Carbon and oxide debris are trapped between each layer. EDS analysis of this area, marked as d in Figure 19c, is shown in Figure 19d and indicates that the main elements in this region are Mg, O, C, and Al. Likewise, the area marked as e in Figure 19c shows the same elements with lower concentration of C and Al. The composition of the bulk material (area marked as 5e in Figure 19c) is similar to that shown in Figure 18e.

Figure 20a shows the surface of the sample rolled with 12% forward slip, the first pass in forward direction and the second pass in the reverse direction. The dashed line in the inserted image shows the path of FIB milling. The cross-section of the FIB milled area shows a layer formed on the surface with average thickness of 150 nm. EDS analysis

of the marked area in (b) shows that the surface layer consists of elements Mg, O, C, and Al. EDS of the area marked as 5e (bulk) is similar to that shown in Figure 17e.

The surface of the sample rolled at -1% forward slip, one pass is shown in Figure 21a. The FIB milling is performed along the dashed line. The cross-section of the FIB milling along the dashed line in Figure 21a is shown in Figure 21b. In this case the layer had an average thickness of 70 nm, and most of the voids are open to the surface. EDS of the area marked c in the layer is shown in Figure 21c and indicates that the main elements in the layer are C, O, Mg, and Al. The composition of the bulk (area marked as 5e) is similar to that shown in Figure 18e.

A depth profile analysis using glow discharge optical emission spectrometry (GDOES) was performed on the surfaces of the samples. The GDOES analysis of the polished surface shows a low Mg and O concentration (Figure 22a). When the alloy is heated to the rolling temperature and held for the duration of the time it takes for one (1) pass to occur, there is an increase in the Mg and O concentration at the surface as shown in Figure 22b. The results of the GDOES for samples rolled at 12% forward slip show that Mg and C have the highest concentration at the surface of the sample after one pass (Figure 23a). When the number of passes is increased to two, there is an increase in the surface concentration of Mg (Figure 23b). The results of the GDOES for samples hot rolled at -1% follow the same trend with an increase in the surface content of Mg when the number of passes increments from one to two (Figures 24a -24b).

In summary, the SEM of the surface of the rolled samples showed deformations in the form of oxides flakes which formed shingles as the passes and forward speed were

increased, gorges and cavities. The EDS of the alloy surface shows it rich in Al, Mg, C and O with defects like the flakes and shingles having a higher concentration of O. On close examination of the shingles through cross section, after one rolling pass the notable features of the disturbed layer were related to localized shear deformations, whereas after two passes in the same direction, the localized deformations exhibited a layered structure (the area surrounded by dashed line in Fig. 19c). GDOES analysis showed the Mg content on the surface varied with the number of passes that were run.

4.2 Hot Forming Experiment

Figure 25 shows the variation of the COF of the polished uncoated pin with time. The polished uncoated pin when run against the polished strip had the highest COF observed under this condition at 1.62. The as-received strip gave a slightly lower COF at 1.42. The coated strips had the lowest COF at 0.69 for the S.B. WS_2 coated strip and 0.40 for the BN coated strip. The SEM image of the surface of the polished uncoated pin run against the polished strip is shown in Figure 26a. It shows material transfer on the pin surface with build-up at the centre of the wear track of the pin. The EDS in Figure 26c confirms that the material transfer comprises Al, Mg, and O. Figure 26b shows the wear track on the polished strip with groove, shingles, and material overlapping at the sides of the wear track, all indicating evidence of material loss. The EDS in Figure 26d shows elements Al, Mg, and O, indicating there was no material transfer from the steel pin onto the Al-Mg strip. The pin surface tested against the as-received strip is shown in Figure 27a. The material adhered to the surface here appears spread across the wear track of the pin in a thin layer on the pin. There is no material build-up observed, and the EDS in

Figure 27c shows that the transferred material comprises O, Mg, and Al. The as-received strip has a wear track with features similar to that of the polished strip, grooves and overlapping, indicating evidence of material loss from the strip as seen in Figure 27b, and its EDS (Figure 27d) shows Al, Mg, and O. Figure 28a shows the surface of the pin against the S.B. WS_2 coated strip. The transfer layer was observed to be in the form of platelets embedded in oxides distributed in small thin layer patches along the wear track on the pin. The EDS, seen in Figure 28c, displays a high amount of O, as well as Fe and trace amounts of W. S and Al were also observed on the surface of the wear track. The S.B. WS_2 coating on the strip as seen in Figure 28b is observed to have surface fractures and cracks exposing the Al-Mg substrate. Unlike the uncoated strips, there were no observably distinct wear tracks found on the S.B. WS_2 coated strip. There were white powdery deposits observed on the coating surface, predominantly at the cracks and fractures on the coating; the EDS seen in Figure 28d shows that these areas are rich in O. Figure 29a shows the pin surface against the BN coated strip. There was no aluminum adhesion observed on the pin surface, a transfer layer however is observed comprised of BN from the strip coating. The BN transfer on the pin was observed to accumulate on the circumference of the wear track, heaviest at the head and the tail of the wear track. It was distributed across the surface of the track in the form of clusters. These clusters are comprised of flakes of BN adhered together. This BN accumulation on the pin could be observed with the naked eye. The EDS in Figure 29c confirmed the material transfer to be comprised of B, N, and Al. The surface of the strip as seen in Figure 29b shows no material loss from the aluminum substrate and no distinguishable wear track. An EDS of

the surface shown in Figure 29d had element peaks of B, N, Al, Mg, Si, and O. The BN coating is an aerosol spray, the Si observed is part of the adhesive solution from the spray.

The variation of the COF of the S.B. WS_2 coated pin with time is given in Figure 30. The highest COF recorded with this pin was against the polished strip (1.80). The COF recorded with the as-received strip was 1.23. The lowest COF were recorded against the S.B. WS_2 coated and the BN coated strips at 0.74 and 0.50 respectively. The SEM analysis of the S.B. WS_2 coated pin against the polished strip displayed in Figure 31a, showed aluminum adhesion and build-up on the pin surface as confirmed by the EDS in Figure 31c. The SEM in Figure 31b shows the surface of the wear track of the strip; it shows features such as overlapping aluminum on the sides of the wear track, shingles, and grooves. The EDS (Figure 31d) shows no evidence of W or S on the surface indicating no material transfer from the pin onto the strip, the elements observed were Al, Mg, and O. Figure 32a shows the surface of the S.B. WS_2 pin run against the as-received aluminum strip. It displays material adhesion dispersed in small thin patches across the surface of the wear track of the pin. The EDS in Figure 32c confirms that the transfer was from the aluminum strip, with peaks in Al, Mg, and O. Figures 32b and 32d display the SEM and EDS of the wear track of the as-received strip respectively. There is no material transfer from the pin surface observed on the wear track of the strip with only peaks in Al, Mg, and O observed and wear track features as overlapping and shingles. The S.B. WS_2 coated pin surface run against the S.B. WS_2 coated strip is shown in Figure 33a; it shows minimal material adhesion on the pin surface. The EDS in Figure 33c was used to

confirm that the material transfer was comprised of Al, Mg, and O. The surface of the S.B. WS_2 coated strip shown in Figure 33b shows cracks and fractures of the coating exposing the alloy surface beneath it; again, there was no distinct wear track observed on the S.B. WS_2 coated strip. Figure 33d displays the EDS of the surface which has peaks of Al, Mg, O, W, S, and C. The S.B. WS_2 coating on both the strips and the pin where observed to have white powdery patches on its surface; the EDS analysis of these areas had peaks of W, S, and O. They are noted to be predominantly occurring at cracks and fractures on the strips. Figure 34a shows the surface of the S.B. WS_2 coated pin when run against the BN coated strip. In this condition, the BN coating is observed to have transferred to the surface of the pin. It is distributed across the surface of the pin in the form of flakes. There is heavy accumulation observed at the middle of the wear track as well as at its head and tail where the flakes accumulate to sometimes form spherical clusters or simply pile up on one another. An EDS of the cluster and flakes as seen in Figure 34b showed B, N, Al, and Si to be present. The BN strip, as with the polished uncoated pin showed no wear track or indication of Al loss from the strip.

When the COF for S.B. WS_2 coated and polished uncoated pins run against the polished strip are compared as seen in Figure 35, it is observed that S.B. WS_2 coated pin (1.80) had a higher COF than the polished uncoated pin (1.62). This implies that at the working temperature of 723 K and $0.04s^{-1}$strain rate, coating the pin with S.B. WS_2 was unable to mitigate high friction. The same test was then repeated at a reduced temperature of 573 K and strain rate of $0.01s^{-1}$ for both the polished uncoated pin and the S.B. WS_2 coated pin. Under this condition the COF of S.B. WS_2 coated pin was recorded as 0.53,

whereas that of the polished uncoated pin was 1.13 as seen in Figure 35. The SEM analysis of the S.B. WS_2 pin is shown in Figure 36: the pin surface displays thin layers of aluminum adhesion spread in small patches across the wear track with no aluminum build up. The adhesion observed on the S.B. WS_2 pin at this lower temperature and strain rate is much less when compared with the wear track of the S.B. WS_2 coated pin surface at 723 K /0.04s^{-1}. The pin surface at 573 K also appears to have less powdery patches across the surface in comparison to the S.B. WS_2 pin surface at 723 K.

An aerosol WS_2 spray was also tried due to the results obtained with the S.B. WS_2 coating. The AA5083 strip was first coated and run against the polished uncoated pin, with a COF of 0.49 being recorded. The A.S. WS_2 coating was then applied on the pin with the time curve shown in Fig 37. The COF for the polished strip against this A.S.WS_2 coated pin was 0.38, and 0.35 was recorded when the A.S. WS_2 coated pin was run against an A.S. WS_2 coated strip. The COF of the pin run against the as-received strip gave a COF of 0.32. The SEM of the A.S. WS_2 coated pin surface run against the polished strip is given in Figure 38a; the wear track shows no aluminum transfer on the pin as confirmed with the EDS in Figure 38c. The wear track however shows a loss of the aerosol coating but with much of the WS_2 platelets still adhering firmly to the pin. The WS_2 appear as platelets held together by an adhesive on the surface of the pin. The EDS also shows evidence of C on the surface from the adhesive and also confirms that W and S are present. An examination of the strip shows, as seen in the SEM in Figure 38b, platelets transferred onto the surface of the strip. These platelets are distributed across the surface of the strip where the pin has been in contact; there is also no material loss

observed from the strip which shows no other distinct signs of a wear track. The platelets are observed by the EDS in Figure 38d to have peaks for the elements W, S, and C, corresponding to the coating from the pin. These same conditions were observed for the pin run against the as-received strip as seen in Figures 39 (a) and (b). The SEM of the pin surface in contact with the A.S. WS_2 coated strip can be seen in Figure 40a. The SEM shows the transfer of WS_2 platelets from the strip to the surface of the pin. Therefore there is a thin accumulation of WS_2 platelets at the surface of the pin in contact with the strip. An EDS in Figure 40c displays peaks of W, S, and C. The A.S. WS_2 coated strip can be observed in Figure 40b with little coating loss observed on the strip. The SEM of the uncoated pin run against the A.S. WS_2 coated strip is shown in Figure 41a. Here platelets are observed adhered on the surface of the pin which has been transferred from the coated strip, as is confirmed from the EDS in Figure 41c. There is no aluminum adhesion observed on the pin surface or on WS_2 platelets. The SEM of the A.S. WS_2 coated strip can be seen in Figure 41b with little coating loss observed which occurs where the pin comes into contact with the strip.

The COF of the BN coated pin with its time curve is displayed in Figure 42. It shows the highest COF recorded when the BN coated pin is run against a BN coated strip (0.49). When the BN was run against a polished strip, the COF was recorded as 0.39, the lowest COF with this pin, whereas against an as-received strip the COF was 0.48. When run against the WS_2 coated strip the COF was 0.40. The BN coated surfaces proved difficult to view under SEM as the BN flakes were not very conductive and so charged easily. Figure 43a shows the SEM of the BN coated pin surface run against the polished

strip. There is coating loss from the surface of the BN coated pin, but the BN still adheres to the surface of the pin so that the steel pin is not exposed. The coating appears as BN flakes piled on top of one another. The EDS of the wear track of the pin (Figure 43c) gives elemental peaks in B, N, C, O, Si, and Al. The SEM of the polished strip is shown in Figure 43b, and BN flakes observed adhered to the surface of the strip. There is no wear track observed on the strip indicating that there has been no material loss from the Al-Mg surface. The surface of the BN coated pin run against the as-received strip (Figure 44a) and the S.B. WS_2 coated strip showed the same surface features with BN coating loss observed; the EDS (Figure 44c) showed peaks in B.N, O, Si, Al, and Au from an Au coating carried out on the surface. The strip surfaces (Figure 44b) had the same features as that of the polished strip with no distinguishable wear track or Al material loss from the surface, but evidence of BN flakes dispersed on the strip surface. The BN coated pin run against the BN coated strip showed BN accumulation on the surface of the BN coated pin.

The TB 40 coated pin COF is shown in the time curves in Figure 45. The COF of this coated pin run against the polished strip was recorded as 1.21 whereas against the as-received strip a COF of 1.05 was observed. The lowest COF were observed when the strip was coated, with a COF of 0.38 recorded against the WS_2 coated strip and 0.42 against BN. The SEM of the surface of the pin against the polished strip is shown in Figure 46a. Aluminum metal transfer was observed adhered to the surface of the pin. The transfer appears from the middle to the tail of the wear track with no material build-up; the wear track itself had a darker appearance than the rest of the surface. There was no

adhesion observed at the start of the wear track. The EDS in Figure 46c of the material adhesion on the TB 40 pin shows peaks heavy in Al, Mg, and O. The polished strip surface is displayed in Figure 46b showing a wear track covered with shingles and grooves. The EDS of the wear track in Figure 46d showed elements Al, Mg, and O; there was no C observed on the surface showing no observable material transfer from the TB 40 coating to the pin. Figure 47a displays the SEM of the pin surface that was run against the as-received strip. The wear track appears darker than the areas of the pin not in contact with the strip. There is little material transfer observed, spread mostly across the tail end of the wear track in small patches. The EDS shown in Fig 47c confirms that the material transfer has the following elements Al, C, O, Co, W, and S. W is part of the chemical composition of the TB 40 coating as observed in Table 6. Figure 47b displays the SEM of the as-received strip run against the TB 40 coated pin; it shows similar features and elemental composition to the polished strip wear track run against the same pin. The SEM of the pin surface that was run against the WS_2 coated strip is shown in Figure 48a. There is material transfer observed in the form of small platelets observed on the surface of the TB 40 pin. These platelets are spread across the surface of the wear track. The EDS analysis shown in Figure 48c confirms that these platelets contain W and S. There was also minimal aluminum adhesion observed. Figure 48b shows the surface of the WS_2 coated strip, this is the only condition where a wear track was observed on the S.B. WS_2 coated strips. The wear track shows no features indicating material transfer or loss. The strip shows similar features as the other S.B. WS_2 strips that is cracking and fractures of the coating exposing the Al-Mg substrate. The EDS of the strip is shown in

Figure 48d with Al, Mg, W, S, and O observed. Figure 49a shows the SEM of the surface of the TB 40 that was run against the BN coated strip. There is material transfer observed covering the surface of the pin, which is confirmed by the EDS in Figure 49b to be B, N with traces of Al. BN covered the surface of the pin in contact with the coated strip with the transfer accumulated at the circumference of the wear track, whereas the centre of the wear track was coated lightly with BN flakes.

The time curve for the TB 41 coated pin is shown in Figure 50. Here the highest COF was observed for the polished strip at 1.72. When this pin was run against the as-received strip, the COF was recorded as 1.28. The lowest COF were again recorded against the strips coated with solid lubricants, with 0.52 observed for the WS_2 coated strip and 0.50 for the BN coated strip. Figure 51a is the SEM of the surface of the TB 41 coated pin in contact with the polished strip. Material transfer adhering to the surface is observed across the wear track with build-up occurring at the tail of the wear track. The EDS analysis shown in Figure 51c confirms that the adhered material has elements Al, Mg, and O. Figure 51b displays the SEM of the wear track of the polished strip, it possesses grooves, shingles, and material displacement overlapping on the side of the wear track. The EDS in Figure 51d confirms the elements Al, Mg, and O present. The SEM of the pin surface against the as-received strip is shown in Figure 52a, where material adhesion is observed on the pin across the tail of the wear track. The adhesion, a thin layer with no build-up was confirmed to be from the as-received aluminum strip with the EDS in Figure 52b. The wear track of the as-received strip showed similar features as that of the polished strip. The surface of the pin against the BN coated strip showed the

strip coating covering the wear track of the pin as seen in Figure 53a. There was BN accumulation in the form of clusters observed at the circumference of the wear track with lighter transfer in the form of flakes observed at the centre. The B, N with traces of Al was confirmed with EDS as seen in Figure 53b on the TB 41 coated pin. The wear track of the pin surface against the WS_2 strip is shown in Figure 54a. There was a very thin layer observed adhered to the surface of the TB 41 pin under this condition. The EDS observed in Figure 54c confirmed that the adhered material was W, S. There was also observed at the edge of the wear track, Al and Mg. The WS_2 coated strip like other cases had shown evidence of fracture and cracking of the surface coating across the surface and can be seen in Figure 54b.

In summary the A.S WS_2 and BN coating performed best during the high temperature simulations, mitigating Al adhesion to the pin and recording low COF under all conditions tested. S.B WS_2 coating performed comparably when coated on the strip, with comparable COF recorded but Al adhesion still observed on the pin. The S.B WS_2 coated pin performed poorly when run against the uncoated strips, with Al adhesion observed in both cases and the highest recorded COF for the experiments recorded when it was run against the polished strip. The DLC coatings were unable to completely mitigate adhesion when run against the uncoated strips. They performed better when run against the coated strips showing comparable COF for both the BN and S.B WS2 coated strips.

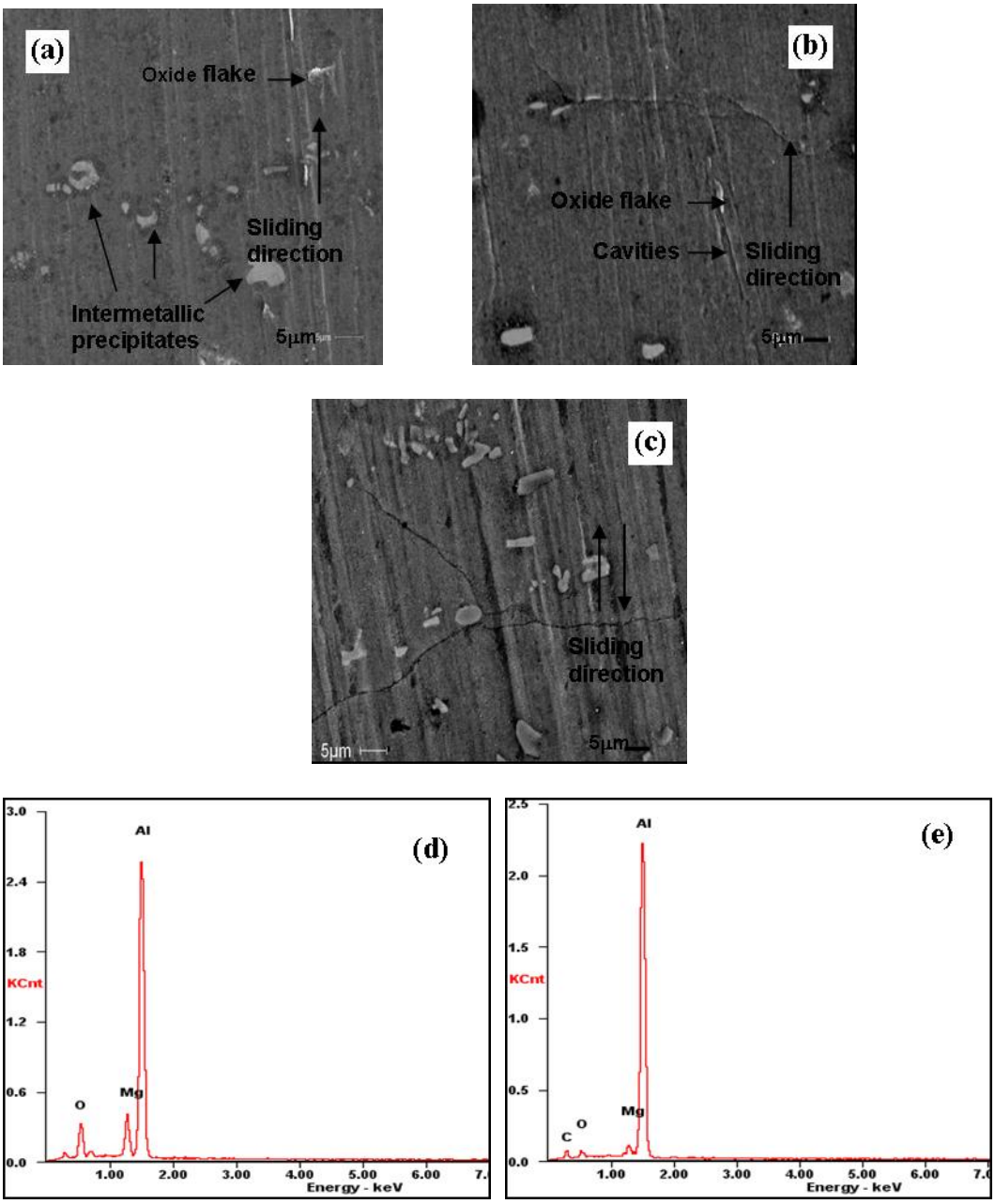

Figure 15 AA3104 surface hot rolled at 753 K and with forward slip 1%, (a) SEM image from the surface after 1 pass, (b) SEM image from the surface after 2 passes in the same direction, (c) SEM from the surface after 2 passes in opposite directions, (d) EDS analysis from the flakes observed and (e) EDS analysis from the bulk surface

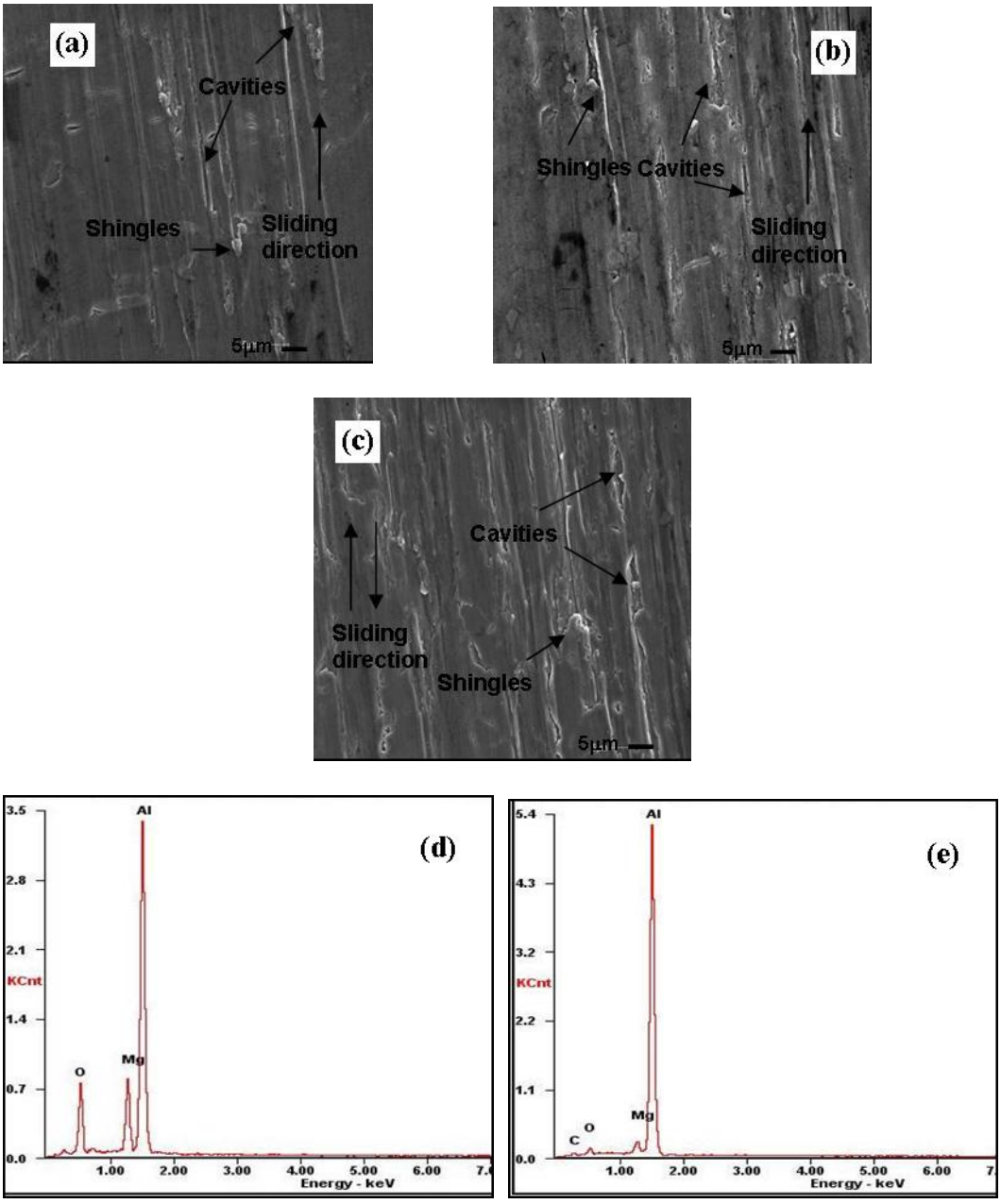

Figure 16 AA3104 surface hot rolled at 753 K and with forward slip 6.5%, (a) SEM image from the surface after 1 pass, (b) SEM image from the surface after 2 passes in the same direction, (c) SEM from the surface after 2 passes in opposite directions, (d) EDS analysis from the shingles observed and (e) EDS analysis from, the bulk surface

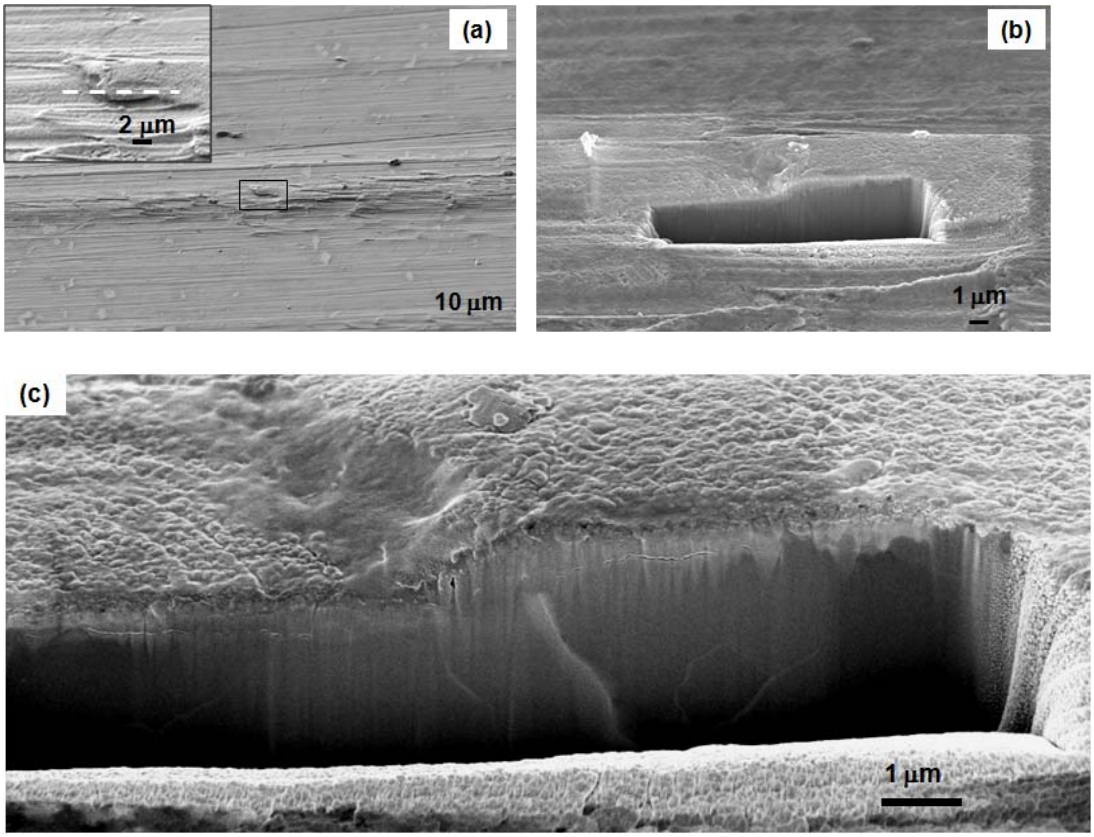

Figure 17 SEM image from the AA3104 surface hot rolled in 1 pass at 753 K and with 12% forward slip, (a) localized shear deformations in the form of shingles, the inserted image magnifies the area in the bracket, (b) low magnification image of the trench after FIB milling the surface was platinum coated first in order to avoid damaging due to exposure to ion beam, (c) cracks formed beneath and parallel to the surface

.

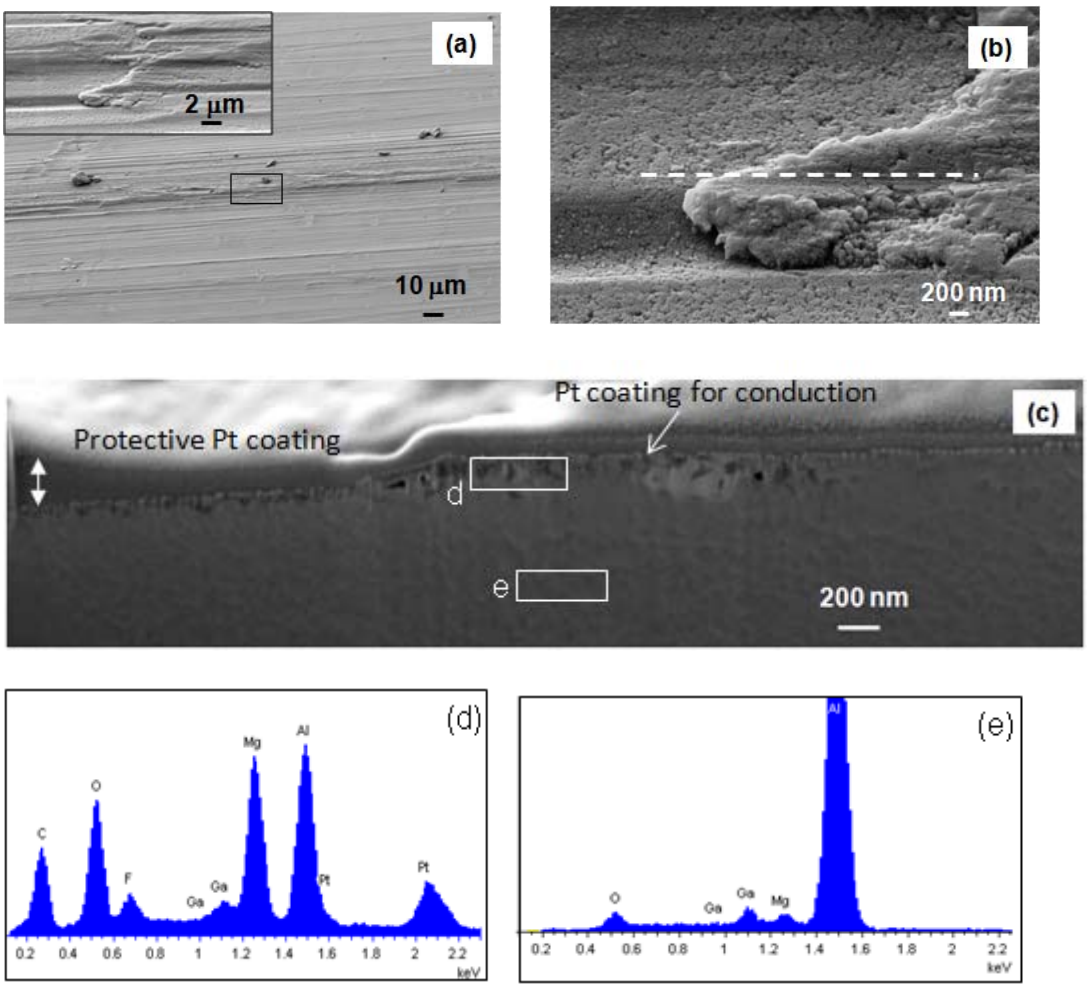

Figure 18 AA3104 surface hot rolled in 1 pass at 753 K and with forward slip 12%, (a) SEM image from the locally deformed areas with the inserted image magnifying the area of interest, (b) the FIB milling is performed along the dashed line, (c) the cross-section shows voids and defects in the near surface area, (d) EDS analysis from the area marked as d; the elements Pt and Ga from the protective coating and the ion source respectively, and (e) EDS analysis from the area marked as e (bulk material)

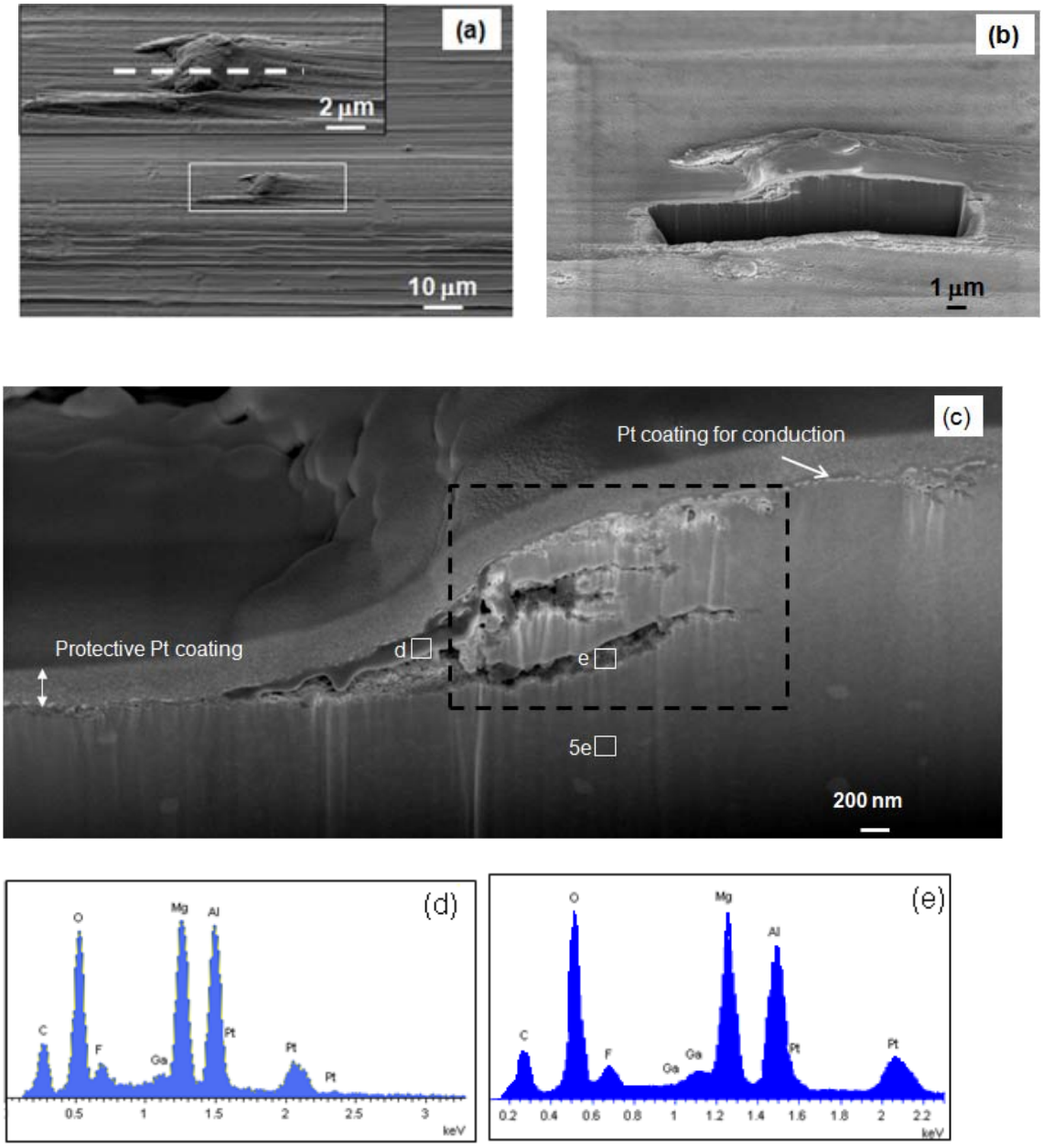

Figure 19 Evolution of AA3104 surface hot rolled in 2 passes in the same direction at 753 K and with 12% forward slip, (a) SEM image, (b) FIB milling performed along the dashed line in (a), (c) the cross-section shows voids and defects on the surface of the dimple and layered features (marked by dashed line), (d) EDS analysis of the area marked as d in (c), and (e) EDS analysis of the area marked as e in (c)

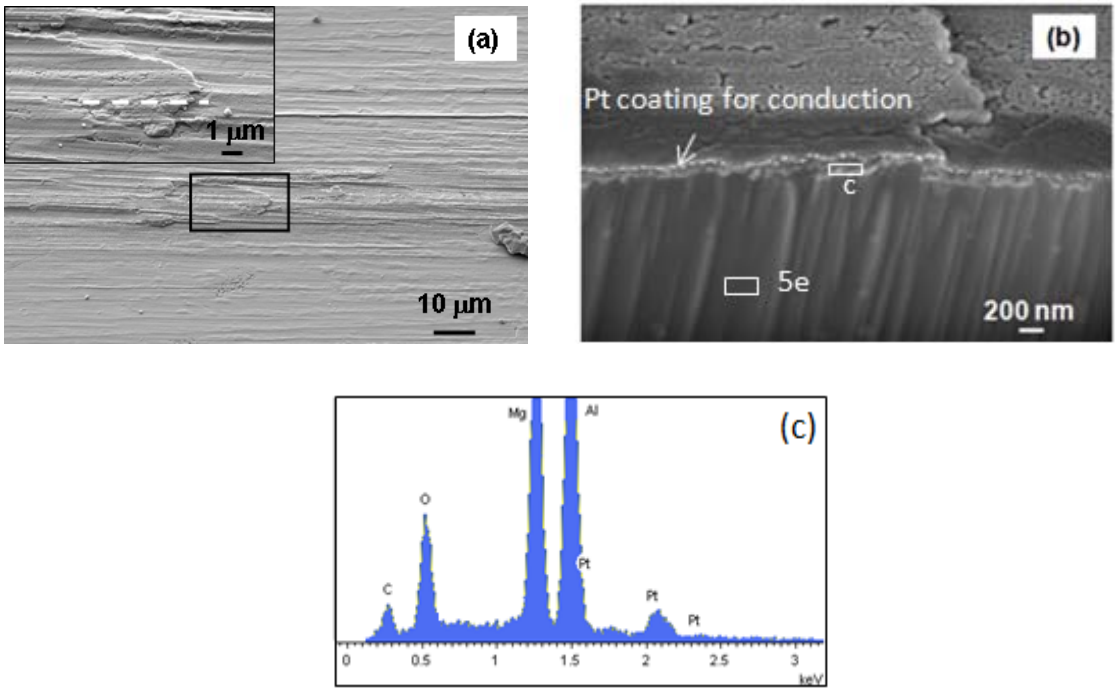

Figure 20 Evolution of AA3104 surface hot rolled in 2 passes (forward-reverse) at 753 K with 12%forward slip of (a) SEM image showing shingles, (b) the cross-section along the dashed line in (a) shows a layer formed on the rolled surface, and (c) EDS analysis of the area marked in (b)

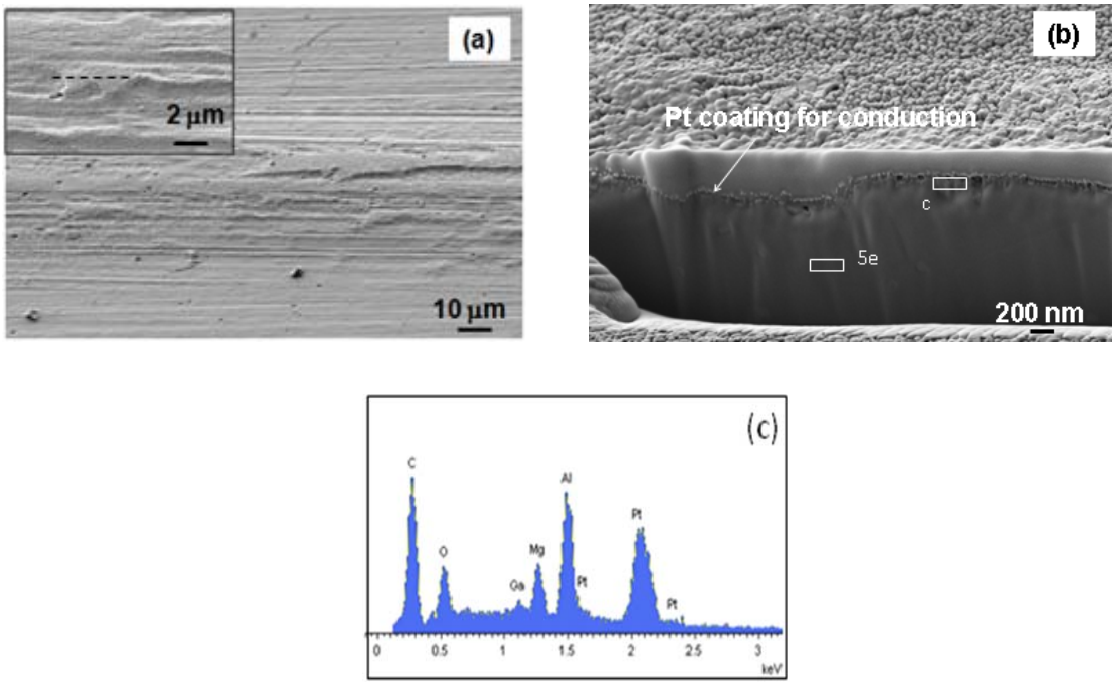

Figure 21 Evolution of AA3104 surface hot rolled in 1 pass at 753 K and with forward speed of -1%, (a) SEM image showing surface smearing, (b) the cross-section along the dashed line in (a) shows a layer formed on the rolled surface, and (c) EDS analysis of the area c marked in (b)

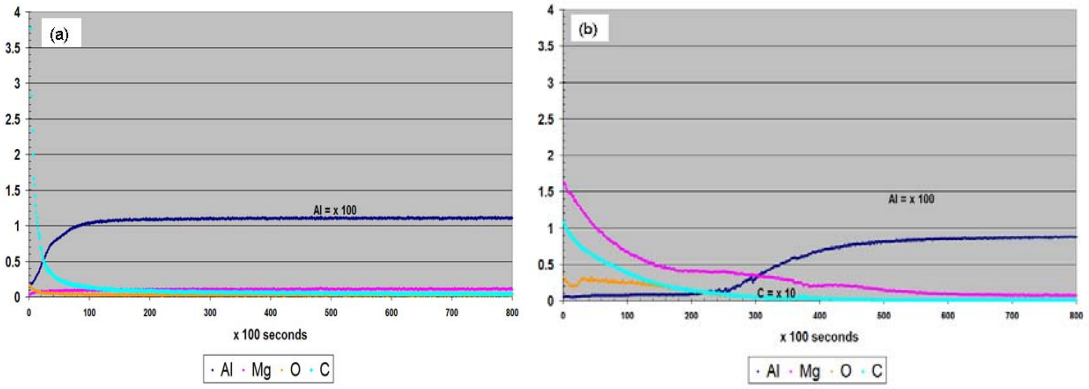

Figure 22 (a) GDOES depth profile analysis from the surface of an as polished sample, (b) GDOES depth profile analysis from the surface of a sample polished and heated to 753 K for 840s.

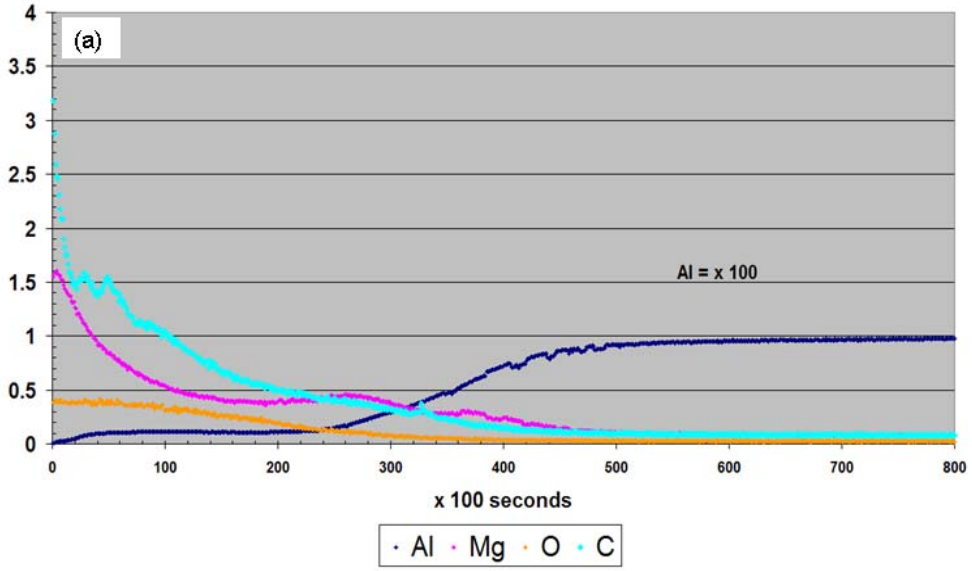

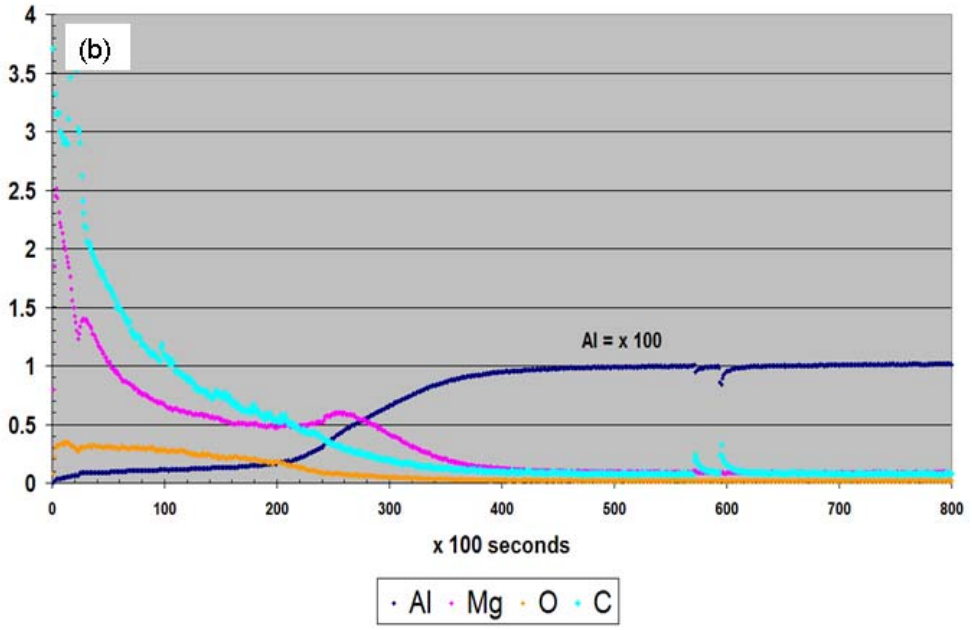

Figure 23 Elemental signal strength as a function of sputter time using GDOES, (a) forward speed 12%, 1 Pass, (b) forward speed 12%, 2 passes in the same rolling direction.

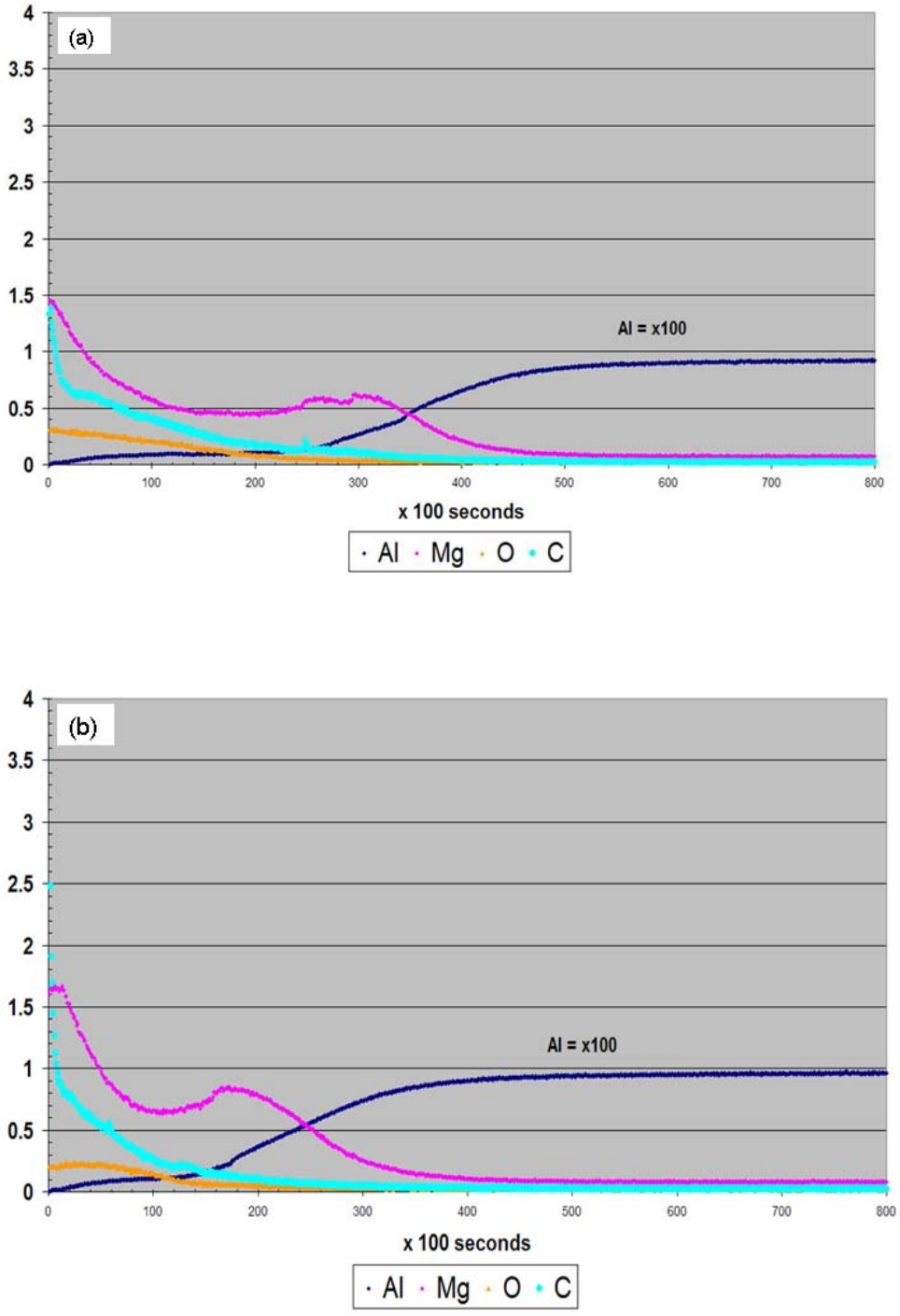

Figure 24 Elemental signal strength as a function of sputter time using GDOES, (a) forward speed -1%, 1 Pass, and (b) forward speed -1%, 2 passes in the same rolling direction.

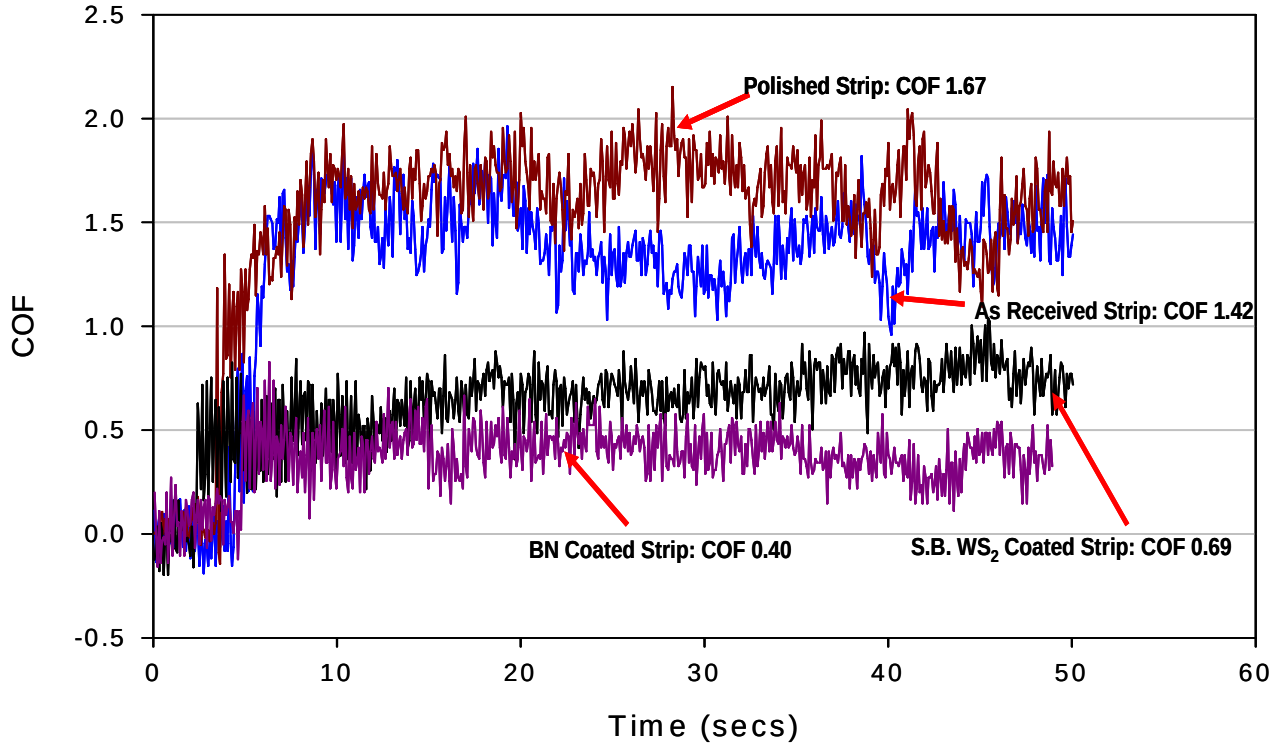

Figure 25 COF-Time curves for the polished uncoated P20 steel pin against the various surface conditions of the AA5083 aluminum strip

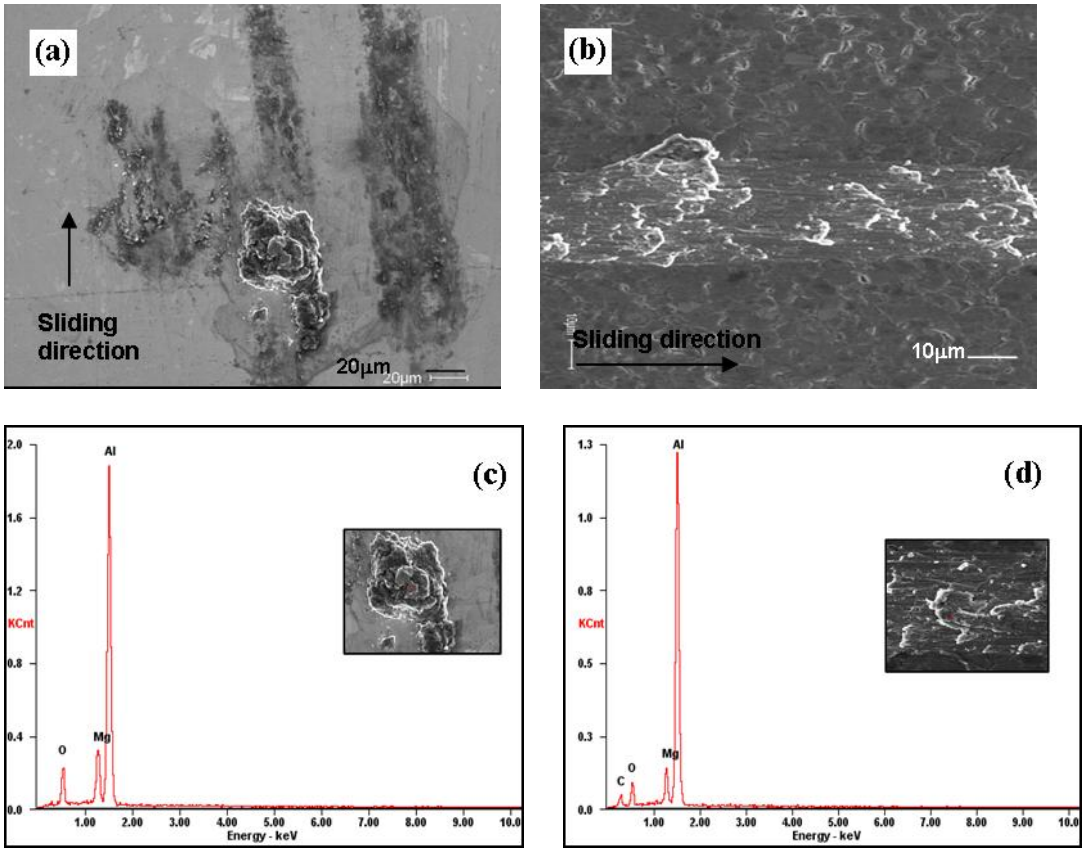

Figure 26 Polished uncoated pin against the polished strip, (a) SEM of polished uncoated pin surface, (b) SEM of polished strip surface, (c) EDS of material adhesion on uncoated pin surface, and (d) EDS of wear track of polished strip

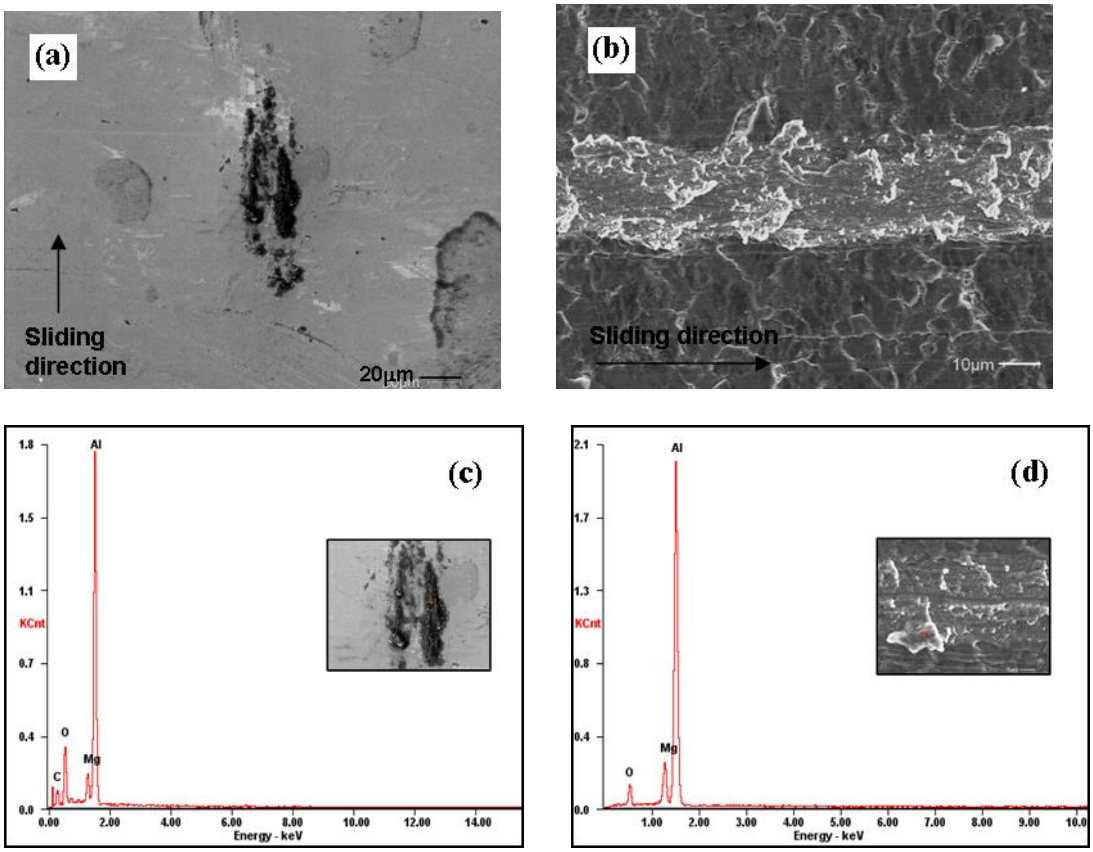

Figure 27 Polished uncoated pin against the as-received strip, (a) SEM of as-received uncoated pin surface, (b) SEM of as-received strip surface, (c) EDS of material adhesion on uncoated pin surface, and (d) EDS of wear track of as-received strip

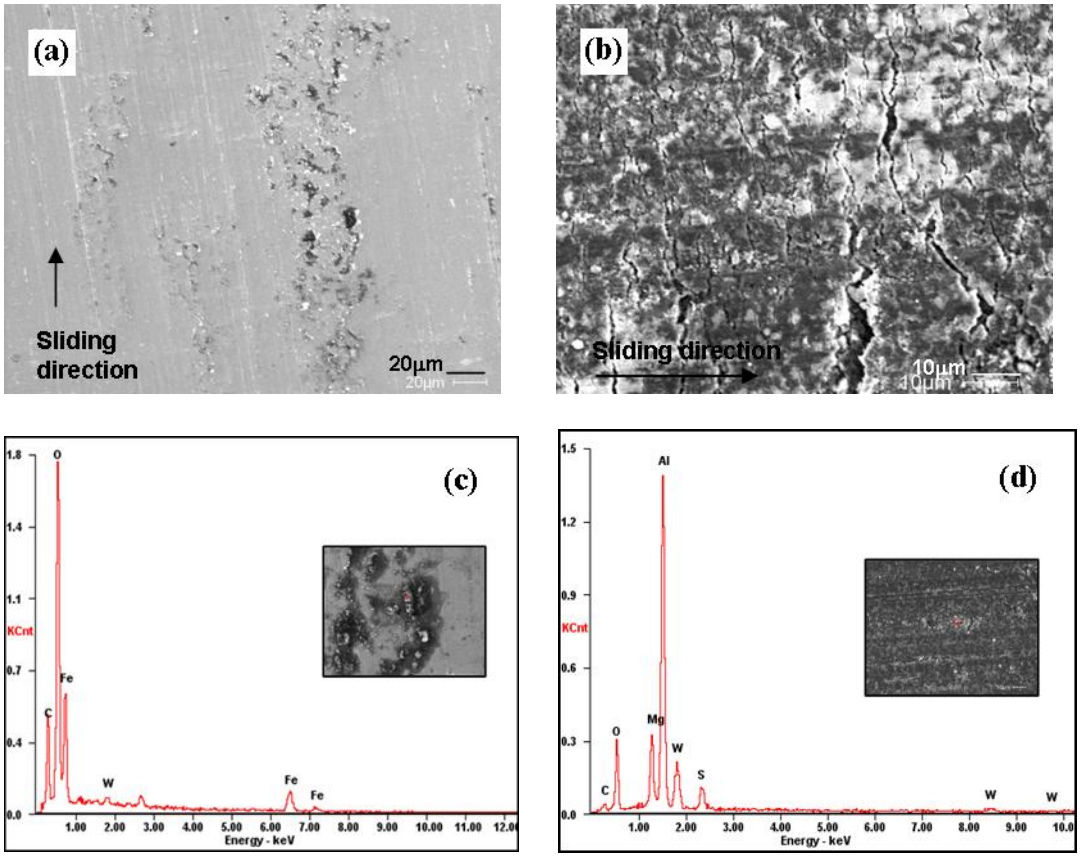

Figure 28 Polished uncoated pin against the WS2 coated strip, (a) SEM of as-received uncoated pin surface, (b) SEM of S.B. WS_2 coated strip surface, (c) EDS of material adhesion on uncoated pin surface, and (d) EDS of wear track of S.B. WS_2 strip

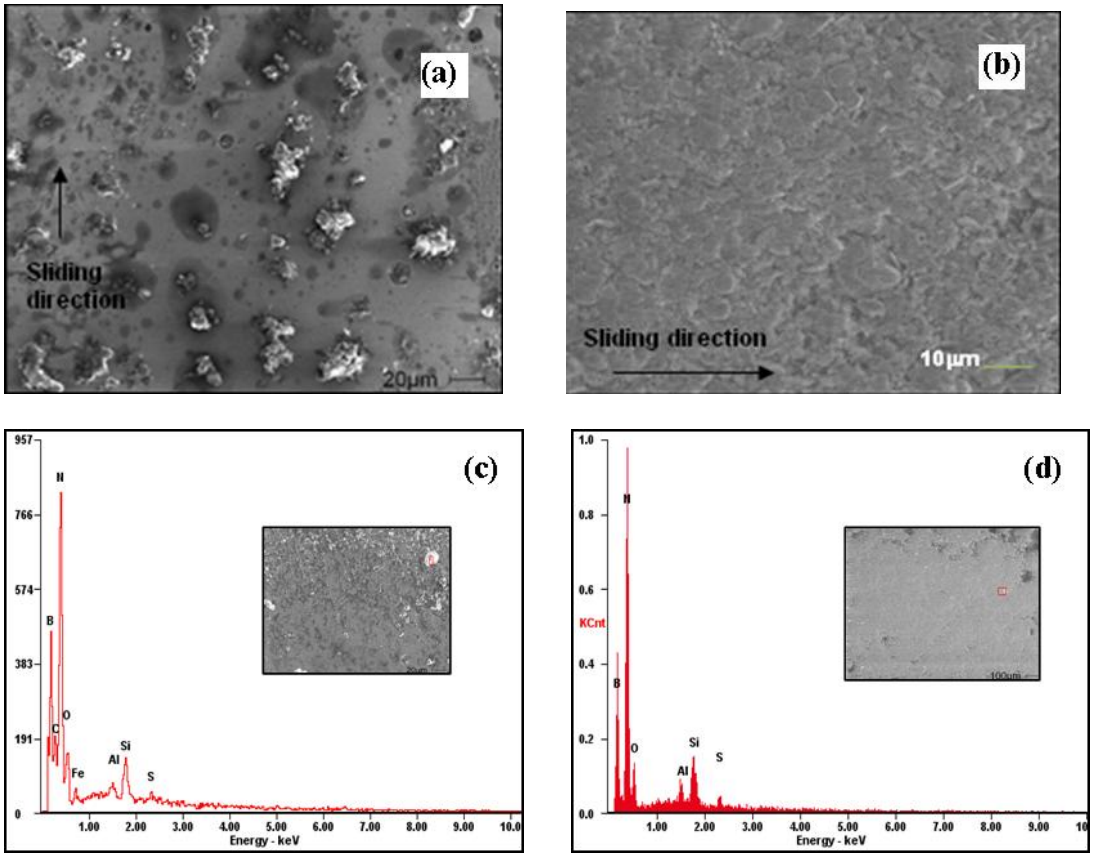

Figure 29 Polished uncoated pin against the BN coated strip, (a) SEM of as-received uncoated pin surface, (b) SEM of BN coated strip surface, (c) EDS of material adhesion on uncoated pin surface, and (d) EDS of wear track of BN strip

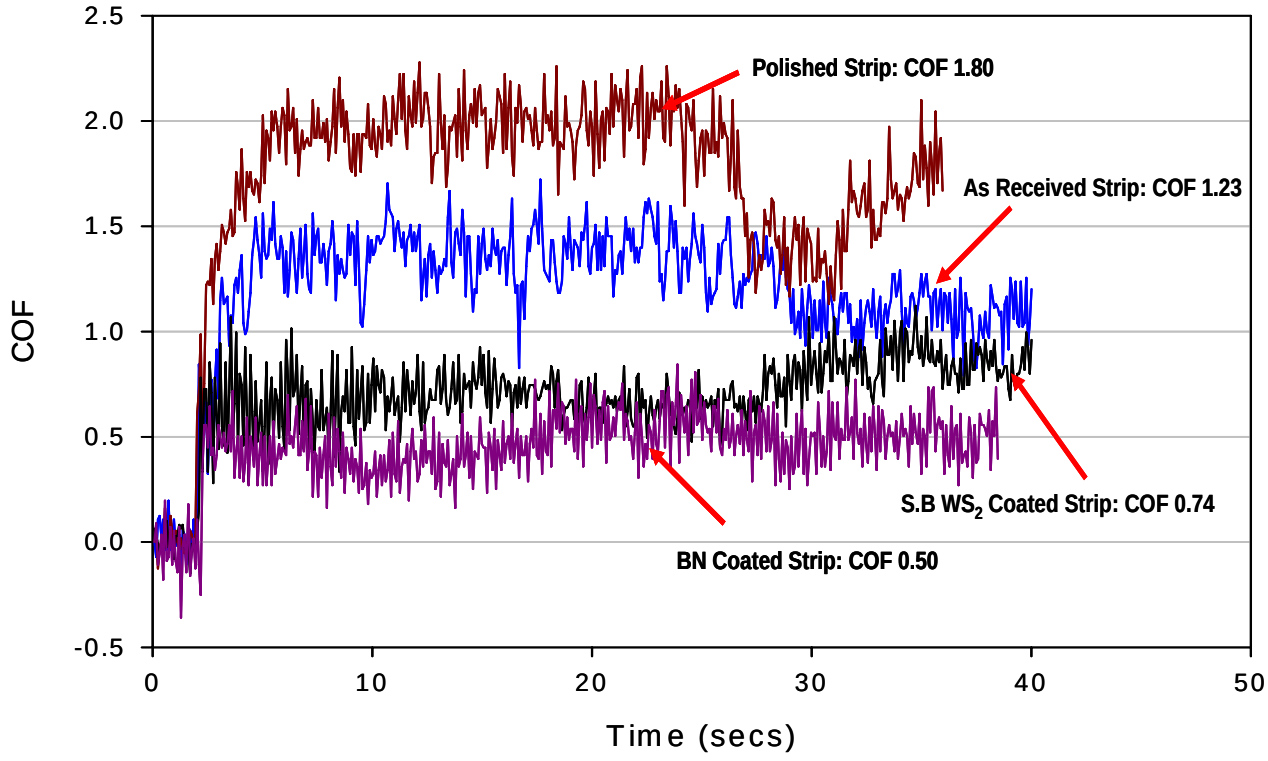

Figure 30 COF-Time curves for the S.B. WS_2 coated P20 steel pin against the various surface conditions of the AA5083 aluminum strip

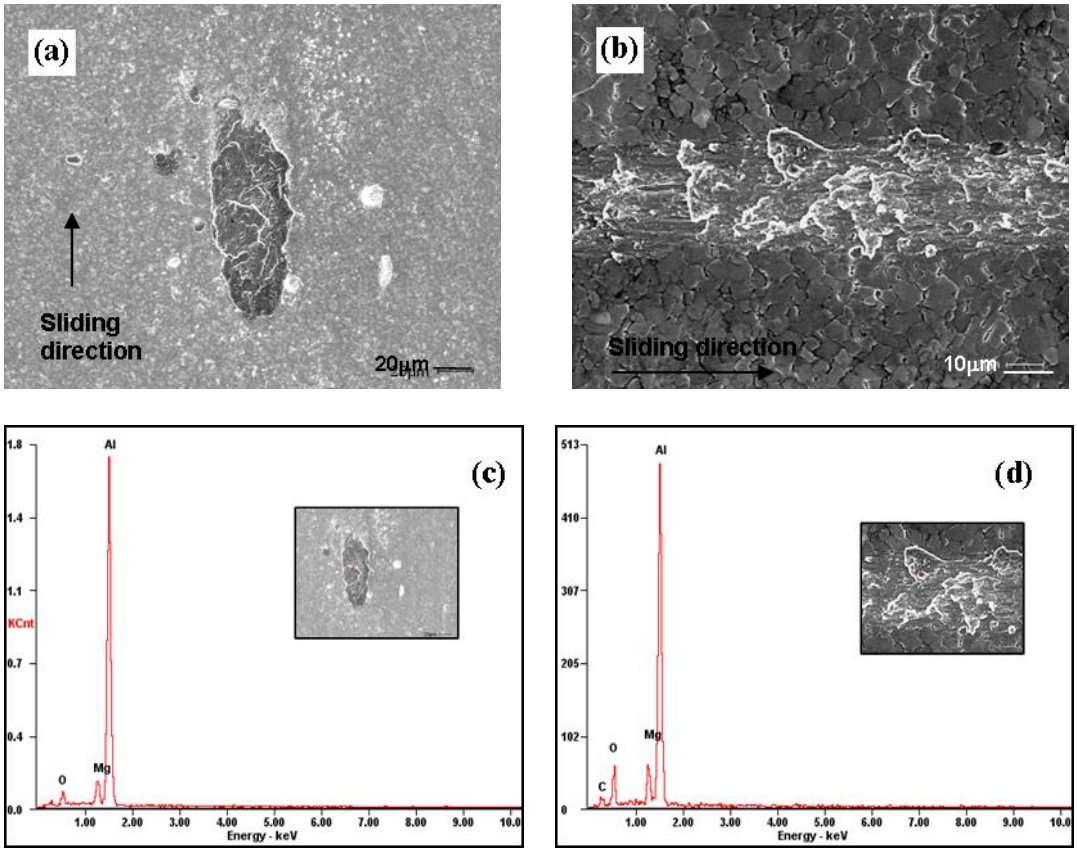

Figure 31 S.B. WS_2 coated pin against the polished strip, (a) SEM of S.B. WS_2 coated pin surface, (b) SEM of polished strip surface, (c) EDS of material adhesion on S.B. WS_2 coated pin surface, and (d) EDS of wear track of polished strip

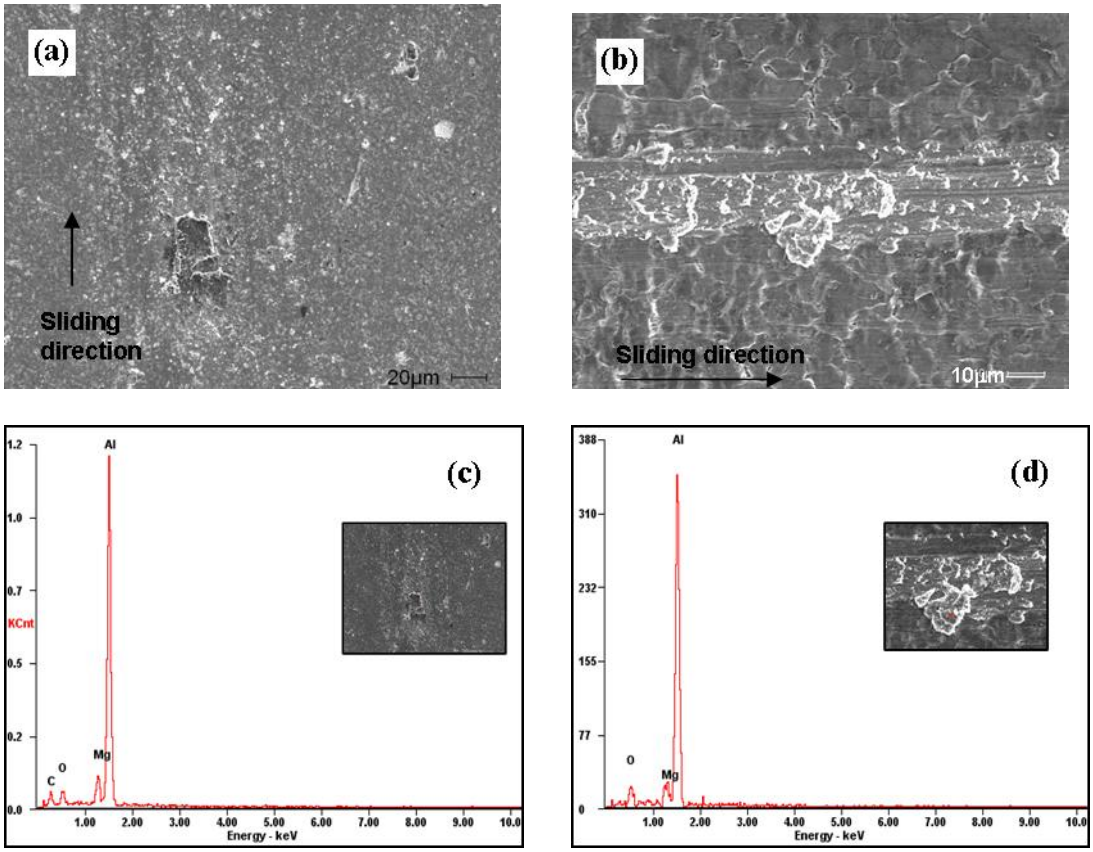

Figure 32 S.B. WS_2 coated pin against the as-received strip, (a) SEM of S.B. WS_2 coated pin surface (b) SEM of as-received strip surface, (c) EDS of material adhesion on S.B. WS_2 coated pin surface, and (d) EDS of wear track of as-received strip

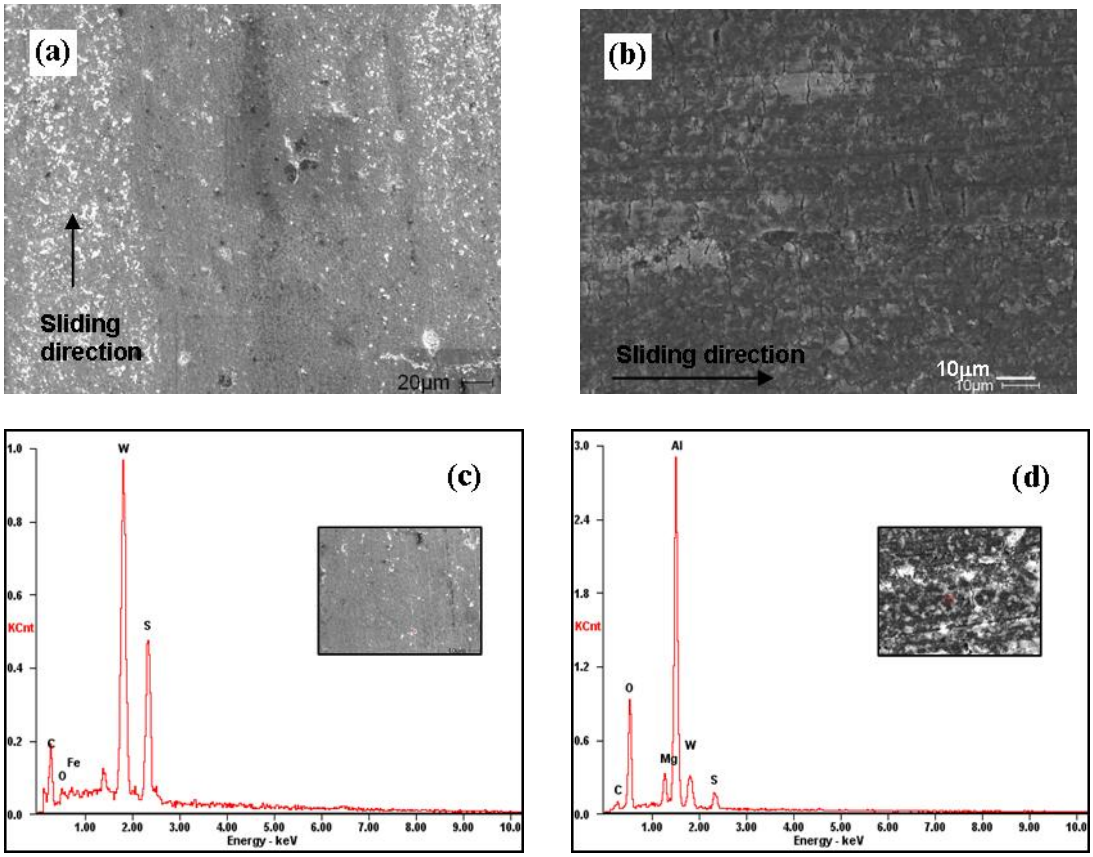

Figure 33 S.B. WS_2 coated pin against the S.B. WS_2 coated strip, (a) SEM of S.B. WS_2 coated pin surface, (b) SEM of S.B. WS_2 coated strip surface, (c) EDS of material adhesion on S.B. WS_2 coated pin surface, and (d) EDS of wear track of S.B. WS_2 strip

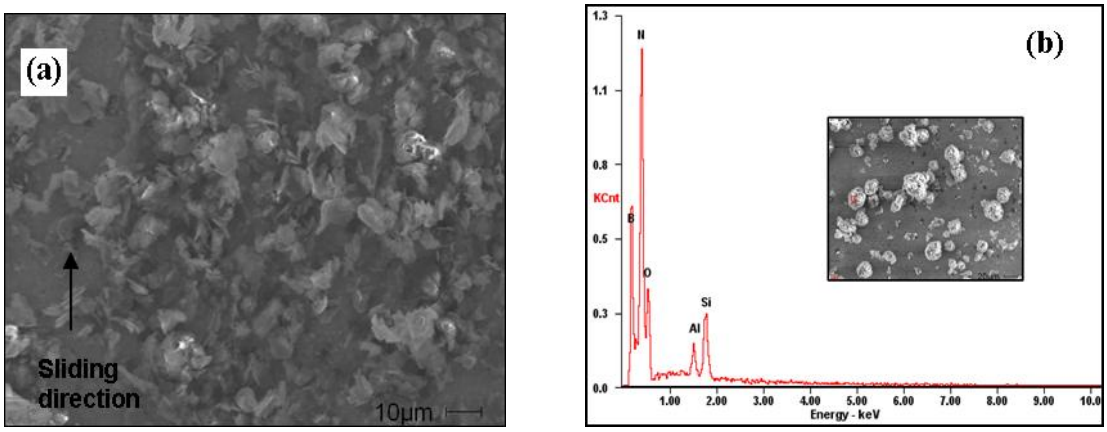

Figure 34 S.B. WS_2 coated pin against the BN coated strip, (a) SEM of S.B. WS_2 coated pin surface, and (b) EDS of material adhesion on S.B. WS_2 coated pin surface

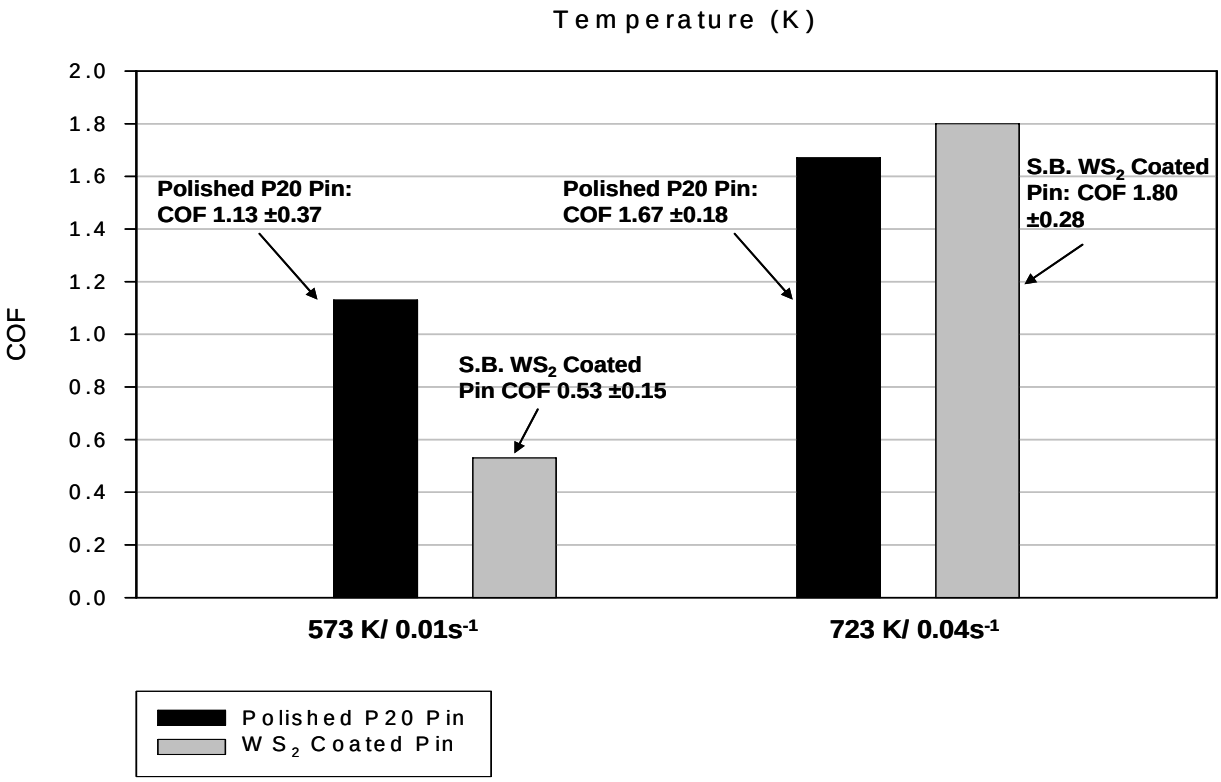

Figure 35 Histogram comparing COF of S.B. WS_2 coated pin against polished strip at 723 K/0.04s^{-1} and 573 K/0.01s^{-1} with the COF of polished uncoated pin against polished strip at 723 K/0.04s^{-1} and 573 K/0.01s^{-1}

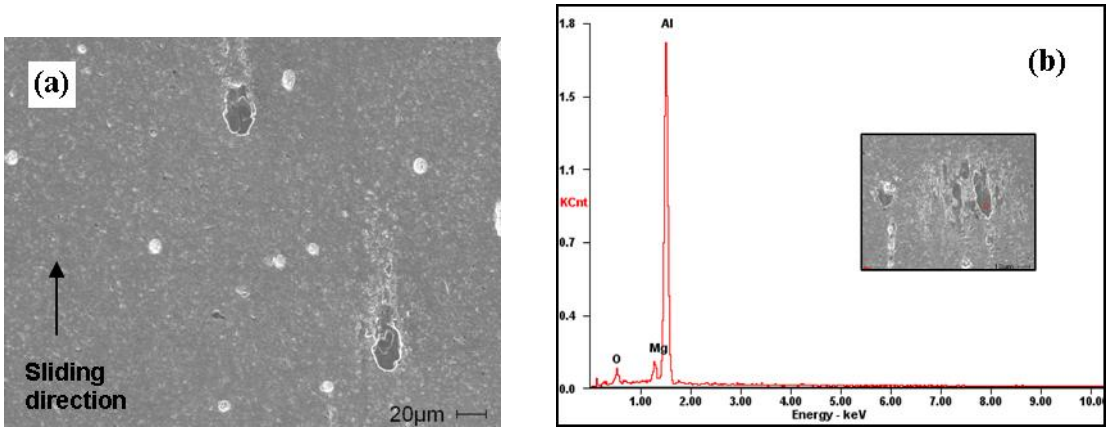

Figure 36 S.B. WS_2 coated pin against the polished strip at 573 K/0.01s^{-1} (a) SEM of S.B. WS_2 coated pin surface, (b) EDS of material adhesion on S.B. WS_2 coated pin surface

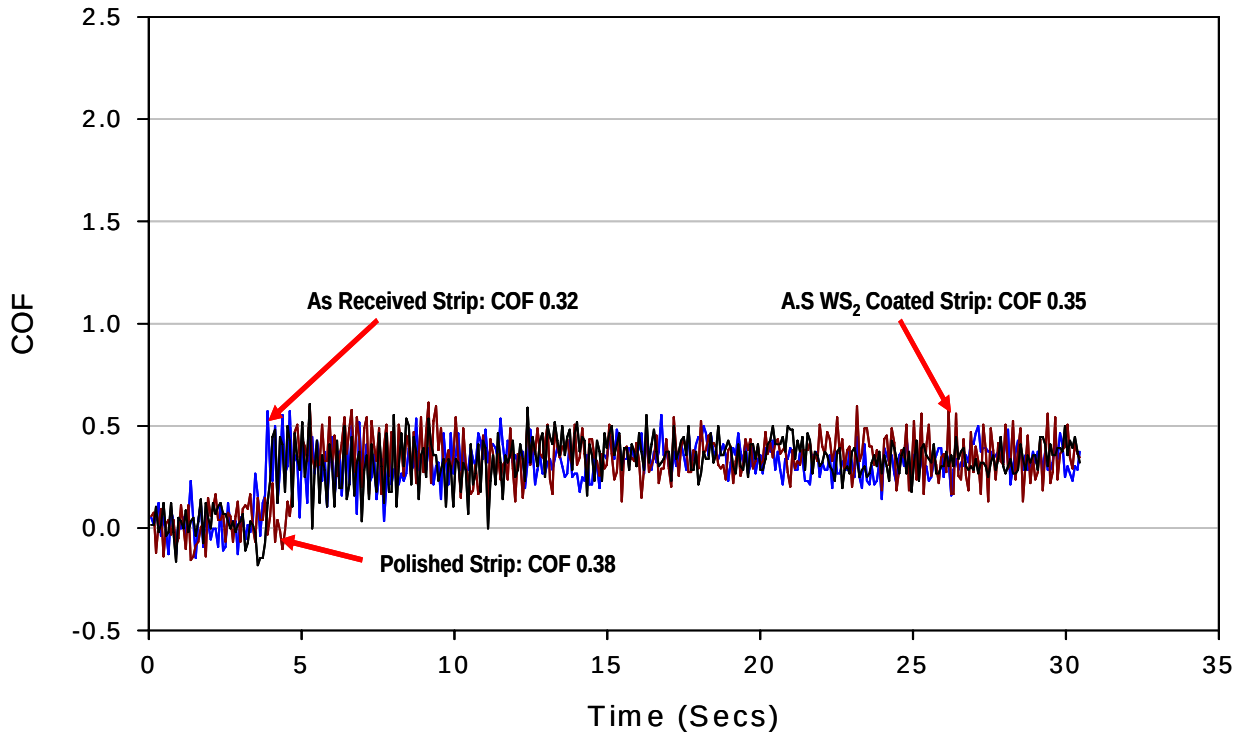

Figure 37 COF-Time curves for the A.S. WS_2 coated P20 steel pin against the various surface conditions of the AA5083 aluminum strip

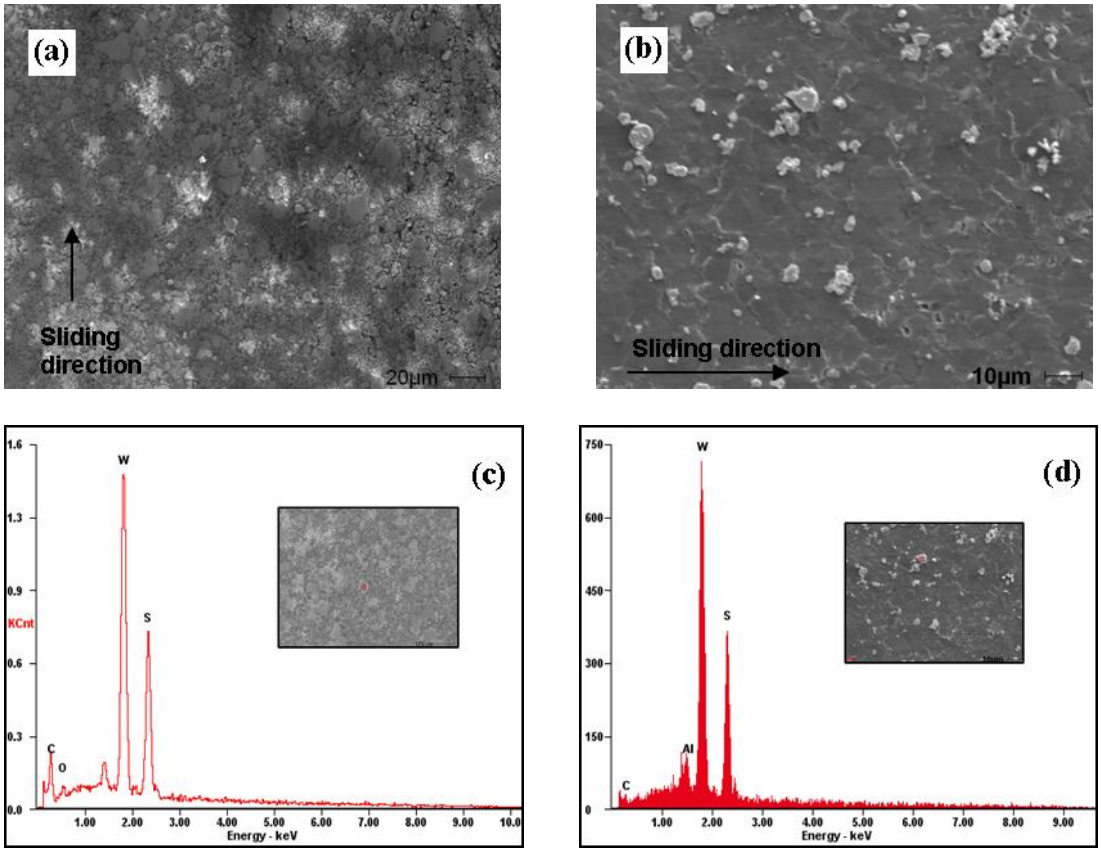

Figure 38 A.S. WS_2 coated pin against the polished strip, (a) SEM of A.S. WS_2 coated pin surface, (b) SEM of polished strip surface, (c) EDS of A.S. WS_2 coated pin surface, and (d) EDS of wear track of polished strip

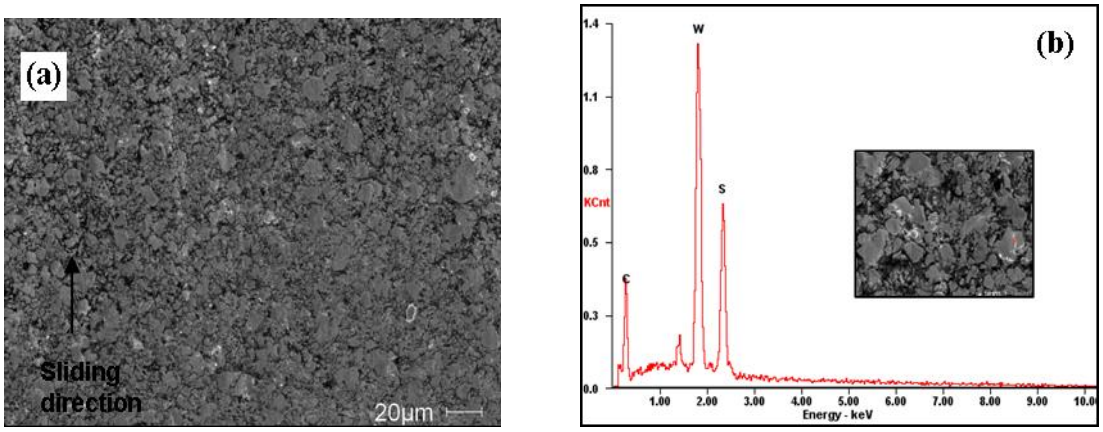

Figure 39 A.S. WS_2 coated pin against the as-received strip, (a) SEM of A.S. WS_2 coated pin surface, (b) EDS of A.S. WS_2 coated pin surface

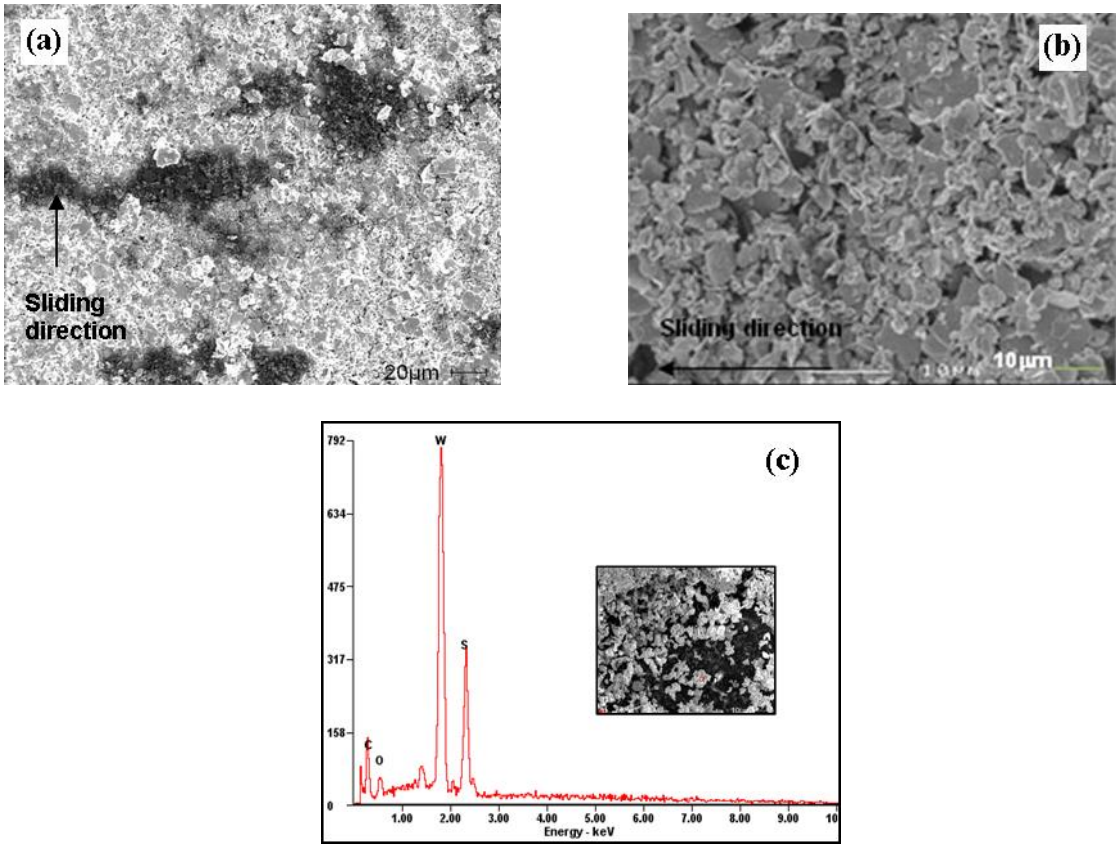

Figure 40 A.S. WS_2 coated pin against the A.S. WS_2 coated strip, (a) SEM of A.S. WS_2 coated pin surface, (b) SEM of A.S. WS_2 coated pin surface, (c) EDS of A.S. WS_2 coated pin surface

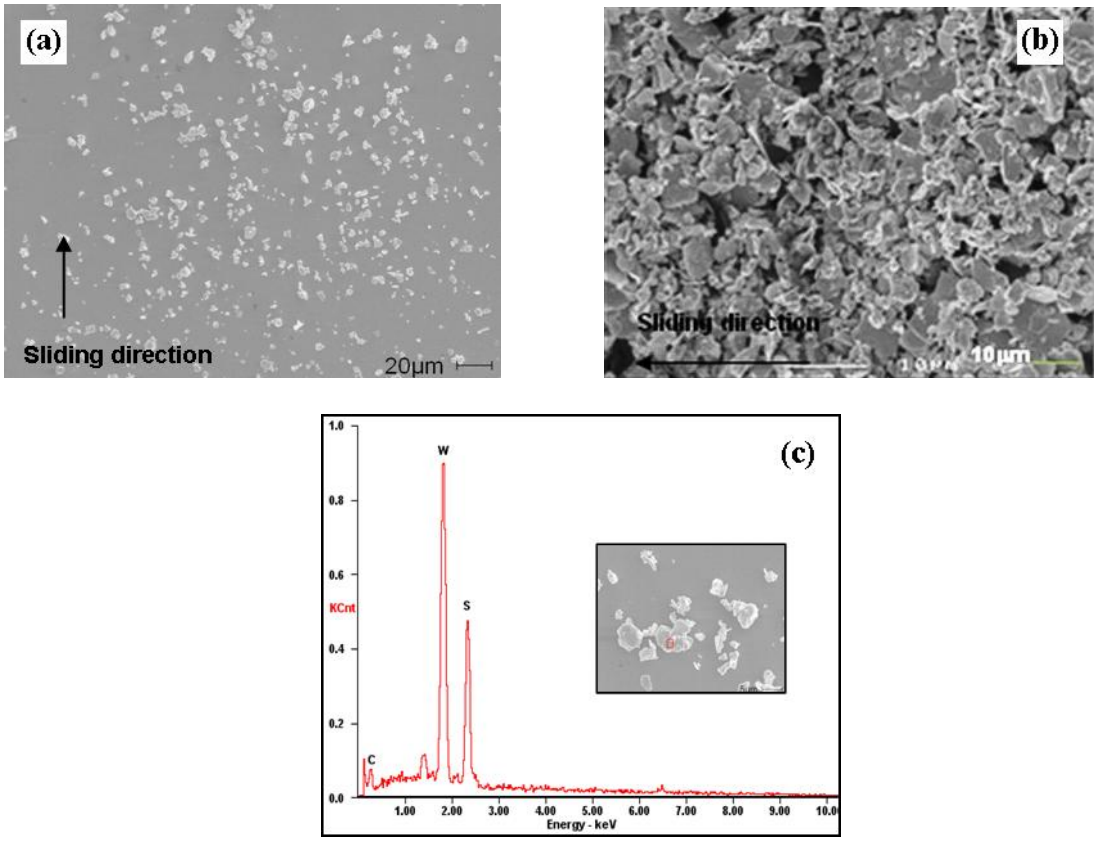

Figure 41 Polished uncoated pin against the A.S. WS_2 coated strip, (a) SEM of polished uncoated pin surface, (b) EDS of material transfer on polished uncoated pin surface

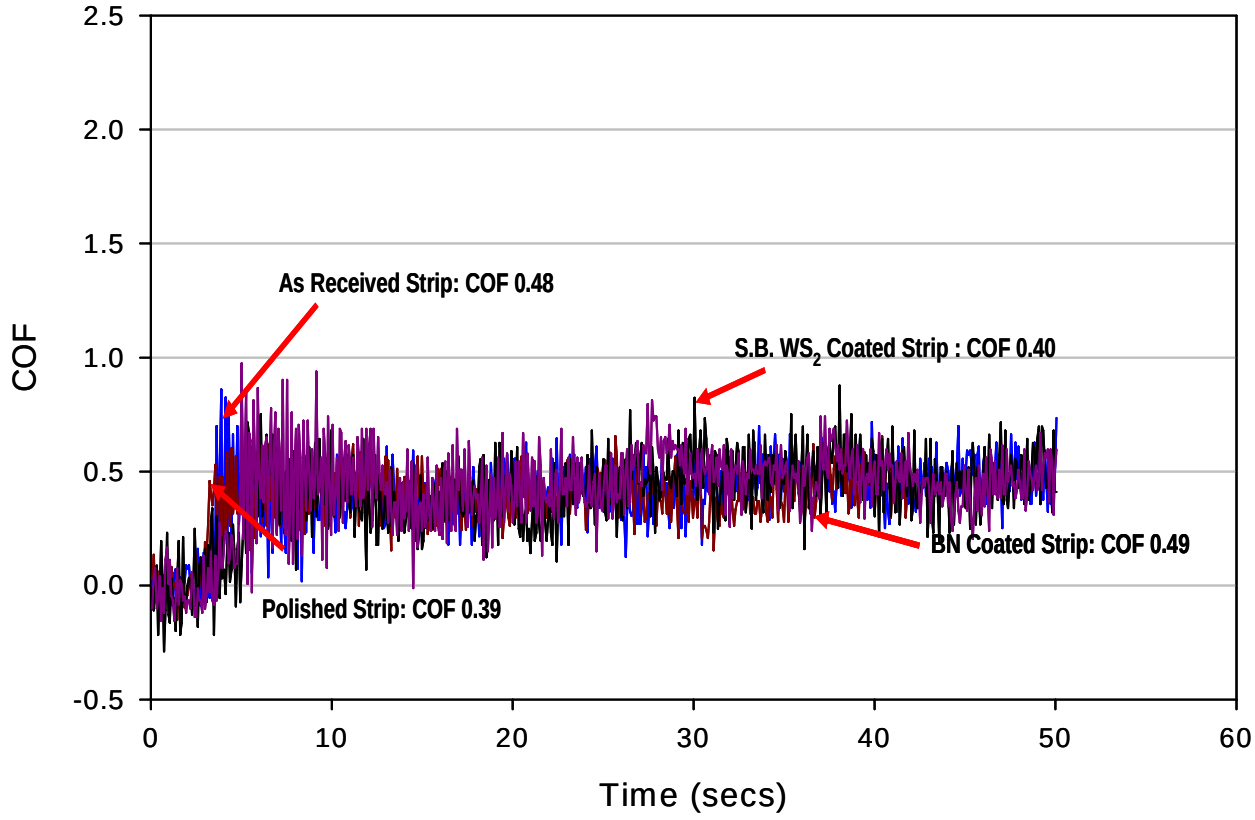

Figure 42 COF-Time curves for the BN coated P20 steel pin against the various surface conditions of the AA5083 aluminum strip

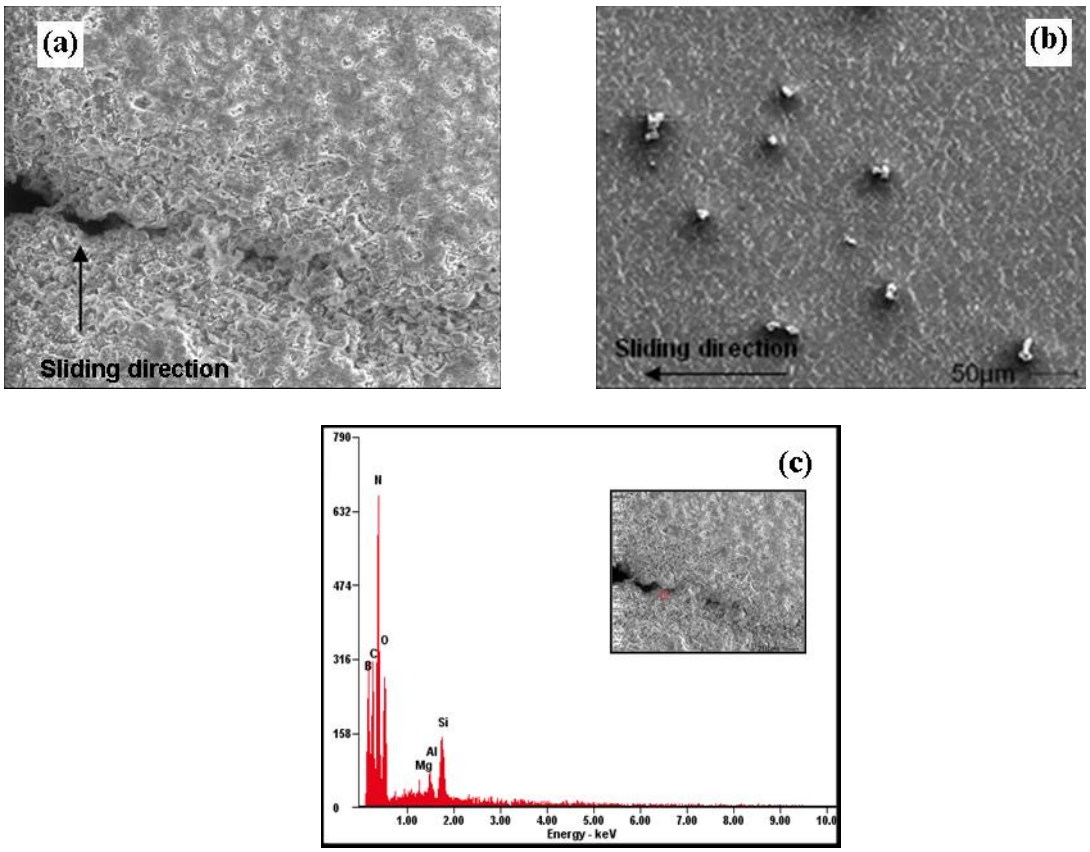

Figure 43 BN coated pin against the polished strip, (a) SEM of BN coated pin surface, (b) SEM of polished strip surface, (c) EDS of BN coated pin surface

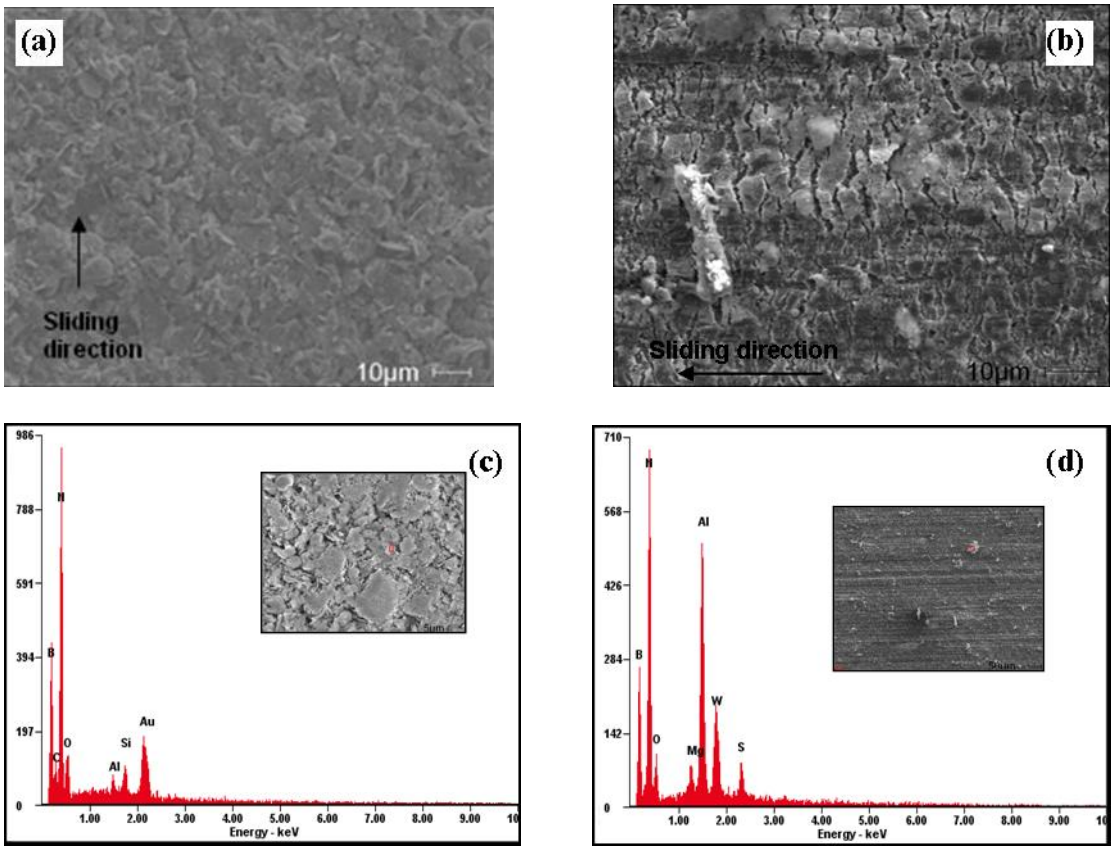

Figure 44 (a) SEM of BN coated pin surface against the as-received strip, (b) SEM of S.B. WS_2 coated strip surface run against BN coated pin, (c) EDS of BN coated pin run against as-received strip surface, (d) EDS of S.B. WS_2 coated strip run against BN coated pin surface

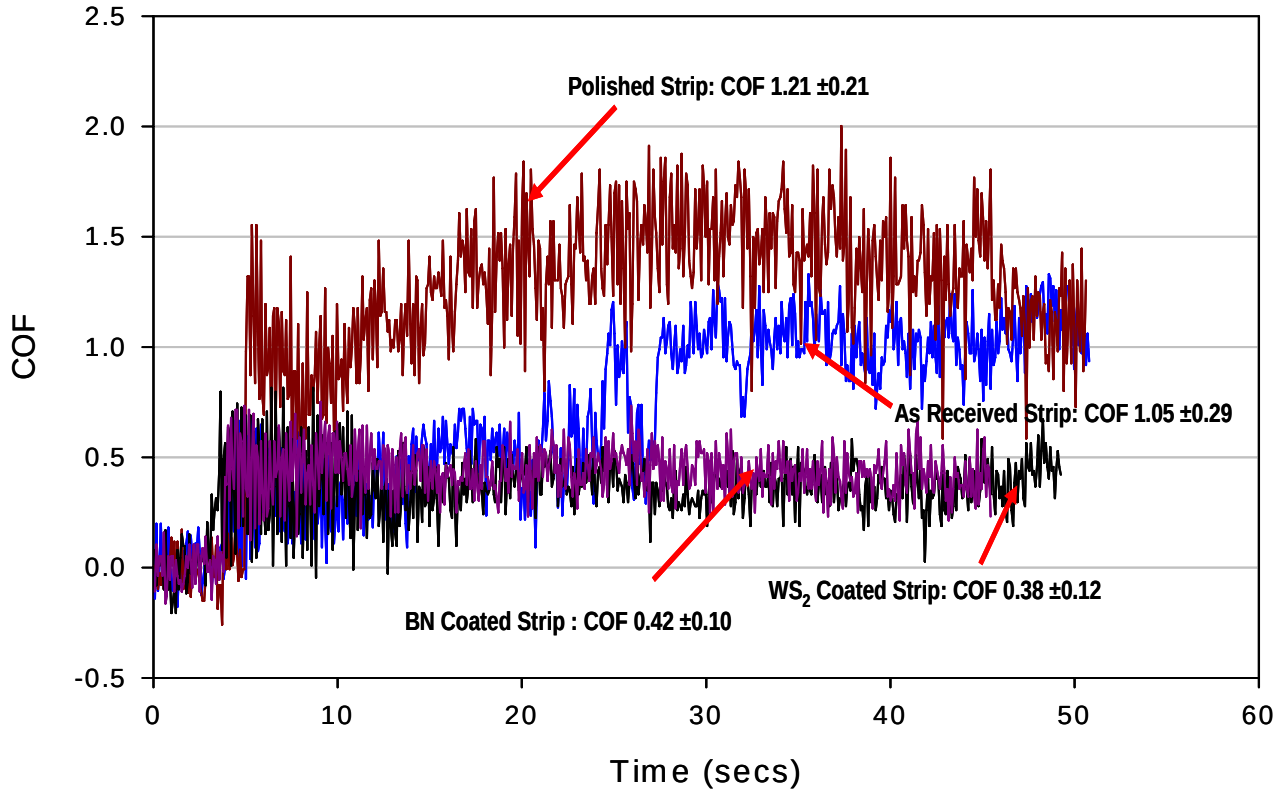

Figure 45 COF-Time curves for the DLC TB40 coated P20 steel pin against the various surface conditions of the AA5083 aluminum strip

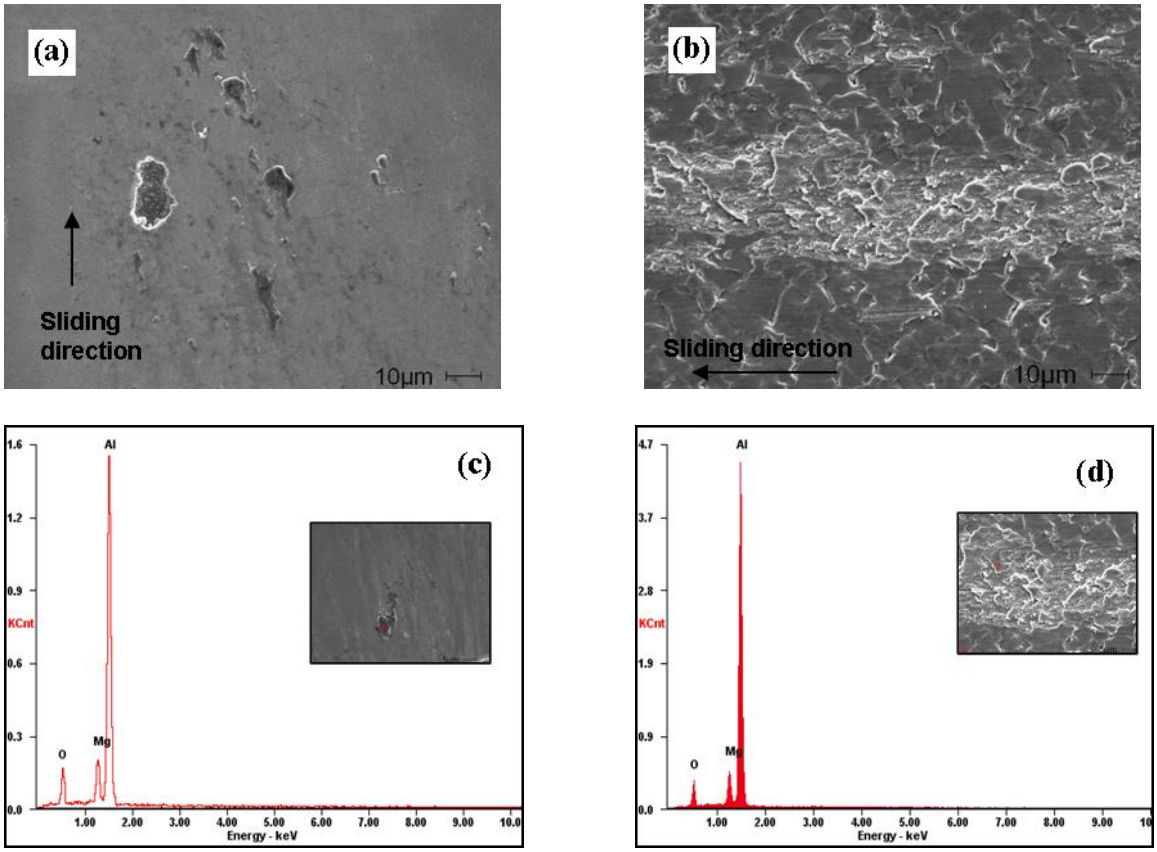

Figure 46 DLC TB40 coated pin against the polished strip, (a) SEM of TB 40 coated pin surface, (b) SEM of polished strip surface, (c) EDS of material adhesion on TB 40 coated pin surface, and (d) EDS of wear track of polished strip

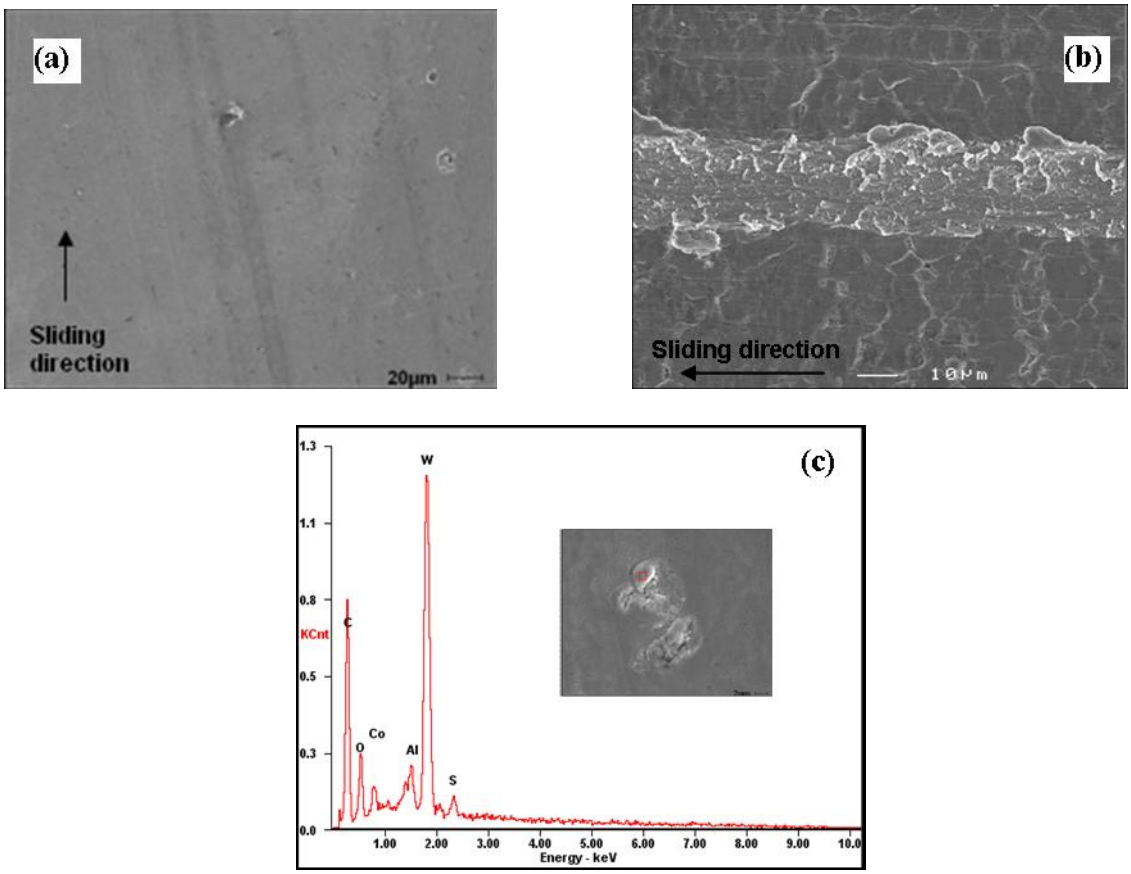

Figure 47 DLC TB40 coated pin against the as-received strip, (a) SEM of TB 40 coated pin surface, (b) SEM of as-received strip surface, (c) EDS of material adhesion on TB 40 coated pin surface

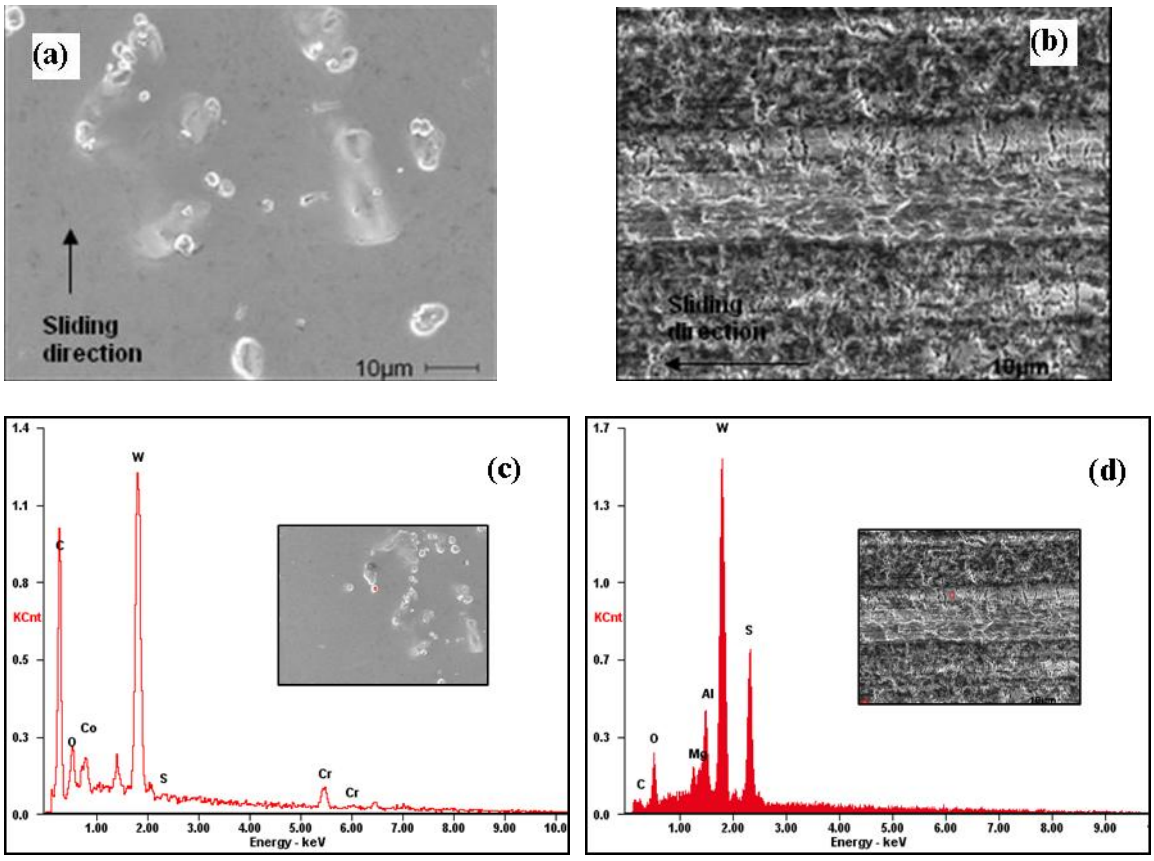

Figure 48 DLC TB40 coated pin against the S.B. WS_2 coated strip, (a) SEM of TB 40 coated pin surface, (b) SEM of S.B. WS_2 coated strip surface, (c) EDS of material adhesion on TB 40 coated pin surface, and (d) EDS of wear track of S.B. WS_2 coated strip

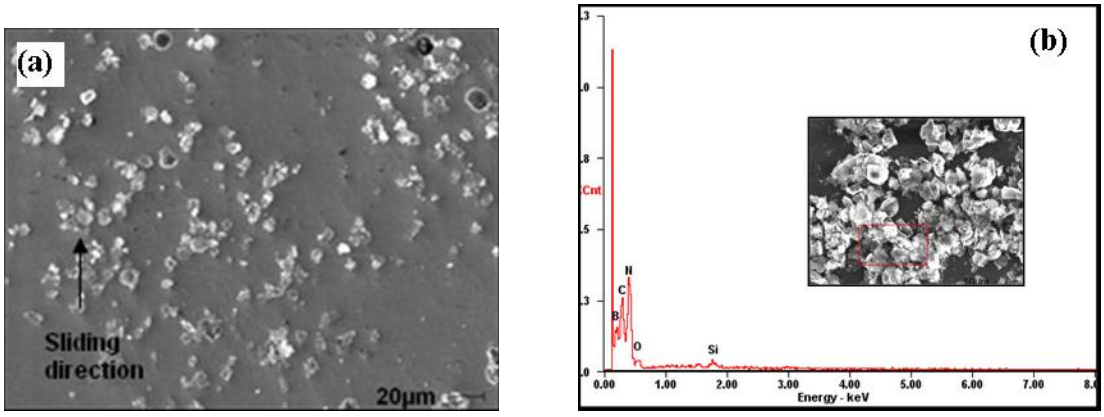

Figure 49 DLC TB40 coated pin against the BN coated strip, (a) SEM of TB 40 coated pin surface, (b) EDS of material adhesion on TB 40 coated pin surface

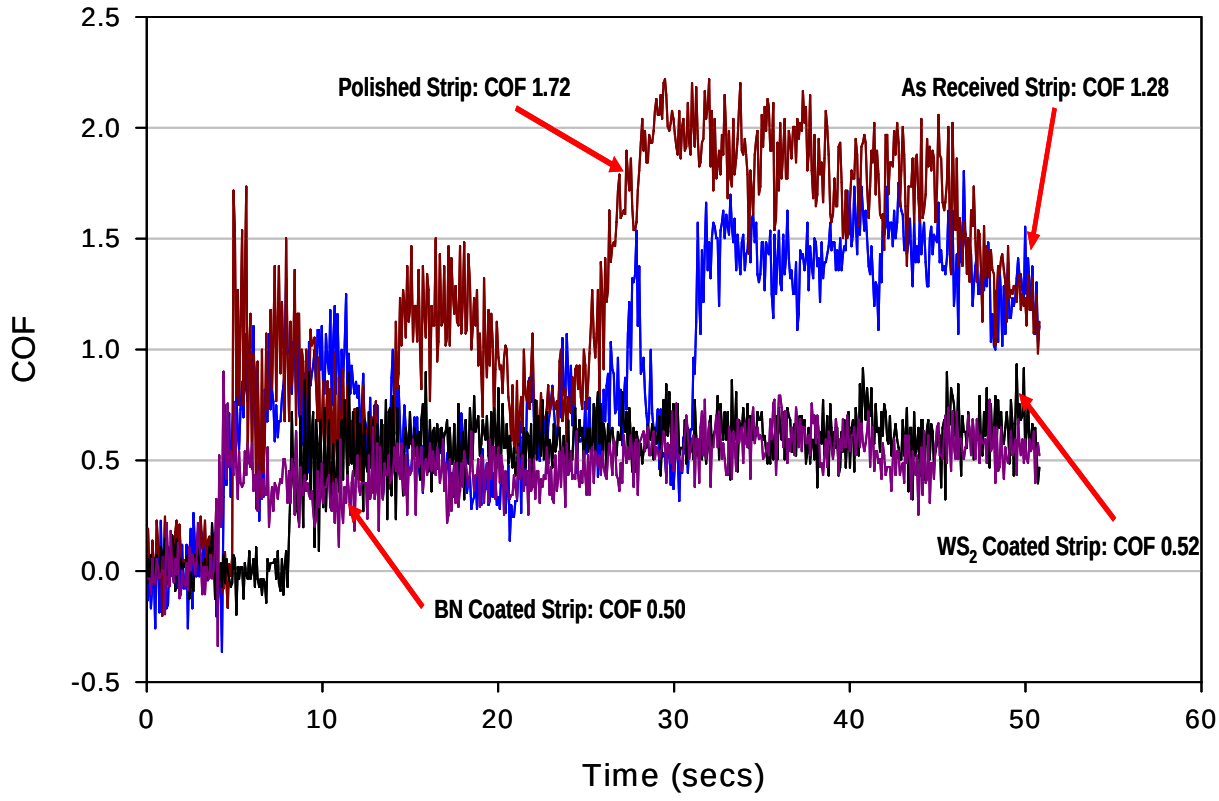

Figure 50 COF-Time curves for TB41 coated P20 steel pin against the various surface conditions of the AA5083 aluminum strip

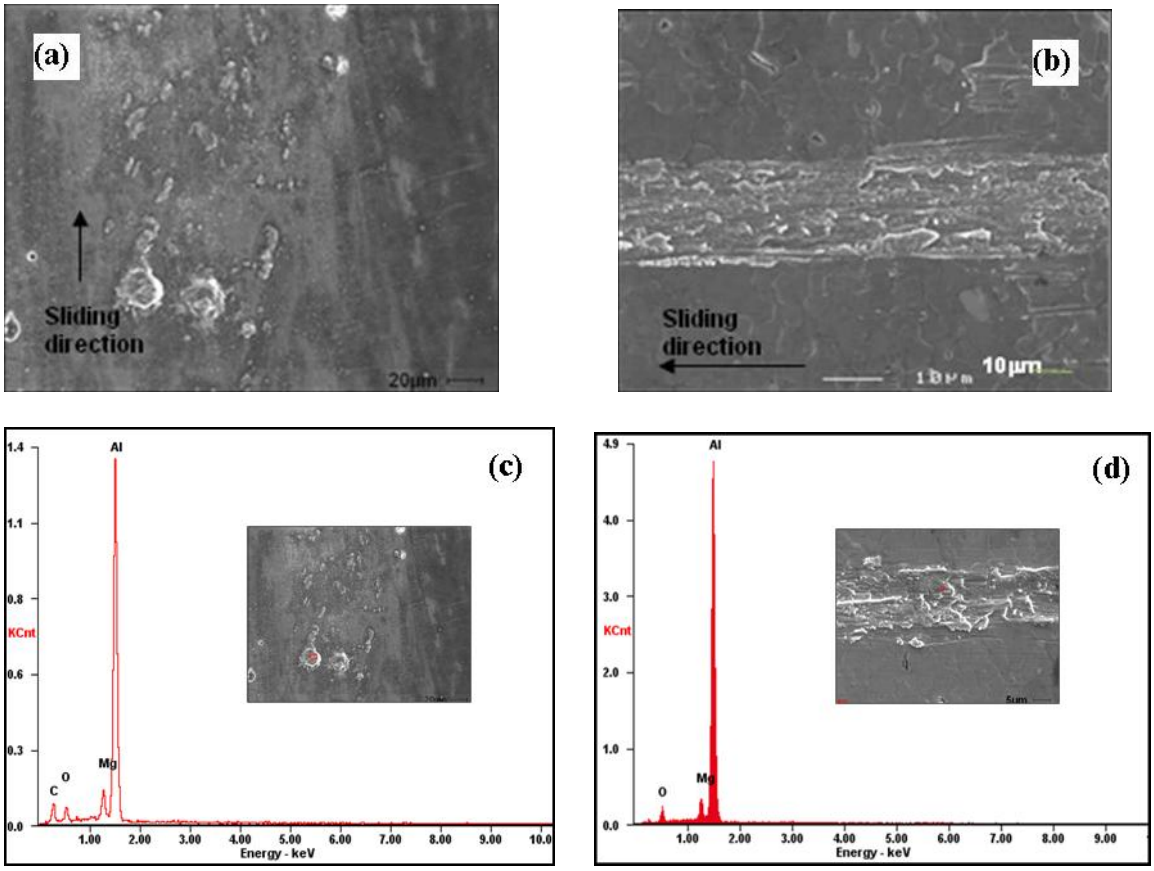

Figure 51 DLC TB41 coated pin against the polished strip, (a) SEM of TB 41 coated pin surface, (b) SEM of polished strip surface, (c) EDS of material adhesion on TB 41 coated pin surface, and (d) EDS of wear track of polished strip

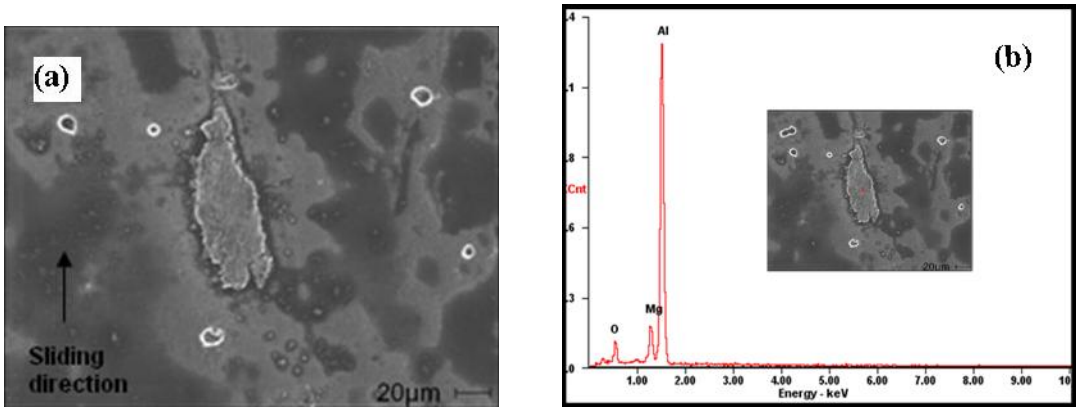

Figure 52 DLC TB41 coated pin against the as-received strip, (a) SEM of TB 41 coated pin surface, and (b) EDS of material adhesion on TB 41 coated pin surface

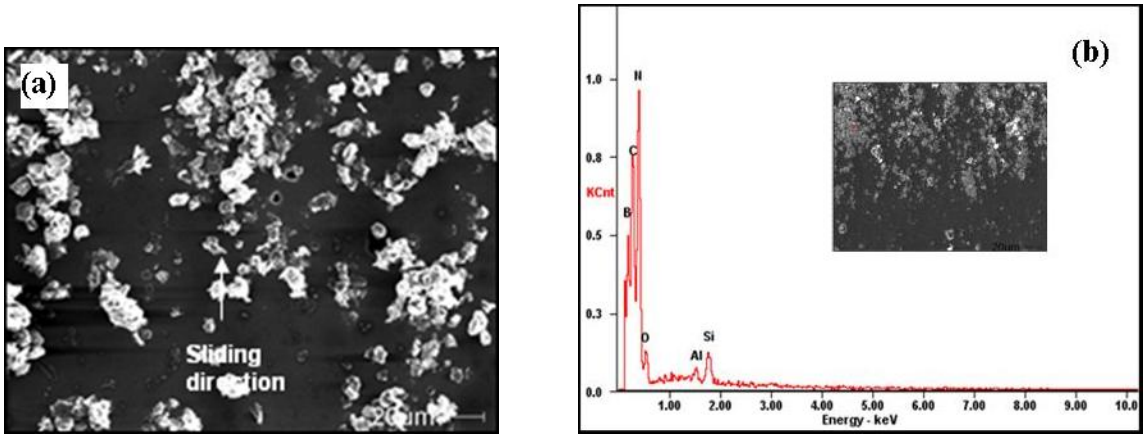

Figure 53 DLC TB41 coated pin against the BN coated strip, (a) SEM of TB 41 coated pin surface, (b) EDS of material adhesion on TB 41 coated pin surface

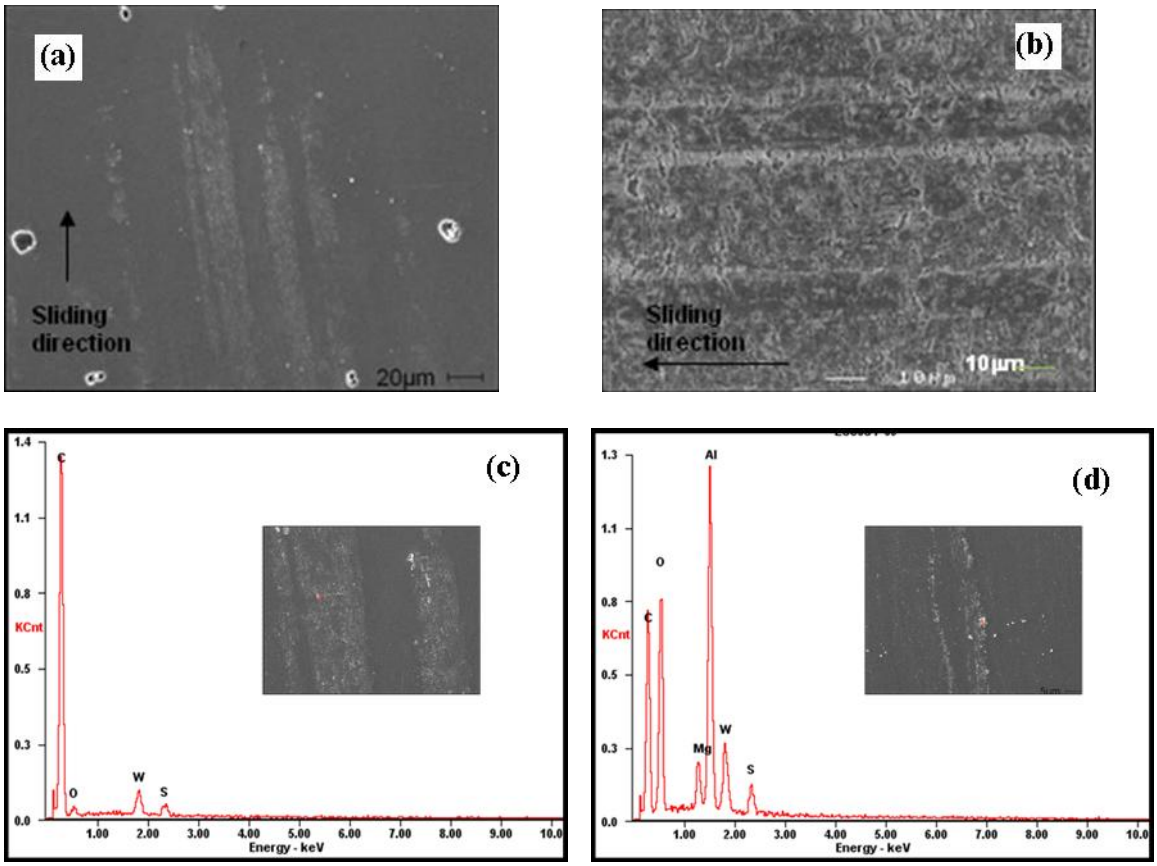

Figure 54 DLC TB41 coated pin against the S.B. WS_2 coated strip, (a) SEM of TB 41 coated pin surface, (b) SEM of S.B. WS_2 coated strip surface, (c) EDS of material adhesion on TB 41 coated pin surface, and (d) EDS of material adhesion on TB 41 coated pin surface

CHAPTER V

DISCUSSION

5.1 Hot Rolling: Local Shear Deformation

The disturbed layer does not have a well-defined structure and composition. However, in the case of aluminum alloys, which often contain magnesium, the disturbed layer is rich of magnesium, especially on the outer layers. The disturbed layer consists of magnesium and aluminum oxides and contains some amount of carbon (from rolling lubricants). The structure can be layered, or it can be just a mixture of oxide and aluminum with micro voids. Due to the high diffusion rate of magnesium towards the aluminum surface, the surface is already rich of Mg when the sample is preheated to the hot rolling temperature (753 K). This is confirmed by the GDOES analysis of the as polished sample and the polished and heated sample (Figures 21a and 21b). Thus the magnesium-rich layer first comes into contact with the roll surface, and any transferred material on the roll surface is rich in Mg [3].

The relative motion between the aluminum workpiece and roll surfaces depends on the amount of forward slip. Taking into consideration the roll surface morphology consisted of discontinuous grinding grooves (Figure 9), the following events are responsible for the surface damage during the initial stages of rolling:

i) During the rolling process, the hot aluminum squeezes into the grooves and forms micro wedges.

ii) These micro wedges contain small volumes of aluminum but have a higher surface area as compared to the flat regions. Since the wedges are under lower constraint,

they undergo plastic deformation easier than the flat surfaces.

iii) As a result, when the squeezed aluminum (micro wedge) is sliding against the groove on the roll surface (due to forward slip), it experiences more severe plastic deformation than the other areas especially if the groove depth is high and lubricant breakdown occurs. This can be seen in Figure 4a on the surface of AA3104 rolled in one (1) pass at 12% forward slip. The localized shear deformations on the wedges appear as shingles. A schematic of this process is shown in Figures 55 and 56.

5.2 Effects of Forward Speed and Rolling Passes

In this study a positive forward slip of 12% (higher than usual values in rolling of aluminum) was selected to accelerate the surface evolutions on the rolled surfaces. It was observed that rolling AA3104 in one pass was enough to cause localized shear deformations on the surface in the form of shingles (Figure 17a). The presence of subsurface cracks shown in Figure 17c suggests that this surface feature might delaminate and transfer to the roll surface in the subsequent contacts. Some of these shingles include small pieces of debris as shown in Figure 18.

The observed high concentration of both Mg and O is consistent with the composition of the disturbed layer formed during the actual rolling process. On the second rolling pass the local presence of severely deformed areas (in the form of shingles) becomes more pronounced. As is shown in Figure 19c, more Mg-rich oxide debris (Figures 19d and 19e) becomes embedded on the generated surface. The deformed layer (tip of the shingle) consists of two sub-layers. This suggests that each sub-layer is formed during each pass of rolling. Considering the shingle feature (defect) in Figure

19a, the total length of the defect is 20 μm. At the sample rolling speed of 21 mm/s, and 12% forward slip, a 20 μm length of the sample slid forward 2.4 μm against the roll surface. The length of the deeper sub-layer in Figure 19c is 2 μm, and the length of the shallower sub-layer is 1.5 μm. The 0.4 μm shorter length of the shallower sub-layer compared with the calculated length can be related to slipping of the surfaces. The deeper sub-layer is 0.9 μm shorter than the calculated value which is probably related to the different surface condition of the roll on the second pass. In the first pass the roll surface was initially clean and as soon as lubricant breakdown occurred, aluminum came into direct contact with steel and adhered to the roll surface (i.e. the coefficient of friction was high), and hence the surface become elongated. However, in the second pass a thin transferred film covered the roll surface. This layer consisted of C, O, Mg, and Al and reduced the coefficient of friction. The roll surface film could also act as a barrier for adhesion of more aluminum to the roll surface as in the case of lubricant breakdown. Therefore, adhesion of the aluminum and roll surfaces was weaker compared to the first pass and led to a shorter and shallower sub-layer in Figure 19c. Hence, it is concluded that each individual layer in Figure 19c was formed during each rolling pass.

When the two rolling passes were in opposite directions, the localized shear deformations were flatter and embedded on the aluminum surface as is shown in Figure 20a. The cross-section of the defect, Figure 20b, shows that the generated layer on the surface is uniform and consists of C, O, Al, and a very high level of Mg (Figure 20c) similar to the composition of the disturbed layer. Therefore, at 12% forward slip the generation of localized shear deformed areas is more pronounced after 2 passes in the

same direction than in a single pass, but is less pronounced with features more embedded in the surface with two passes in the opposite directions.

In order to observe the effect of forward slip on the generation of surface defects, a comparison can be made of the AA3104 hot rolled surfaces at a forward slip of 1% (Figure 15) and those rolled at 6.5% (Figure 16). At 1% forward slip, visible loss of the total reflectance can be observed due to the burning in of C from the lubricant. Surface defects here appear as oxide flakes and gorges. At a forward slip of 6.5% there is more severe deformation observed on the surface with cavities, shingle formation being more prominent. Comparing both forward slips after 1 pass, at 1% (Figure 16a) the surface defects are in the form of oxide flakes and broken intermetallic precipitates covering the surface. At 6.5% forward slip, the surface is covered with shingles and cavities with no visible intermetallic precipitates which are likely embedded underneath the shingles. An increase in the forward slip from 1% forward slip to 6.5% forward slip thus induces more severe deformation on the surface as highlighted by the increase in severity of surface defects observed.

The -1% forward slip specimens produced after a single rolling pass were also selected for analysis. As is shown in Figure 21b, a thin, non-uniform layer (with average thickness of 70 nm) consisting of high amounts of O, Mg, and Al and a high amount of C (Figure 21c) was formed on the surface. The thickness of the disturbed layer formed during rolling with -1% forward slip was thinner than that produced at 12% forward slip in one pass (150 nm thick layer shown in Figure 18c). This indicates that the thickness of the disturbed layers is higher at higher forward slips.

5.3 Mechanisms of Generation of Disturbed Layer

The trend of surface evolution as a function of forward slip and number of rolling passes, described above, is consistent with the results obtained from GDOES for elemental depth profiling analysis. The concentration of Mg on the polished-heated sample (Figure 22b) is the same as the Mg concentrations on the samples rolled in one pass at 12% and -1% forward speeds (Figures 23a and 24a, respectively). Therefore, there is no considerable transfer to-and-from the roll taking place during rolling in the first pass: it is assumed that the removal of the Mg rich layer from the surface provides sufficient energy to enhance the diffusion of Mg towards the surface. However, after two passes in the same rolling direction, at 12% forward slip (Figure 23b), there is 60% increase in the concentration of Mg and a slight increase in the concentration of Mg at -1% forward speed (Figure 24b) compared to that of polished-heated sample. This increase in the Mg concentration may be related to the local shear deformations similar to the multi-layer features as those shown in Figure 19c.

The above interpretation sheds light on the generation mechanism of the disturbed layer. During the initial stages of the formation of the disturbed layer, it was found that the changes on the morphology, thickness, and composition of the defects on the rolled surfaces were functions of the forward speed and the number of rolling passes. More specifically, the results suggest that at higher number of rolling passes, some of the localized shear deformed areas on the surface can delaminate (see Figure 17c), transfer to the roll surface, and back transfer to the rolled surfaces on consequent contacts. During this process, a large fraction of the delaminated debris oxidizes and becomes

contaminated with the rolling lubricant. Finally, when it transfers back to the sheet surface and becomes embedded in this surface, it becomes a part of the disturbed layer. One might also expect that some of this back-transferred debris accumulates on top of each other or in the localized shear deformed areas. This would lead to an increase in the thickness of the disturbed layer and changes to the structure of the re-deposited layer. According to Figure 19c, multi-layered types of disturbed layers can also be generated during the tandem rolling process, for which the rolling in all passes is in the same direction, as explained above. At higher coefficients of friction and higher forward slips, the layered structures elongate and become more pronounced. On the other hand, during the reversing mill process the disturbed layer is not multi-layer, can be generated faster (Figure 20b), and cover more surface area of the rolled product, especially due to the higher number of passes compared to, say, tandem mills.

5.4 Hot Forming: Solid Lubricant Coating Performance – Aluminum Adhesion

The high COF recorded during the experiments were observed to be accompanied by aluminum adhesion to the steel pin with aluminum build-up being observed for the highest COF recorded. This high COF was observed for four of the six pins run against the uncoated strips; both polished and as-received the two exceptions being the pins coated with BN and A.S. WS_2. The lowest COF were accompanied with little to no aluminum adhesion to the pins, the likelihood of which increased when the aluminum strips were coated. The highest COF observed for five of the six pins were noted when the pins were run against the polished strips. During hot forming simulations the Al-Mg strips were stretched at a constant strain rate and high temperature, thus experiencing

surface deformation as well as oxidation. The performance of a coating applied to the alloy surface to mitigate aluminum adhesion would be expected to either be able to match the stretching ability of the alloy in order to protect the substrate or depend on a transfer layer initiated on mating surface to mitigate aluminum transfer.

The S.B. WS_2 coated pin recorded the highest COF against the polished strip, with the pin surface showing aluminum build-up on the surface. The white powdery patches observed on the surfaces of the coated pin (Figure 31a) are an indication of the oxidation of the WS_2 coating, as noted by Prasad et al., who distinguished WS_2 particles to appear as platelets and its oxidation to be in the form of a white powder [84]. The EDS analysis of the powdery patches confirmed the presence of O. The WS_2 coating on the surface of the pin can therefore be thought to be undergoing oxidation while it was running against strips stretched at 723 K. WO_3, a product of the oxidation of WS_2, is known to disrupt the transfer of WS_2 to the mating surface which is an essential process for WS_2 lubrication [79, 80, 84]. There was no evidence of W or S observed on either the polished strip which confirms that WS_2 transfer to the strip might not have occurred. The formation of $Al_2 (WO_4)_3$ has been noted to result from the interaction of the solid phase or molten Al_2O_3 with WO_3, the formation of which would disrupt the lubricating action of the WS_2 coating [91]. At the reduced temperature and strain rate of 573 K/0.01s^{-1}, the aluminum adhesion was observed to have reduced, appearing more as splatter on the wear surface with no of build-up occurring. It can be said then that this particular coating is better suited for lower temperature operations such as warm forming or hot stamping.

WO_3 disrupting the WS_2 coating transfer would also explain the high COF

observed in the case of the as-received strip against the S.B. WS_2 coated pin at 723 K. There is aluminum adhesion observed on the pin under this condition as well, but here there is no aluminum build-up on the pin (Figure 32a). The reduced adhesion and COF could be attributed to the increased amount of MgO on the surface of the strip due to the presence of a disturbed layer. It is expected that this layer would aid in reducing adhesion as well as COF due to the high MgO presence, which itself acts as a lubricant, on the surface of the disturbed layer. Riahi and Alpas have already shown that adhesion in Al-Mg alloys at high temperature reduces with an increase in magnesium content [63]. This in turn would explain the slight reduction in friction observed with the as-received strip against most of the pins.

The lower COF observed when the S.B. WS_2 coated pin is run against the S.B. WS_2 coated strip, was most likely due to the two WS_2 surfaces running against each other, as WS_2 does not adhere to itself. The formation of WO_3 observed on the surface of the strips at the high temperature could be contributed by the cracks and fractures observed on the coating, noticed in all cases of the S.B. WS_2 coated strips. Cracks and fractures are sites for dangling bonds which are the activation sites for oxidation of WS_2. It was observed that most of the powdery patches noticed occurred at these areas on the coating (Figure 28b). WO_3 though, is lubricious at high temperatures and on its own could possibly aid the COF reduction [79, 80]. The aluminum adhesion observed on the pins run against the S.B. WS_2 coated strips was possible due to the exposure of the Al-Mg alloy below the WS_2 coating at the fractured areas of the coating.

The polished uncoated pin recorded a low COF when run against the S.B. WS_2

coated strip. WS_2 transfer from the strip to the pin is suspected to have occurred as noted from the EDS of the pin in Figure 28c. The EDS also showed a high percentage of oxygen present on the surface of the pin, which could indicate the presence of WO_3 transferred from the oxidized coating or aluminum oxide having transferred from the substrate exposed at the fractures of the coating. The WS_2 transfer aids in the reduction of friction, encouraging the occurrence of WS_2 sliding over WS_2. There was no WS_2 accumulation observed on the pin as was the case with the uncoated pin run against BN coated strip observed when comparing Figure 28a and 29a. Their COF however, were comparable as seen in Figure 25. The COF for the uncoated polished pin against the uncoated strip were high due to the amount of aluminum adhesion which was observed in the SEM seen in Figures 26a and 27a.

The low COF recorded by the A.S. WS_2 can be generally attributed to the efficient transfer of the WS_2 platelets to the mating surface. This occurred when it was used as a coating for the pin and when it was used to coat the aluminum strip. It can be said that WS_2 sliding over WS_2 effectively occurred in all cases leading to the low COF with no aluminum adhesion observed. It also gave better protection of the substrate, not exposing any part of it as was the case with the S.B. WS_2 coating on the strips. It could be suggested that the presence of carbon could contribute to WS_2 performance; one of the noted application methods for WS_2 is mixing it with oil or grease to enhance the lubrication properties and improve the high temperature performance of the mixture [87]. Taking into consideration also that the lowest COF observed during this study was for the S.B.WS_2 coated strip run against the DLC TB 40 pin, a carbon based coating, and that the

A.S. WS_2 coating had comparably the lowest COF observed for all the coatings it could be suggested that the WS_2/C indeed offers a lower COF combination The coating thickness also comes into play seeing that the thicker aerosol coating was better able to mitigate aluminum adhesion. The thin S.B. WS_2 coating adheres to the surface through mechanical interlock, conforming to the surface, and during the stretching of the strip, the coating cracks and fractures, exposing the alloy substrate, as shown in Figure 57. The A.S. WS_2 on the other hand adheres to the substrate with the aid of the carbon based adhesive allowing for its thicker coating as seen in Figure 58. The coating fractures do not expose the substrate to aluminum transfers nor adhesion.

An A.S. WS_2 spray exists in the market at present, but when this was tested, it gave off harmful fumes at high temperatures due to isobutene and other chemical contents. A laboratory prepared aerosol WS_2 spray, based on a carbon adhesive was also tested, and this formula gave off no hazardous fumes with equal results to the market formula. Unlike the market product, the laboratory prepared aerosol spray could be applied indoors and did not require outdoor spaces for application. It was, therefore better suited to high temperature operations.

The TB 40 coated pin recorded a lower COF against all the strip conditions than the TB 41 coated pin. The TB 40 coated pin also performed better in mitigating aluminum adhesion as there was less aluminum observed on this pin surface under all conditions in comparison to that adhered to the TB 41 coated pin. Against the polished strip there was aluminum adhesion observed on the TB 40 coated pin which was splattered across the surface of the wear track in thin layers (Figure 46a), whereas there

was mild build-up observed as two dimples towards the tail of the wear track on the TB 41 coated pin. There was a reduction in COF and aluminum adhesion when both pins were run against the as-received strips. Again the TB 40 coating showed a lower COF with little aluminum adhesion observed at the tail of the wear track, whereas the TB 41 coated pin - with the higher COF comparable to that the COF of the S.B. WS_2 pin against the as-received strip – showed, a larger aluminum adhesion observed on its surface, appearing as a thin layer. Although these DLC coatings performed better than the S.B. WS_2 coated pin but against the uncoated strips they were still unable to mitigate aluminum adhesion under hot forming conditions against the uncoated strips. They performed much better when run against the coated strips with the lowest COF observed for the TB 40 coated pin run against the S.B. WS_2 coated strip. Here WS_2 transfer onto the pin was deduced based on the EDS in Figure 48c and the SEM in Figure 48a, which would aid in the COF reduction. Both DLC pins recorded a low COF when run against the S.B. WS_2: with the W and S observed on the pin surface (Figure 53 and 53c) suggesting that WS_2 transfer could have occurred. The mild aluminum adhesion observed on both pins was due to the WS_2 coating on the strip fracturing and exposing the aluminum alloy substrate. The low COF recorded against the S.B. WS_2 strips were comparable with those recorded against the BN coated strips but without the lubricant accumulation that was observed in the case of the BN coated surfaces. Taking into consideration the COF and aluminum adhesion mitigation qualities of both DLCs, the TB 40 coating appears better suited for high temperature forming operations than the TB 41 coating, especially when it is run against a WS_2 coated surface, which seems to be the

ideal condition for the lowest COF observed.

The BN coating performed well in reducing the COF and mitigating aluminum adhesion, by the transfer of BN flakes onto the mating surface which protected against metal to metal contact. This transfer was effective regardless of which surface was coated with BN. The flakes of BN were observed to accumulate in the form of spherical clusters on the mating surfaces. These BN clusters and flakes observed transferred to the pins from the BN coated strips showed traces of Al and sometimes Mg on them. This most likely occurred due to the loose oxides on the strip surface adhering to the BN coating (consisting of flakes) closest to the substrate. These BN clusters with loose oxide debris are transferred to the mating pin when it is run against the BN coated AA5083 strips. This also occurs for the BN coated pins run against the uncoated strips as seen in from the EDS in Figure 43c. Therefore, although BN can protect against aluminum adhering to the mated surface, it does not protect against loose debris adhering to its flakes.

Using this information gathered from these SEM observations a chart can be obtained as shown in Table 9. This adhesion chart correlates the tendency of adhesion, from the visual observations made with the SEM, with the surface conditions of both the P20 pin and the AA5083 strip. High adhesion is used to refer to aluminum build-up that was observed, medium adhesion represents the thin layer aluminum adhesion observed adhered to the pin surface, low adhesion refers to mainly minute patches of aluminum observed on the surface of the pin and finally no adhesion is used to describe the condition where no aluminum was observed adhered to the surface of the pin. This chart can be used to predict the possibility of adhesion occurring during hot forming with the

several combinations of coatings under the surface conditions tested. For example, the chart shows that no adhesion was observed for the combination of the uncoated polished pin run against the A.S. WS_2 coated strip, which from the discussion is due to the effective transfer of WS_2 platelets to the mating surface.

5.5 Solid Lubricant Coating Integrity Comparison

The integrity of the solid lubricant coatings were compared after the experiments with regard to adhesion of the coating and its loss from the substrate. The BN coated samples had the worst coating integrity; the BN coating was applied by aerosol spray and could easily be wiped clean off the substrate with the fingers. The coating also dislodged easily from the substrates during the hot forming experiments and accumulated on the mating surfaces. The accumulation occurred as flakes which adhered easily to one another, forming spherical clusters. These clusters accumulated and distributed on the wear track. The BN coating was able to protect the substrates and the mating surfaces from damage and defects despite loss of coatings due to coating transfer and accumulation. The accumulation of coating on the mating surface however is undesired during hot forming. The coating flakes of BN also picked up loose oxides from the aluminum strip during the hot forming run, which were transferred to the mating pin.

The A.S. WS_2 also displayed loss of coating from the substrates due to material transfer to the mating surfaces. The coating however adhered better to the substrate and was not removed or rubbed off by the finger. The coating loss only occurred during the hot forming tests. The WS_2 transferred were in the form of platelets that do not adhere to each other, so there is no accumulation of WS_2 on mating surfaces. There were no loose

oxide debris observed on the platelets, and aluminum adhesion to the mating surfaces was effectively mitigated by the coating.

The S.B. WS_2 had minimum loss of coating which could not be confirmed visually but only by the platelets of WS_2 observed transferred to the mating surfaces. The WS_2 platelets were mechanically interlocked with the substrate, could not be removed by rubbing, and showed better adhesion to the substrate than the BN and A.S. WS_2. This coating however was most effective in mitigating aluminum adhesion when applied to the aluminum strip. It was unable to mitigate aluminum adhesion while applied to the pin and run at 723 K.

Figure 59 shows the surfaces of the BN coated pin, the A.S. WS_2 coated pin, and the S.B. WS_2 coated pin right after the completion of the hot forming tests. The wear track of the BN coated pin and the A.S. WS_2 pin are easily observed here showing a distinct loss of coating. There is no visual confirmation of a wear track although on the surface of the S.B. WS_2, this can only be observed under close examination with an SEM. The wear track on the BN coated pin, observed with the naked eye, appears to have a larger coating loss with a larger wear track observed than that of the A.S. WS_2 pin.

Both DLCs also showed good adherence to the substrate with no confirmed material transfer from the coating observed on any of the mating surfaces they were run against. There was also no visual of coating for any of the DLC solid lubricants. They were not effective against mitigating aluminum adhesion against the uncoated aluminum strips but were most effective when run against the coated aluminum strips.

5.6 Solid Lubricant Coating Comparison: A.S. WS_2 and S.B. WS_2

From the earlier discussion a comparison can be derived between both WS_2 coatings. S.B. WS_2 was industrially applied and required both pre-coating and coating at high pressure. It relies on the mechanical interlocking of its platelets into the crevices of the substrate and was observed to have nano-sized platelets. At high temperature it did not effectively form a WS_2 transfer on the mating surface under most conditions tested. Its platelets are meant to conform to the substrate surface and on stretching, on a superplastic alloy, it cracked and fractured creating oxidation sites. It did not effectively protect the AA5083 substrate on stretching. There was no coating loss observed when the surface was examined visually. The A.S. WS_2 had to be applied in ventilated spaces; this restriction applies only to the industrially marketed A.S. WS_2 which produces hazardous fumes on spraying. The A.S. WS_2 that was locally prepared in the laboratory did not give off such fumes and therefore could be applied anywhere. Both, A.S WS_2 relied on a carbon based binder to adhere the coating to the substrate. The platelet sizes were observed to be much larger in comparison as seen in Figure 60. At high temperature both A.S WS_2 effectively formed a WS_2 transfer layer under all conditions tested. The platelets were not observed to crack or fracture, and due to a thick coating were able to protect against aluminum adhesion. Although the industrial A.S. WS_2 gave off harmful fumes at high temperature, the laboratory prepared A.S. WS_2 did not. Both, A.S. WS_2 showed visual coating loss after each experiment. A summary table of the comparison of these coatings is given in Table 8.

Table 8 Comparison between S.B. WS_2 and A.S. WS_2 coatings

Properties	S.B. WS_2	A.S. WS_2
Application method	Sand or spray blasted to substrate at 120psi	Aerosol spray
Platelet Adhesive mechanism	Mechanical Interlock	Carbon-based adhesive
Platelet size	Nano-sized	Micro-Sized
Substrate Protection	Unable to properly protect substrate due to thin coating fracture exposing substrate	Able to protect substrate due to thick coating, therefore no substrate exposure
Coating Integrity	WS_2 cracked and fractured on stretching creating oxidation sites	WS_2 did not crack or fracture, platelets were separated on stretching
Coating Adhesive Performance	No coating loss observed	Some coating loss observed

5.7 Solid Lubricant Coating Performance: COF

An average COF chart shown in Figure 61 was compiled. The chart displays all the COF data recorded in a 3D format which effectively compares all the pins surface conditions against the various strip surface condition. The chart shows distinctively the that COF of the BN coated pin and that of the A.S. WS_2 coated pin were the lowest recorded of all the pins. The COF of these pins can be observed to be quite comparable. It also shows that the lowest COF observed were for the coated strips as stated earlier.

The summary in Table 10 of all the COF obtained with the various coating

combinations was also compiled. It can be used to select specific surface conditions required to attain any desired COF. From this chart different surface conditions can be combined and used at different parts of the die to attain different COF at different locations during hot forming. If the summary tables for COF (Table 10) and that for adhesion (Table 9) are both combined, it can be observed the DLC TB 40 coating possess a lower COF and better aluminum adhesion mitigating tendencies than the DLC coating TB 41. One can also observe here the lowest (TB 40 against S.B. WS_2) and highest COF (S.B. WS_2 against Polished) recorded during these simulations in relation to the relative amount of aluminum adhesion that occurred under these combinations. These tables also show that under most conditions, the lowest COF is observed when the AA5083 strip is coated; this condition also leads to the least amount of aluminum adhesion to the pin.

These tables can be used during coating selection for combining specific surface conditions, for the die and the workpiece, to obtain an approximate COF combined with an idea of the possible aluminum adhesion tendencies under those conditions. As a low COF is not always required, as this increases the tendency of necking over sharp radii, during hot forming it is advised to have low friction for most of the tool but high friction in specific areas [13]. Therefore, using these tables, one can select a coating combination for areas that require low COF and another matching combination for areas requiring a higher COF.

A practical example is shown in the schematic diagram in Figure 62 where the die surface is coated with A.S. WS_2 for most of the surface and TB 40 at the sharp edges of the die. Here the aluminum workpiece is as-received, there would be little adhesion but a

high COF recorded at the TB 40 coated edges but a low COF with no adhesion for the rest of the surfaces coated with A.S. WS_2. The aluminum strip can also be coated with S.B. WS_2 and the die left uncoated where a high COF is required and TB 40 where a low COF is needed. There are various combinations that could possibly be used depended on the desired out come. Again these tables could also be used independently, depending on if aluminum adhesion is more of an issue or if the COF is the major issue.

These tables are specific for the researched coatings at 723 K/ $0.04s^{-1}$ and can be used as a reference for possible coating combinations with predictable results.

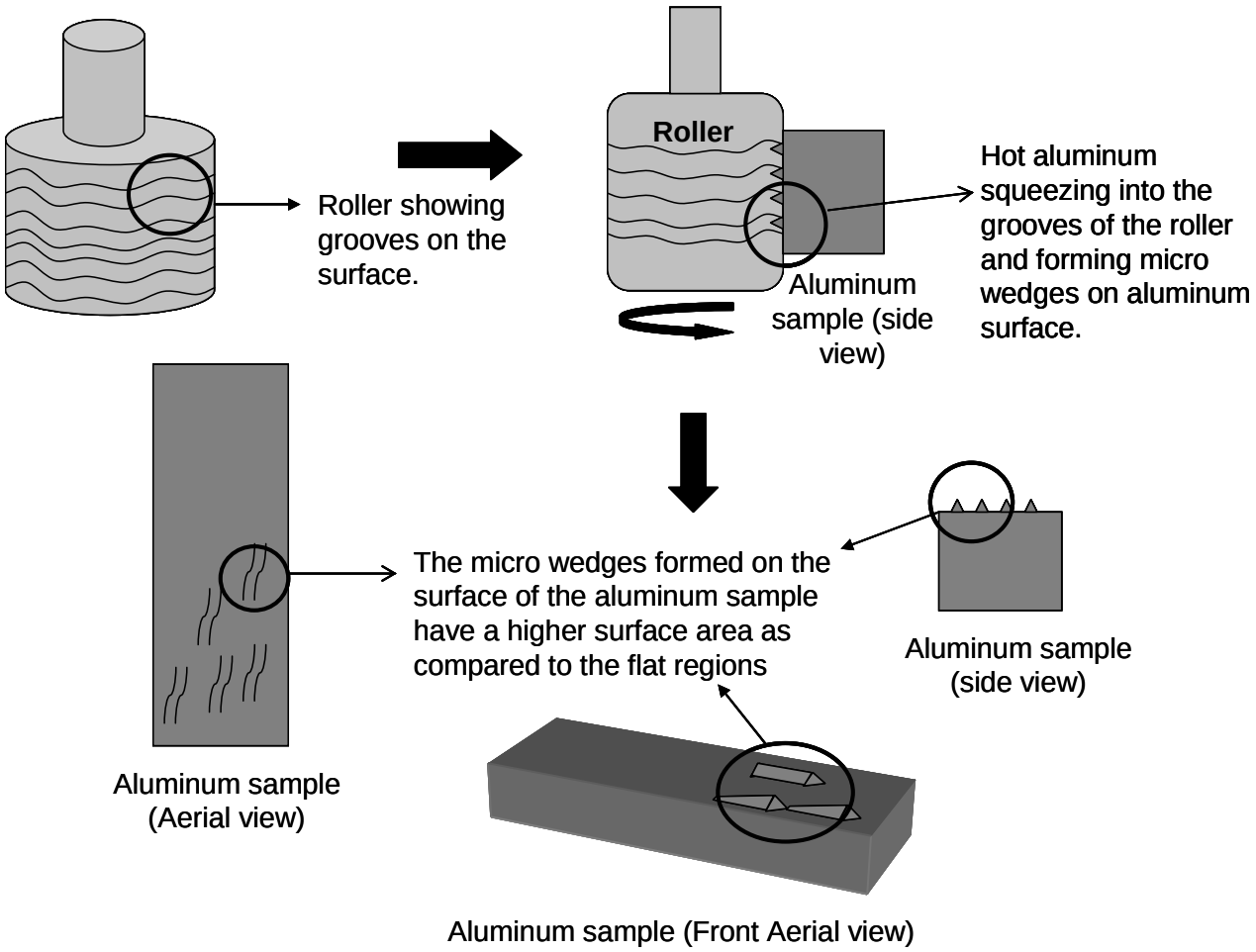

Figure 55 Formation of Microwedges on the aluminum stock rolled against the steel roll

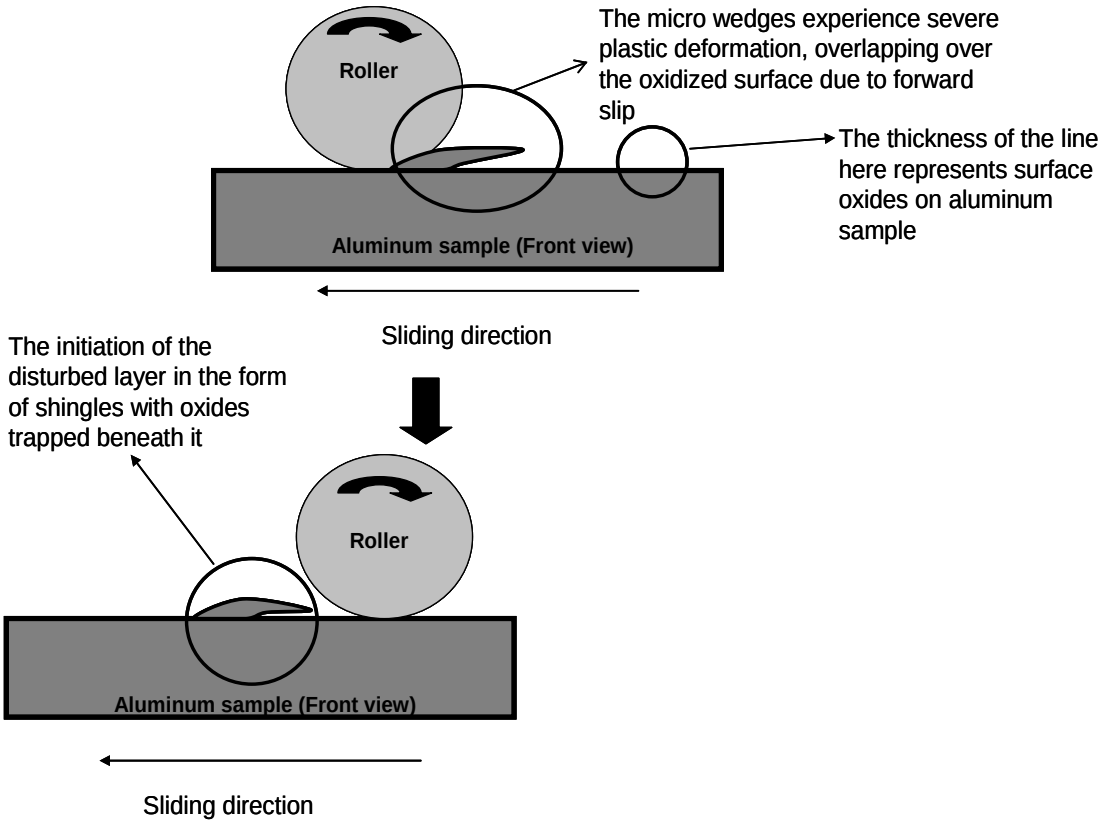

Figure 56 The influence of the first rolling pass

Figure 57 SEM of the cracks on S.B. WS_2 coating showing the exposed AA5083 substrate

Figure 58 SEM of the cracks on A.S. WS_2 coating showing no exposure of AA5083 substrate due to coating thickness

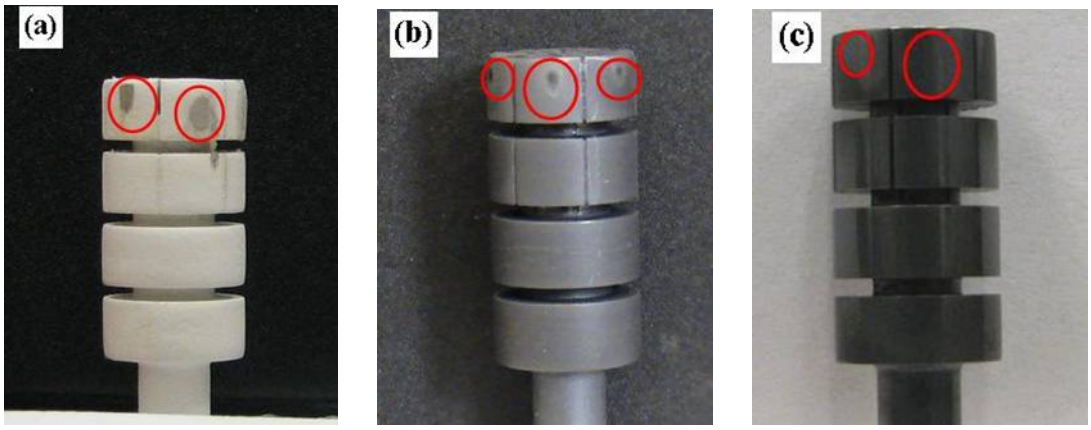

Figure 59 Pictures of the surfaces of the, (a) BN coated pin, (b) A.S. WS_2 coated pin, and (c) S.B. WS_2 coated pin after the hot forming experiment with red rings around strip contact areas showing visual coating loss

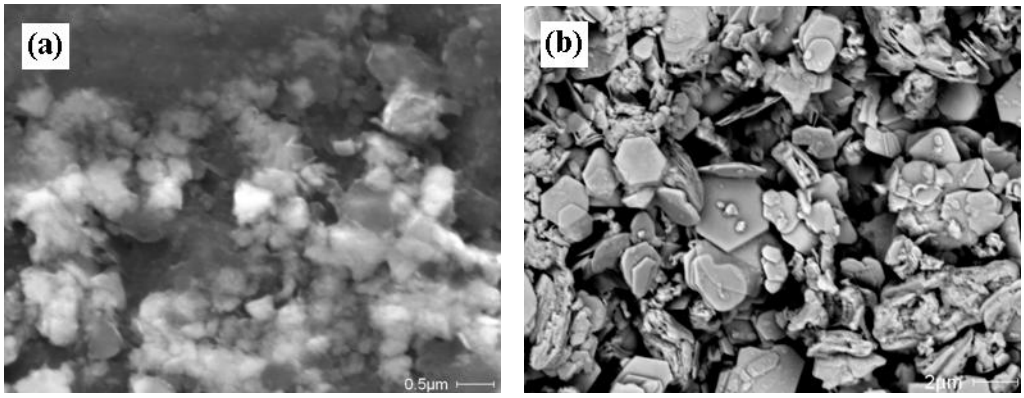

Figure 60 A Comparisons of the platelet sizes for (a) S.B. WS_2 coating (b) A.S. WS_2 coating

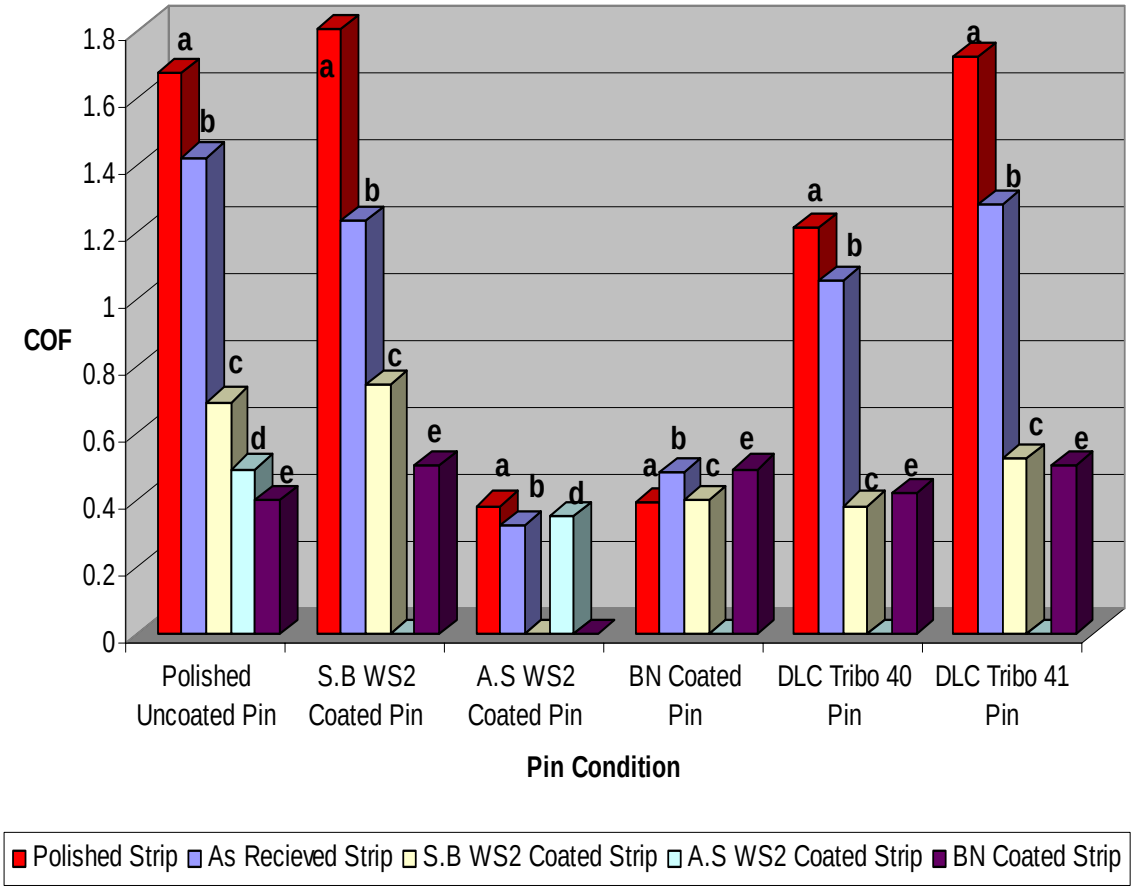

Figure 61 Average COF Chart ; (a) depicts the polished strip, (b) as-received strip, (c) S.B. WS_2 coated strip, (d) A.S. WS_2 coated strip, (e) BN coated strip

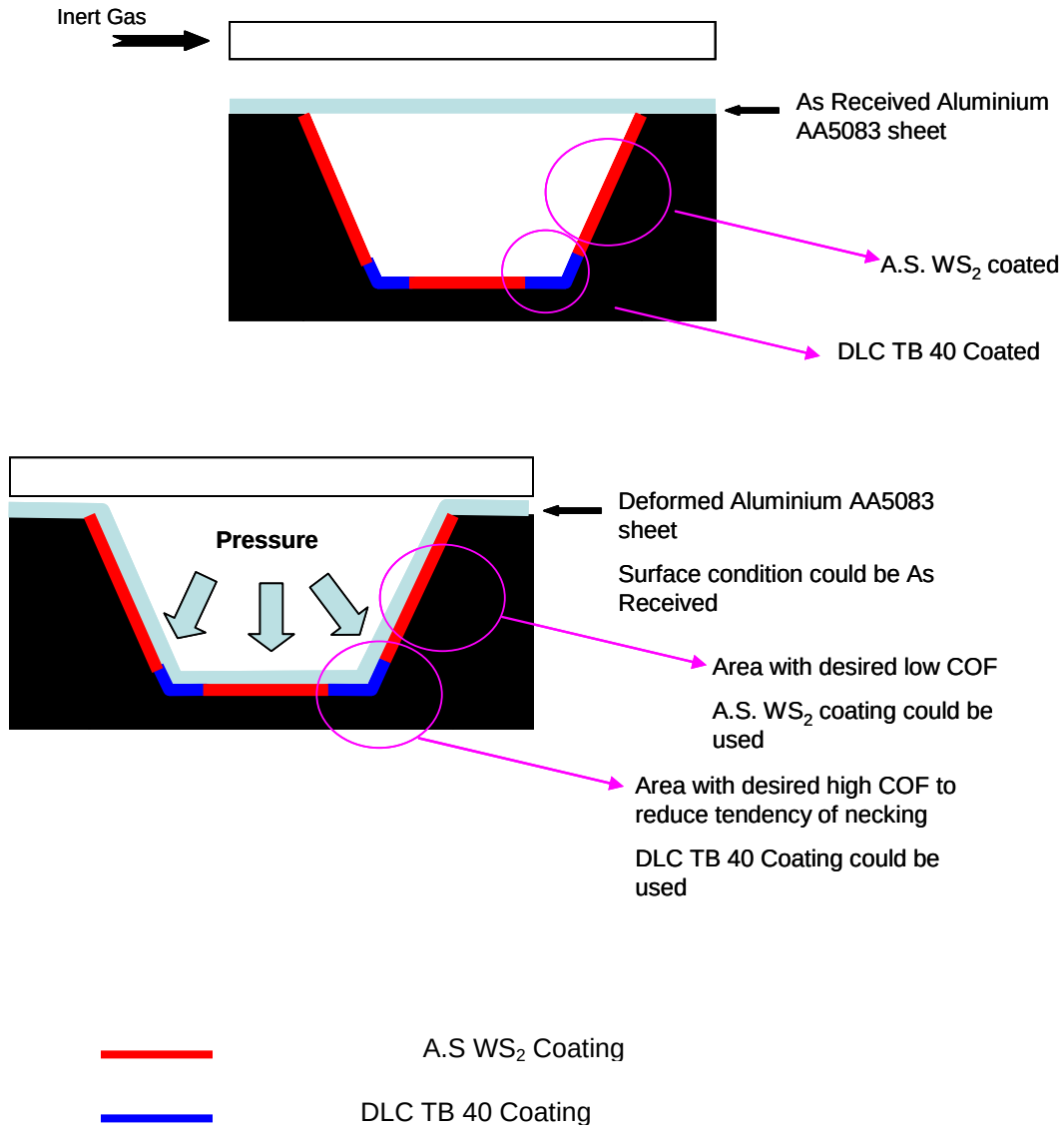

Figure 62 A Schematic diagram displaying ways solid lubricant coatings can be combined to attain high COF at high radii areas and low COF at other areas

Table 9 Summary Table showing the adhesion tendencies for all the experimental conditions

	As Received Strip	Polished Strip	S.B WS_2 Coated Strip	A.S WS_2 Coated Strip	BN Coated Strip
Polished Uncoated Pin	Medium Adhesion	High Adhesion	Low Adhesion	No Adhesion	No Adhesion
S.B WS_2 Coated Pin	Medium Adhesion	High Adhesion	Low Adhesion		No Adhesion
A.S WS_2 Coated Pin	No Adhesion	No Adhesion		No Adhesion	
BN Coated Pin	No Adhesion	No Adhesion	No Adhesion		No Adhesion
DLC Tribo 40	Medium Adhesion	High Adhesion	Low Adhesion		No Adhesion
DLC Tribo 41	Medium Adhesion	High Adhesion	Low Adhesion		No Adhesion

Table 10 Summary Table showing the average COF for all the experimental conditions examined

	As Received Strip	Polished Strip	S.B WS_2 Coated Strip	A.S WS_2 Coated Strip	BN Coated Strip
Polished Uncoated Pin	1.42 ±0.16	1.67 ±0.18	0.69 ±0.18	0.49 ±0.10	0.40 ±0.11
S.B WS_2 Coated Pin	1.23 ±0.19	1.80 ±0.28	0.74 ±0.15		0.50 ±0.14
A.S WS_2 Coated Pin	0.32 ±0.07	0.38 ±0.11		0.35 ±0.11	
BN Coated Pin	0.48 ±0.12	0.39 ±0.10	0.40 ±0.13		0.49 ±0.11
DLC Tribo 40	1.05 ±0.16	1.21 ±0.29	0.38 ±0.08		0.42 ±0.11
DLC Tribo 41	1.28 ±0.21	1.72 ±0.29	0.52 ±0.12		0.50 ±0.11

CHAPTER VI

CONCLUSIONS AND RECOMMENDATIONS

Simulated hot rolling and hot forming experiments were conducted using aluminum alloys, AA3104 (Al-Mn-Mg) and AA5083 (Al-Mg) in order to study the surface defects that occurred during these high temperature operations and the parameters that influence them. The hot rolling experiments centered on the effects of forward speed and number and direction of rolling passes on the generation of disturbed layer. The hot forming experiments looked into the effect of COF on the surface defects induced on aluminum surfaces. The results show that:

1) The surface defects, such as cavities, gorges and shingles, observed during the high temperature rolling experiments were similar to those found in the industry, proving these high temperature processes can be successfully replicated in the laboratory to study the surface defects.

2) The surface defects such as shingles, appear on the rolled surfaces at the initial stage of disturbed layer generation due to the local deformation of the micro wedges. These surface defects were observed in single pass tests, using roll surfaces without aluminum build-up.

3) The surfaces formed during sliding at high forward slip display more pronounced surface defects, such as shingles (local shear deformations).

4) The increase in the number of rolling passes increases the frequency of the surface defects, surface concentration, and depth of magnesium.

5) When the second rolling pass is conducted in the reverse direction to the

previous one, local shear deformations appear to be shallower and flattened compared to those observed with both rolling passes conducted in the same direction.

6) The COF observed during hot forming operations can be related to the aluminum adhesion observed on the die. A high COF is observed to be accompanied by aluminum build-up while low COF is accompanied by no adhesion or little adhesion.

7) WS_2 spray blasted (S.B. WS_2) on the surface of the aluminum strip offers similar COF to that of the BN coated surfaces but displays a higher durability than the BN coating at the temperatures and strain rates tested. The BN coating displayed the worst durability of all the coatings (TB40. TB41, S.B. WS_2 and A.S. WS_2), being easily lost by rubbing and accumulating on mating surfaces

8) The highest COF (1.80) was observed with the WS_2 coating spray blasted onto the pin run against the polished strip at 723 K /0.04s^{-1}. A reduction of the COF to 0.53 was recorded however when the temperature and strain rate were reduced to 573 K /0.01s^{-1}. This suggests that this method can best be used for such operations as warm forming and hot stamping.

8) As a solid lubricant coating WS_2 aerosol spray (A.S. WS_2) recorded the lowest against all mating surfaces (0.32-0.49), evenly matching the BN coating (0.39-0.49) with regards high friction reduction. It offered good durability and did not accumulate on mating surfaces as compared to BN. There was also no aluminum adhesion observed when this coating was used, either on the coating platelets or the die surface unlike the BN coating which easily picked up oxide debris.

10) An aerosol spray WS_2 coating was locally developed and proved to be as

effective in reducing COF and mitigating aluminum adhesion as the industrially marketed aerosol WS_2 spray but without the release of harmful gases of that plagues the industrial aerosol WS_2.

11) Two summary tables were developed in Tables 9 and 10. The first can be used to as a reference for combining coatings during hot forming operations in relation to the aluminum adhesion tendency. It shows the suitable combinations for mitigation of aluminum adhesion. The second is related to the COF, showing combinations of solid coatings as lubricants during hot forming in relation to this parameter. Combining the information from both tables can be used to select a coating combination based on a desired COF and aluminum adhesion tendency.

REFERENCES

[1] Sanders R. E., Hollinshead P. A., Simielli E. A., "Industrial Development of Non-Heat Treatable Aluminum Alloys", Materials Forum, Vol.28, 2004 pp 53-64

[2] Polmear I. J., "Wrought Aluminium Alloys Light Alloys: Metallurgy of the Light Metals", Butterworth – Heinemann, London 1995

[3] Totten G. E., MacKenzie D. S., "Handbook of Aluminum Volume 1: Physical Metallurgy and Processes", Marcel Dekker Inc., 2003, New York

[4] Metals Handbook, Welding, Brazing and Soldering, Vol. 6, ASM International, 1993 pp 1363

[5] Lu L., Man O. L., "Mechanical Alloying", Springer. 1998, Massachusetts

[6] Metals Handbook 10th Ed., Metallography and Microstructures, Vol. 9, ASM International, 2004 pp 1714

[7] Groover M. P., "Fundamentals of Modern Manufacturing: Materials, Processes and Systems 3rd Ed." John Wiley and Sons Inc. 2007

[8] Le H. R., Sutcliffe M. P. F., Williams J. A., "Friction and Material Transfer in Micro-Scale Sliding Contact between Aluminium Alloy and Steel" Tribology Letters. Vol. 18, 2005 pp 99-104

[9] Dieter E. G., "Mechanical Metallurgy", McGraw-Hill, 1998, New York

[10] Metals Handbook, Metalworking: Sheet Forming, Vol. 14B, ASM International, 2006 pp 583

[11] Energetics Incorporated., "Aluminum Industry Roadmap for the Automotive Market: Enabling Technologies and Challenges for Body Structures and

Closures", The Aluminum Association Inc., 2006, Washington

[12] Hanna M. D., "Tribological Evaluation of Aluminum and Magnesium Sheet Forming at High Temperatures", Wear 267, 2009 pp 1046-1050

[13] Krajewski P. E., Morales A. T., "Tribological Issues During Quick Plastic Forming", Journal of Materials Engineering and Performance Vol. 13., 2004 pp700-709

[14] Chen Z., Thomson P. F., "Friction Against Superplastic Aluminium Alloys", Wear 201., 1996 pp227-232

[15] Shakeri H. R., "Superplastic Forming of Aluminium Alloys", Aluminium Technology Centre., 2004

[16] Totten G. E., "Handbook of Lubrication and Tribology Vol. I", CRC Taylor and Francis Group. New York 2006

[17] Timothy S. P., Yiu H. L., Fine J. M., Ricks R. A., "Simulation of Single Pass of Hot Rolling Deformation of Aluminium Alloy by Plane Strain Compression", The Institute of Metals, 1991 pp 255-261

[18] Ambat R., Davenport A. J., Afseth A., Scamans G., "Electrochemical Behavior of the Active Surface Layer on Rolled Aluminum Alloy Sheet", Journal of The Electrochemical Society 151, 2004 pp B53-B58

[19] Fishkis M. and Lin J. C., "Formation and Evolution of a Subsurface Layer in a Metalworking Process", Elsevier, Wear 206, 1997 pp 156-170

[20] Buytaert G., Premendra., de Wit H. H. W., Katgerman L., Kernig B., Brinkman H. J., Terryn H., "Electrochemical Investigation of Rolled-in Subsurface Layers in Commercially Pure Aluminium Alloys with the Micro-Capillary Cell Technique",

Surface and Coatings Technology 201, 2007 pp 4553-4560

[21] Frolish M. F., Walker J. C., Jiao C., Rainforth W. M., Benyon J. H., "Formation and Structure of a Subsurface Layer in Hot Rolled Aluminium Alloy AA3104 Transfer Bar" , Elsevier, Tribology International 38, 2005 pp 1050-1058

[22] Frolish M. F., Krzyzanowski M., Rainforth W. M., Benyon J. H., "Oxide Scale Behaviour on Aluminium and Steel Under Hot Working Conditions" , Journal of Materials Processing Technology 177, 2006 pp 36-40

[23] Premendra., Philippe L., Terryn H., de Wit J. H. W., Katgerman L., "Understanding the Electrochemical, Microstructural and Morphological Changes During Hot Rolling from a Corrosion Perspective" Surface and Coatings Technology Vol. 201, 2006 pp 828-834

[24] Afseth A., Nordlien J. H., Scamans G. M., Nisancioglu K., " Effect of Thermo-Mechanical Processing on Filiform Corrosion of Aluminium Alloy AA3005" Corrosion Science Vol. 22, 2002 pp 2491-2506

[25] Zhou X., Liu Y., Thompson G. E., Scamans G. M., Skeldon P., Hunter J. A., "Near-Surface Deformed Layers on Rolled Aluminum Alloys", Metallurgical and Materials Transactions A, 2010 pp 1-13

[26] Ambat R., Davenport A. J., Afseth A., Scamans G., "Electrochemical Behavior of the Active Surface Layer on Rolled Aluminum Alloy Sheet", Journal of The Electrochemical Society 151, 2004 pp B53-B58

[27] Leth-Olsen H., Nordlien H. J., Nisancioglu K., "Filiform Corrosion of Aluminium Sheet. III. Microstructure of Reactive Surfaces" Corrosion Science, Vol. 40, No.

12, 1998 pp 2051-2063

[28] Buytaert G., Kernig B., Brinkman H. J., Terryn H., "Influence of Surface Pre-Treatments on Disturbed Rolled-in Subsurface Layers of Aluminium Alloys" , Elsevier, Science Direct 201, 2006 pp 2587-2598

[29] Hahin C., Buchheit R. G., "Filiform Corrosion", ASM Metals Handbook Vol. 13A, 2003 pp 248-256

[30] Buytaert G., Terryn H., Van Gils S., Kernig B., Grzemba B., Mertens M., "Study of the Near-Surface of Hot- and Cold-Rolled AlMg0.5 Aluminium Alloy" Surf. Interface Anal. 37, 2005 pp 534-543

[31] Premendra., Chen H. J., Tichelaar F. D., Terryn H., deWit J. H. W., Katgerman L., "Optical and Transmission Electron Microscopical Study of the Evolution of Surface Layer on Recycled Aluminium Along the Rolling Mills" Surface and Coatings Technology Vol. 201, 2007 pp 4561-4570

[32] Kuypers s., Buytaert G., Terryn H., "Depth Profiling of Rolled Aluminium Alloys by Means of GDOES" , Surf. Interface Anal. 36, 2004 pp 833-836

[33] Scamans G., "Shear Processing of Aluminium Alloy Surfaces and its Influence on Corrosion" Innoval Technology Limited, Oxfordshire

[34] Xia X., "Precipitation and Recrystallization in Al-Mn AA3104 Alloy" Scripta Metallurgica Vol. 28, 1993 pp 1213-1218

[35] Plassart G., Aucouturier M., Penelle R., "Microstructure and Chemistry of an Al-4.7 wt.%Mg Alloy Subsurface After Cold-Rolling" , Scripta Materialia Vol. 41, N 10, 1999 pp 1103-1108

[36] Delplancke J. L., Berger S., Lefebvre X., Maetens D., Pourbaix A., Heymans N., "Filiform corrosion: Interactions between electrochemistry and mechanical properties of the paints", Progress in Organic Coatings., Vol. 43 2001 pp 64-74.

[37] Bautista A., "Filiform Corrosion in Polymer-Coated Metals", Progress in Organic Coatings, Vol. 28 1996 pp 49-58

[38] Davis J. K., "Corrosion: Understanding the Basics" JASM International, Ohio, 20

[39] Zhou X., Thompson G. E., Scamans G. M., "The Influence of Surface Treatment on Filiform Corrosion resistance of Painted Aluminium Alloy Sheet", Corrosion Science, Vol.45, 2003 pp 1767-1777

[40] Revie R. W., Uhlig H. H., "Corrosion and Corrosion Control, 4th Edition" John Wiley and Sons, New Jersey, 2008

[41] Sastri V. S., Ghali E., Elboujdaini M., "Corrosion Prevention and Protection"John Wiley and Sons, West Sussex 2007

[42] Slabaugh W. H., Grotheer M., "Mechanism of Filiform Corrosionl", Industrial and Engineering Chemistry, Vol. 46; 1954 pp 1014-1016

[43] Hoch G. M., "A Review of Filiform Corrosion" , Localized corrosion, Vol. 159-160, 1974 pp 134-142

[44] Jenkins A. T. A., Armstrong R. D., "The Breakdown in the Barrier Properties of Organic Coatings due to Filiform Corrosion", Corrosion Science, Vol. 38 1996 pp 1147-1157

[45]Vargel. C., "Corrosion of Aluminum", Elsevier Ltd., Oxford, 2004

[46] LeBoze N., Persson D., Thierry D., "In Situ Studies of the Initiation and Propagation

of Filiform Corrosion on Aluminum", Journal of The Electrochemical Society, Vol. 151 2004 pp 440-445

[47] Scamans G. M., Afseth A., Thompson G. E., Liu Y., Zhou X., "Corrosion of Paint Aluminium Sheet", Materials Science Forum, Vol. 519-521, 2006 pp 647-654

[48] de Wit J. H. W., "New Knowledge on Localized Corrosion Obtained from Local Measuring Techniques" Electrochimica Acta ., Vol. 46 2001 pp 3641-3650

[49] Scamans G. M., Afseth A., Thompson G. E., Zhou X., "Ultra-Fine Grain Sized Mechanically Alloyed Surface Layers on Aluminum Alloys" Materials Science Forum, 2002 pp 1461-1466

[50] Buytaert G., Terryn H., Van Gils S., Kernig B., Grzemba B., Mertems M., "Investigation of the (Sub) Surface of Commercially Pure Rolled Aluminium Alloys by means of Total Reflectance, R.F GDOES, SEM/EDX and FIB/TEM Analysis" Surface and Interface Analysis, 2006 pp 272-276

[51] Roberge P. R., "Corrosion Engineering: Principles and Practice", McGraw Hill, New York, 2008.

[52] Carlsson P., "Surface Engineering in Sheet Metal Forming", Acta Universitatis Upsaliensis, Uppsala. 2005

[53] Hanna M. D., Krajewski P. E., Schroth J. G., "Tribological Testing of Graphite and Boron Nitride Lubricant Formulations for High Temperature Aluminum Sheet Forming Processes", Proceedings of ASME/STLE International Joint Tribology Conference, pp 705-707

[54] Lange. K., "Handbook of Metal Forming", McGraw-Hill., New York, 1985

[55] Hao S., Klamecki B. E., Ramalingam S., “Friction Measurement Apparatus for Sheet Metal Forming”, Wear, 1999 pp 1-7

[56] Matuszak A., “Factors Influencing Friction in Steel Sheet Forming”, Journal of Materials Processing Technology, 2000 pp 250-253

[57] Han S. S., “The Influence of Tool Geometry on Friction Behavior in Sheet Metal Forming”, Journal of Materials Processing Technology, 1999 pp 129-133

[58] Menezes P. L., Kumar K., Kishore., Kailas S. V., “Influence of Friction During Forming Processes – A study using a Numerical Simulation”, International Journal of Advanced Manufacturing Technology, 2009 pp 1067-1076

[59] Lovell M. R., Deng Z., Khonsari M. M., “Experimental Characterization of Sliding Friction: Crossing from Deformation to Plowing Contact”, Journal of Tribology, Vol. 122 2000 pp 856-863

[60] Hanson M., Hogmark S., Jacobson S., “Influence from Tool Roughness on the Risk of Work Material Adhesion and Transfer”, Materials and Manufacturing Processes, Vol. 24 2009 pp 913-917

[61] Hanson M., “On Adhesion and Galling in Metal Forming”, Acta Universitatis Upsaliensis, Uppsala. 2008

[62] de Rooij M. B., Schipper D. J., “Analysis of Material Transfer from a Soft Workpiece to a Hard Tool: Part II – Experimental Verification of the Proposed Lump Growth Model”, Journal of Tribology, Vol. 123 2001 pp 474-478

[63] Riahi A. R., Edrisy A., Alpas A. T., “Effect of Magnesium Content on the High Temperature Adhesion of A-Mg Alloys to Steel Surfaces”, Surface and Coatings

Technology 2009 pp 2030-2035

[64] Wei J, Erdemir A, Fenske G. R., “Dry Lubricant Films for Aluminum Forming”, Tribology Transactions, Vol. 43 2000 pp 535-541

[65] Kuhlman G. W., “Forging of Aluminum Alloys”, ASM Metals Handbook Vol. 14, 2005 pp 299-312

[66] Schey A. J., “Mechanical Deformation Process (Friction and Lubrication)”, Marcel Dekker Inc., New York. 1970

[67] Booser R. E., “CRC Handbook of Lubrication (Theory and Practice) Vol. II”, CRC Press LLC. New York 1983

[68] Toros S., Ozturk F., Kacar I., “Review of Warm Forming of Aluminum-Magnesium Alloys”, Journal of Materials Processing Technology. Vol.207. 2008 pp1-12

[69] Sakurai T., “The Latest Trends in Aluminum, Alloy Sheets for Automotive Body Panels”, Kobelco Technology Review. Vol.28. 2008 pp22-28

[70] Mang T., Dresel W., “Lubricant and Lubrication”, Wiley-VCH Verlay GmbH. Weinheim. 2007

[71] Ngaile G. and Botz F., “Performance of Graphite and Boron-Nitride-Silicone Based Lubricants and Associated Lubrication Mechanisms in Warm Forging of Aluminum”, Journal of Tribology Vols. 130, 2008 pp 1-7

[72] Hanna M. D., Franetovic V., “The Effect of Boron Nitride Lubricant Thickness and Steel Surface Condition on Tribological Behavior of P20 Steel/5083 Aluminum Sliding Pairs at High Temperature”, Proceedings of the STLE/ASME International Joint Tribology Conference. 2008

[73] Allam I. M., "Solid Lubricants for Applications at Elevated Temperatures", Journal of Materials Science 24. 1991 pp3977-3984

[74] Riahi A. R., Alpas A. T., "Adhesion of AA5182 Aluminum Sheet to DLC and TiN Coatings at 25oC and 420oC", Surface and Coatings Technology, 2007 pp 1055-1061

[75] Riahi A. R., Morales A. T., Alpas A. T., "Evaluation of Vitreous and Devitrifying Enamels as Hot Forming Lubricants for Aluminum AA5083 Alloy", Journal of Materials Engineering and Performance, 2008 pp 387-394

[76] Morales A. T., "Evaluation of Die Coatings for Superplastic Forming Process", Advances in Superplasticity and Superplastic Forming, 2004 pp 51-64

[77] Rai A. K., Bhattacharya R. S., Zabinski J. S., Miyoshi K., "A Comparison of the Wear Life of As-Deposited and Ion-Deposited WS_2 Coatings", Surface and Coatings technology Vols. 92, 1997 pp 120-128

[78] Prasad S. and Zabinski J., McDevitt N. T., "Friction Behavior of Pulsed Laser Deposited Tungsten Disulfide Films", Tribology Transactions Vol. 38, 2006 pp 57-62

[79] Zabinski J. S., Donley M. S., Prasad S. V., "Synthesis and Characterization of Tungsten Disulphide Films Grown by Pulsed Laser Deposition", Journal of Materials Science Vols. 29, 1994 pp 4834-4839

[80] Scharf T. W., Prasad S. V., Dugger M. T., Kotula P. G., Goeke R. S., Grubbs R. K., "Growth, Structure and Tribological Behaviour of Atomic Layer Deposited Tungsten Disulphide Solid Lubricant Coatings with Applications to MEMS" ,

Acta Metarialia Vol. 54, 2006 pp 4713-4743

[81] Martin-Litas I., Vinatier P., Levasseur A., Dupin J. C., Gonbeau D., Weil F., "Characterisation of R.F. Sputter Tungsten Disulfide and Oxysulfide Thin Films" , Thin Solid Films. Vol. 416, 2002 pp 1-9

[82] Isshiki T., Nishio K., Yabuuchi Y., Takahashi N., Saijo H., "High Resolution Transmission Electron Microscopy of Layer Structure and Stacking Faults in Tungsten Disulphide Lubricants", Wear 170, 1993 pp 55-61

[83] Srivastava S. K. and Avasthi N. B., "Layer Type Tungsten Dichalcogenide Compounds: Their Preparation, Structure, Properties and Uses", Journal of Materials ScienceVol. 20, 1985 pp 3801-3815

[84] Prasad S. and Zabinski J., "Tribology of Tungsten Disulphide (WS_2): Characterization of Wear Induced Transfer Films", Journal of Materials Science Letters Vols. 12, 1993 pp 1413-1415

[85] Scharf T. W., Rajendran A ., Banerjee R., Sequeda F., "Growth, Structure and Friction Behavior of Titanium Doped Tungsten Disulphide (Ti-WS_2) Nanocomposite Thin Films" , Thin Solid Films. 517, 2009 pp 5666-5675

[86] www.lowerfriction.com

[87] http://www.ws2oil.com/what-is-ws2.html

[88] Prasad S. V., McDevitt N. T., Zabinski J. S., "Tribology of Tungsten Disulfide Films in Humid Environments: The Role of a Tailored Metal Matrix Composite Substrate" , Wear, Vol. 230 1999 pp 24-34

[89] Prasad S. and Zabinski J., "Super Slippery Solids", Nature 387, 1997 pp 761-763

[90] Scharf T. W., Diercks D. R., Gorman B. P., Prasad S. V., Dugger M. T., "Atomic Layer Deposition of Tungsten Disulphide Solid Lubricant Nanocomposite Coatings on Rolling Element Bearings", Tribological Transactions. Vol. 52, 2009 pp 284-292

[91] Scharf T. W., Prasad S. V., Mayer M. T., Goeke R. S., Dugger M. T., "Atomic Layer Deposition of Tungsten Disulphide Solid Lubricant Thin Films", J. Mater. Res. Vol. 19, 2004 pp 3443-3446

[92] Cohen S. R., Rapoport L., Pomomarev E. A., Cohen. H., Tsirlina T., Tenne R., Levy-Clement C., "The Tribological Behavior of Type II Textured MX2 (M=Mo, W; X=S, Se) Films", Thin Solid Films Vol. 324, 1998 pp 190-197

VITA AUCTORIS

NAME:	Olufisayo Gali
PLACE OF BIRTH:	Ikeja, Lagos
YEAR OF BIRTH	1978
EDUCATION:	University of Ibadan, Oyo State
	1994- 2000 B.Sc
	University of Windsor, Windsor, Ontario
	2009- 2011 M.Sc